ISTANBUL MEDENIYET UNIVERSITY
INSTITUTE OF GRADUATE STUDIES
DEPARTMENT OF MOLECULAR BIOLOGY AND GENETICS

Generating A Novel Targeted Cancer Therapy By Using A Combination Of Cellulose Nanoparticles With Cellulase Enzyme In The Tumor Microenvironment

Master's Thesis

Ruken Sarıboğa

June 2025

ISTANBUL MEDENIYET UNIVERSITY
INSTITUTE OF GRADUATE STUDIES
DEPARTMENT OF MOLECULAR BIOLOGY AND GENETICS

Generating A Novel Targeted Cancer Therapy By Using A Combination Of Cellulose Nanoparticles With Cellulase Enzyme In The Tumor Microenvironment

Master's Thesis

Ruken Sarıboğa

Supervisor

Assist. Prof. Ömer Faruk Sarıoğlu

June 2025

THESIS JURY APPROVAL

This Master thesis titled "Generating A Novel Targeted Cancer Therapy By Using A Combination Of Cellulose Nanoparticles With Cellulase Enzyme In The Tumor Microenvironment" written by SARIBOĞA, Ruken at the Department of Molecular Biology and Genetics was accepted by our jury.

JURY MEMBERS **SIGNATURE**

Supervisor:

Assist. Prof. Ömer Faruk Sarıoğlu

Istanbul Medeniyet University

Other Jury Members:

Assist. Prof. Ümmühan Demir

Istanbul Medeniyet University

Assist. Prof Canan Bağcı

Bahçeşehir University

Date of Defense: 25.06.2025

STATEMENTS

Style and Reference Manual Statement

Having reviewed this thesis written under my supervision, I confirm that it has been written in accordance with Chicago Manual of Style 16th edition and used its [footnote/in text] reference format consistently throughout the entire text.

Signature
Assist. Prof. Ömer Faruk Sarıoğlu

Declaration of Originality

I hereby declare that all information in this dissertation has been obtained and presented in accordance with academic rules and ethical conduct. I also declare that, as required by these rules and conducts, I have fully cited and referenced all material and results that are not original to this work.

Signature
Ruken Sarıboğa

ACKNOWLEDGEMENTS

First and foremost, I would like to express my sincere gratitude to my supervisor, Assist. Prof. Ömer Faruk SARIOĞLU, for giving me the opportunity to be a part of this project and for his invaluable support and guidance throughout the entire study. I am also deeply thankful to Assist. Prof. Ümmühan DEMİR for her expertise and kind guidance, especially in the cell culture studies, which significantly contributed to the success of this work.

Among all, I wish to express my heartfelt thanks to my dear friend and colleague, Hande GÜZEL, who has been not only a long-time companion but also my greatest support throughout this journey. Her encouragement, understanding, and presence meant the world to me.

I would also like to sincerely thank Damla Nur ÇAMLI for both her experimental contributions and for being a constant source of support and motivation during this process. Her presence made the challenges much more manageable.

Additionally, I thank my colleagues Nilay DİNÇKURT and Ünal ARABACI for their consistent encouragement and supportive companionship throughout this journey.

My deepest gratitude goes to my family, who have always stood by me through every challenge and moment of doubt. I especially thank my mother and father for their endless support throughout my academic journey, and my siblings for bringing joy and meaning into my life.

Lastly, I gratefully acknowledge TÜBİTAK for supporting the 3501 project of my supervisor and providing me with a scholarship through the ARDEB program (Project no: 123S091).

CONTENTS

CONTENTS ..... **III**
LIST OF SYMBOLS ..... **VII**
LIST OF ABBREVIATIONS ..... **VIII**
LIST OF FIGURES ..... **XII**
LIST OF TABLES ..... **XVI**
ABSTRACT ..... **XVII**
ÖZET ..... **XIX**
1. INTRODUCTION **1**
1.1. CELLULOSE 1
1.1.1. Cellulose: Structural Features and Dissolution 2
1.2. CELLULOSE BIOMATERIALS 4
1.2.1. Antimicrobial Material Design 5
1.2.2. Food Packaging 6
1.2.3. Tissue Engineering 7
1.2.4. Drug Delivery and Targeting 8
1.3. RUMINANT MICROORGANISMS AND CELLULASE 9
1.3.1. Endogenous Metabolism of Ruminant Bacteria 9
1.3.2. Microbial Turnover Through Lysis and Predation in the Rumen 10
1.3.3. Microbial Rumen Fermentation 10
1.3.4. Cellulase 11
1.4. CANCER 11
1.4.1. Hallmarks of Cancer 13
1.4.2. Molecular and Cellular Mechanisms of Cancer 14
1.4.3. Types of Cancer 15
1.5. DOXORUBICIN 20
1.5.1. Molecular Mechanisms of Doxorubicin 23
1.6. TARGETED DRUG DELIVERY TECHNIQUES 25
1.6.1. Active Targeting 26

1.6.2. EPR effect and Passive Targeting 26
1.6.3. ThermoDOX 28
2. MATERIALS & METHODS 29
2.1. ISOLATION AND IDENTIFICATION OF CELLULOSE DIGESTIVE BACTERIA FROM THE RUMEN 29
2.1.1. Collection of Samples From the Cattle Rumen Fluid 29
2.1.2. Isolation of Cellulose-Digesting Bacteria 29
2.1.3. Cellulase Enzyme Activity Analysis with Congo Red Assay 29
2.2. DNS ENZYME ACTIVITY ASSAY 30
2.2.1. Partial Isolation of Cellulase Enzyme 30
2.2.2. Preparation of DNS Solvent 31
2.2.4. gDNA Isolation from the Newly Isolated Bacteria 31
2.2.5. Sequencing 16S rRNA for Species Identification 32
2.2.6. Scanning Electron Microscopy for Bacteria 32
2.3. GROWTH AND ENZYMATIC ANALYSIS OF THE *RUMINOCOCCUS FLAVEFACIENS* BACTERIA 33
2.3.1. Preparing An Anaerobic Growth Media 33
2.3.2. Growth of *Ruminococcus Flavefaciens* Bacteria 33
2.3.3. Cellulase Enzyme Activity Analysis with Congo Red Assay 33
2.4. CELLULASE ENZYME ACTIVITY ANALYSIS AT DIFFERENT PH LEVELS WITH DNS ENZYME ACTIVITY ASSAY 34
2.4.1. Partial Isolation of Cellulase Enzyme 34
2.5. PRODUCTION AND CHARACTERIZATION OF DOXORUBICIN ENTEGRETED SPHERICAL CELLULOSE NANOPARTICLES 35
2.5.1. Preparation of Doxorubicin 35
2.5.2. Cellulose Nanoparticle Production with Ionic Solvent 35
2.5.3. Cellulose Nanoparticle Production with Alkali Mixture 36
2.5.4. Nanoparticle Production with Thiourea & Urea 37
2.5.5. Characterization of Cellulose Nanoparticles with TEM 37
2.5.6. Characterization of Cellulose Nanoparticles with DLS/Zeta Sizer 37
2.5.7. Characterization of Cellulose Nanoparticles with FT-IR 37
2.6. BACTERIAL CAPACITY FOR CNP DEGRADATION AND DRUG RELEASE 38
2.6.1. Use of Cellulose Nanoparticles as a Carbon Source in Bacterial Culture 38

2.6.2. Investigation of Doxorubicin Release 38
2.6.3. Release Test and Washing Method for Cellulose Nanoparticles 38
2.7. *IN VITRO* TRIALS ON LNCaP, CaCo-2, and PNT1A CELL LINES 39
2.7.1. Cell Lines 39
2.7.2. Cell Culturing, Counting, and Seeding 39
2.7.3. Viability Test with Crystal Violet 41
2.7.4. WST-8/CCK8 Viability Test 42
2.7.5. IC50 Calculation For LNCaP, CaCo-2, and PNT1A Cell Lines 42
2.7.6. Conducting a Preliminary Study to Determine the Values at Which Enzyme and CNPs Can Be Applied Before the Experimental Treatment Method 43
2.7.7. Exposure of Bacteria-Treated Cell Lines to Empty and Doxorubicin-Containing Cellulose Nanoparticles 43
2.7.8. Cellular Uptake Assays 43
3. RESULTS 44
3.1. ISOLATION & IDENTIFICATION OF CELLULOSE DIGESTIVE BACTERIA 44
3.1.2. DNS Enzyme Activity Assay 45
3.1.3. Phylogenetic Analysis with MEGA Software 46
3.1.4. Analysis of *ROBY* Strain on SEM 46
3.2. CELLULOLYTIC ACTIVITY OF ANAEROBIC *RUMINOCOCCUS FLAVEFACIENS* BACTERIA 47
3.2.1. Congo Red Assay 47
3.2.2. DNS Enzyme Activity Assay 48
3.3. CELLULOSE NANOPARTICLES 48
3.3.1. Preparation of the Doxorubicin (Dox) 48
3.3.2. Production of CNP by EMIMAc Method 49
3.3.3. Production of CNP by Alkali Solvent Mixture 51
3.3.4. Production of Cellulose Nanoparticles with Urea/Thiourea 53
3.3.5. Comparison of CNP Production Methods 54
3.4. BACTERIAL CAPACITY TO DEGRADE CNP AND DRUG RELEASE 55
3.5. CELL CULTURE 57
4. DISCUSSION 64
5. REFERENCES: 74

6. SUPPLEMENTARY DATA 84
PUBLICATIONS DERIVED FROM THESIS 90

LIST OF SYMBOLS

°C: Degree Celsius

μ: Micro

LIST OF ABBREVIATIONS

ADT	Androgen deprivation therapies
AICR	American Institute for Cancer Research
ALT	Alanine aminotransferase
AMIMCI	1-allyl-3-methylimidazolium chloride
AR	Androgen receptor
ARSi	AR signal transducers
AST	Aspartate transaminase
ATP	Adenosine triphosphate
BC	Bacterial cellulose
BMIMCI	1-butyl-3-methylimidazolium chloride
BH	Bushnell Haas
BHM	Bushnell Haas Medium
BNC	Bacterial nanocellulose
BPH	Benign prostatic hyperplasia
CFU	Colony-forming unit
CIMP	Cpg island methylator phenotype
CIN	Chromosomal instability
CMC	Carboxymethyl cellulose
CNC	Cellulose nanocrystal

CNF	Cellulose nanofiber
CNP	Cellulose nanoparticle
CR	Congo Red
CRPC	Castration-resistant prostate cancer
DAPI	4',6-diamidino-2-phenylindole
DBD	DNA-binding domain
DHT	Dihydrotestosterone
DLS	Dynamic light scattering
DMEM	Dulbecco's Modified Eagle Medium
dMMR	DNA mismatch repair
DMSO	Dimethyl sulfoxide
DNA	Deoxyribonucleic acid
DNS	Dinitro salicylic acid
Dox	Doxorubicin
DOX-CNP	Doxorubicin-loaded cellulose nanoparticle
EBV	Epstein-Barr virüs
EGFR	Epidermal growth factor
EMIMAc	1-Ethyl-3-methylimidazolium acetate
EPR	Enhanced permeability and retention
FBS	Fetal bovine serum
FT-IR	Fourier-transform infrared spectroscopy
gDNA	Genomic DNA
HBV	Hepatitis B virus
HCV	Hepatitis C virus
HHV-8	Human herpes virus 8

HIV	Human immunodeficiency virus
HPV	Human papillomavirus
HTLV	Human T-cell lymphotropic virus
IARC	International Agency for Research on Cancer
ILs	Ionic liquids
LBD	Ligand binding domain
MCC	Microcrystalline cellulose
MEGA	Molecular Evolutionary Genetics Analysis Software
mPTP	Mitochondrial permeability transition pore
mRNA	Messenger RNA
MSI	Microsatellite instability
NOX	NAPD oxidases
NTD	N-terminal transactivation domain
PBS	Phosphate buffered saline
PTS	Phosphotransferase system
RFA	Radiofrequency ablation
ROS	Reactive oxygen species
RPMI	Roswell Park Memorial Institute
rRNA	Ribosomal ribonucleic acid
SEM	Scanning electron microscope
TEM	Transmission electron microscope
TME	Tumor microenvironment
TSL	Temperature-sensitive liposomes
UV	Ultraviolet
VFA	Volatile fatty acids

WCRF	World Cancer Research Fund
YE	Yeast Extract

LIST OF FIGURES

Figure S1. A standard curve that refers to A540 results according to different glucose concentrations.

Figure S2. Doxorubicin standard curve

Figure 1. The general chemistry of cellulose is schematized with covalent linkages between glucose monomers via β-1,4-glycosidic bonds (Awais et al. 2021)

Figure 2. Basic scheme of amorphous and crystalline forms in the structure of cellulose. While amorphous structure has higher hydrophilicity, reactivity, and enzymatic digestibility, the crystalline form has less due to the non-covalent interactions (Quiroz Castañeda and Folch-Mallol 2013).

Figure 3. An example of a visual indicator for food freshness is indicated by pH changes (Moradi et al. 2019).

Figure 4. Enzymatic action of cellulase (Mathew et al. 2008).

Figure 5. Global burden of diseases that cause death in the world in 2021.

Figure 6. Hallmarks of Cancer (Hanahan 2022).

Figure 7. Prostate cancer physiology (Illustrated with BioRender.com).

Figure 8. Illustration of mRNA and protein sequences of the androgen receptor (AR) (Fujita and Nonomura 2019).

Figure 9. Representation of molecular pathways of androgen-positive and androgen-negative prostate cancer (Formaggio, Rubin, and Theurillat 2021).

Figure 10. Chemical structure of the Doxorubicin chemotherapy drug (Carvalho et al. 2009).

Figure 11. Schematic summary of injuries caused by Doxorubicin chemotherapy, including cognitive, circulatory, digestive, and urinary system injuries induced by the drug.

Figure 12. The molecular mechanisms of the Doxorubicin drug (Varela-López et al. 2019).

Figure 13. The EPR effect and the passive targeting model of nanoparticles in TME (Illustrated with BioRender.com).

Figure 14. Thermodox treatment combines temperature-sensitive liposomal nanoparticles with radiofrequency ablation to generate a targeted drug release method in TME based on hyperthermia(Regenold et al. 2022).

Figure 15. Congo red assay result of isolated cellulolytic bacteria from the rumen liquid. Zones around colonies result from the breaking of β-glycosidic linkages in the chemical structure of cellulose by the secreted cellulase enzyme from the isolated cellulolytic bacteria.

Figure 16. Relative enzyme activity analysis for the partially isolated cellulase enzyme from *A. pittii* was analyzed concerning different pH levels via the DNS enzyme activity assay.

Figure 17. The phylogenetic tree of the isolated cellulolytic bacteria, *Acinetobacter pittii ROBY* strain (Figure was illustrated with MEGA-Molecular Evolutionary Genetics Analysis Software).

Figure 18. Scanning electron microscope view of the *Acinetobacter pittii* ROBY Strain.

Figure 19. Congo red assay results of *Ruminococcus flavefaciens* Sijpesteijn 1948 strain visualized with zones around colonies, which represent secretion of cellulase enzyme and existence of cellulolytic activity.

Figure 20. Relative enzyme activity analysis for partially isolated cellulase enzyme from *R. flavefaciens* was analyzed with respect to different pH levels via the DNS enzyme activity assay.

Figure 21. Absorbance value changes of the Doxorubicin drug under conditions of exposure to different temperatures.

Figure 22. TEM views of (A) free cellulose nanoparticles (CNPs) and (B) Doxorubicin integrated cellulose nanoparticles (Dox-CNP) produced by EMIMAc.

Figure 23. DLS/ZetaSizer results of (A) Dox-CNP and (B) CNP, and Zeta potential results of (C) Dox-CNP and (D) CNP produced with EMIMAc.

Figure 24. FT-IR spectroscopy results of (A) CNP and (B) Dox-CNP.

Figure 25. TEM views of (A) CNP and (B) Dox-CNP produced with the Alkali solvent system (NaOH, Thiourea, and Urea). The average CNP size is calculated as 280 nm.

Figure 26. DLS/ZetaSizer results of (A) Dox-CNP and (B) CNP, and Zeta potential results of (C) Dox-CNP and (D) CNP produced with Alkali solvent.

Figure 27. FT-IR results of (A) free Dox, (B) CNP, and (C) Dox-CNP.

Figure 28. TEM views of cellulose nanoparticles produced with thiourea and urea and stabilized with CMC.

Figure 29. Bacterial capacity for degradation of cellulose nanoparticles is examined in the presence of CNPs and Dox-CNPs with VCC (Viable cell counting assay) by calculating CFU (colony forming units) per mL over time.

Figure 30. Illustration of the percentage of drug release in the presence of partially isolated enzymes from *A. pittii* and *R. flavefaciens*, compared to the control group containing only Dox-CNP.

Figure 31. Illustration of the percentage of cumulative release of Dox from the nanoparticles at 37˚C.

Figure 32. IC50 values for all three cell lines were determined using the CCK-8 viability test in duplicate. This value was calculated as 0.07475 μM (R^2=0.9994) for the PNT1A cell line, 0.1784 μM (R^2=0.9996) for the CaCo-2 cell line, and 0.1226 μM (R^2=0.9945) for the LNCaP cell line.

Figure 33. Crystal violet viability assay results of enzymes isolated intracellularly and extracellularly from both *A. pittii* and *R. flavefaciens* bacteria species are illustrated.

Figure 34. Crystal violet viability assay results of CNP and Dox-CNP without CMC coating.

Figure 35. Crystal violet viability assay results of CNP and Dox-CNP with 0.5% CMC coating.

Figure 36. Crystal violet viability test results of treatment with TU (Thiourea & Urea) +Dox+heat+ultrasonication combination, Dox+heat+ultrasonication combination, and free Dox are illustrated. Therefore, chemicals, heat, or ultrasonication in the nanoparticle production process do not change the effectiveness of the drug.

Figure 37. Combinations of the intracellularly isolated cellase enzyme from *A. pittii* and cellulose nanoparticles were analyzed with the CCK-8 assay. CNP and enzyme (CE), Dox-CNP and enzyme (DCE), and Dox-CNP and enzyme combination that is incubated for 2 hours before treatment (DCE 2h) are analyzed on the LNCaP cell line.

Figure 38. DAPI staining and Dox drug uptake into the cell are analyzed with Fluorescent microscopy with four groups: Control, Free Dox, Dox-CNP, and enzyme (DCE).

LIST OF TABLES

Table S1. List of instruments that are utilized.

Table S2. List of chemicals that are utilized

Table 1. Biotechnological applications of cellulose-based materials and their corresponding cellulose types.

Table 2. Cell culture planning conditions

Table 3. Comparison of cellulose nanoparticles produced with EMIMAc ve Alkali solvents

ABSTRACT

Generating A Novel Targeted Cancer Therapy By Using A Combination Of Cellulose Nanoparticles With Cellulose-Digesting Anaerobic Bacteria In The Tumor Microenvironment

SARIBOĞA, Ruken

Master's Thesis, Molecular Biology and Genetics Department

Supervisor: Assist. Prof. Ömer Faruk SARIOĞLU

June 2025

Recently, cellulose has been widely used to produce sustainable and biodegradable products with low toxicity and less risk to human health. Cellulose is a good example that reaches these characteristics. In this project, we attempted to generate a targeted therapy by using a combination of cellulose nanoparticles loaded with Doxorubicin (Dox) chemotherapy drug and bacterial cellulase enzyme, which accomplishes an enzymatic breakdown of cellulose and releases the drug. By the way, the release of the drug was aimed to be carried out specifically at the tumor microenvironment. The main purpose ot this targeted therapy is to reduce the risks of the chemotherapy drug for damage to healthy tissues. The isolation of cellulose-digesting bacteria was conducted with a rumen sample, and samples were inoculated on a selective medium. Bacterial colonies obtained from samples cultured on a solid medium containing Bushnell-Haas (BH) and CMC were stained with Congo red, and cellulase enzyme secretion was examined. In addition, the enzyme activity of the partially isolated cellulase was analyzed with the DNS enzyme activity assay in acidic and basic conditions. To produce cellulose nanoparticles and integrate the drug Dox, three different nanoparticle synthesis methods were tested. In the first method, EMIMAc ionic liquid was used; however, due to the high toxicity and high cost of the resulting nanoparticles, alternative methods were explored. Subsequently, a mixture that contains NaOH, thiourea, and urea was utilized to produce nanoparticles with the dissolution of MCC. Nevertheless, issues such as salt precipitation and neutral zeta potential led to further refinement of the nanoparticle formulation. NaOH was removed from the formulation, and CMC was used as a coating agent to provide a negative surface charge. The finalized nanoparticle method was analyzed using TEM. To confirm that the

nanoparticle synthesis process did not affect the drug's efficacy, the chemicals, heat, and sonication steps used in the process were also applied in cellulose-free conditions, and viability did not significantly change. Furthermore, both drug-loaded and unloaded nanoparticles were tested without bacterial cellulase on LNCaP and PNT1A cell lines at concentrations ranging from 0.1 to 10 μM, and nearly 100% cell viability was observed for both samples. These results suggest that the produced cellulose nanoparticles are non-toxic to cells, even if they are loaded with Dox, and the integrated drug retains its therapeutic efficacy without releasing uncontrollably. During the study, direct application of the bacteria to the cells was also attempted, but high contamination levels significantly interfered with viability test results. For this reason, partially isolated enzymes were used instead; however, due to insufficient enzyme purity and not achieving optimal activation conditions, consistent results could not be achieved. When cell culture experiments with partially isolated enzymes were applied in 3 replicates, a decrease in enzyme activity was observed over time. For future studies, it is anticipated that obtaining cellulase enzymes with higher purity and optimal activation conditions will allow the successful drug release from cellulose nanoparticles.

Keywords: Cellulose Nanoparticles, Doxorubicin, Drug-Integration, Targeted cancer therapy

ÖZET

Tümör Mikroçevresindeki Selüloz Sindiren Anaerobik Bakterilerle Selüloz Nanopartiküllerinin Bir Kombinasyonunu Kullanarak Yeni Bir Hedefli Kanser Tedavisi Üretmek

SARIBOĞA, Ruken

Yüksek Lisans, Moleküler Biyoloji ve Genetik

Danışman: Dr. Öğr. Üyesi Ömer Faruk SARIOĞLU

Haziran 2025

Son yıllarda, sürdürülebilir ve biyolojik olarak parçalınabilir biyomalzemelere, ve bu malzemeler sayesinde daha düşük toksisiteye ve insan sağlığı için daha az riske sahip biyomalzemelere olan ilgi artmaktadır. Selüloz bu özellikleri karşılayabilen biyomalzemelere iyi bir örnektir. Bu projede, Doksorubisin kemoterapi ilacı ve selülozun enzimatik parçalanmasını gerçekleştiren ve ilacı serbest bırakan bakteriyel selülaz enzimi ile yüklenen selüloz nanopartiküllerinin bir kombinasyonunu kullanarak hedefli bir tedavi üretildi. Bu süreçte, ilacın salınımının özellikle tümör mikroçevresinde gözlemlenmesi ve bu hedefli tedavide kemoterapi ilacının sağlıklı dokudaki hasar riskini azaltması amaçlanmıştır. Öncelikle selüloz giderimi yapabilen bakteri izolasyonu rumen örneğinden alınarak gerçekleştirilmiştir. Bushnell Haas ve CMC içeren katı besiyerinde büyütülen örneklerden elde edilen bakteri kolonileri Kongo kırmızısı ile boyanmış ve selülaz enzim salınımı incelenmiştir. Ayrıca, DNS enzim akticvitesi testi kullanılarak farklı pH değerlerindeki kısmi olarak izole edilmiş olan selülaz enziminin aktivasyonu incelenmiştir. Selüloz nanoparçacıklarının üretimi ve Dox ilacının entegrasyonu için 3 farklı yöntem ile nanoparçacık üretimi denenmiştir. İlk yöntemde EMIMAc iyonik çözeltisi kullanılmıştır ancak oluşturulan nanoparçacıkların yoğun toksisitesi sebiyle farklı yöntemler araştırılmıştır. Daha sonra NaOH, tiyo üre ve üre kullanılarak birçözücü oluşturulmuş ve nanoparçacıklar yine aşarı ile üretilmiştir. Ancak oluşturulan nanoparçacıklarda tuz çökelmesi ve nötral zeta potansiyel gibi problemler nedeniyle nanoparçacık formülasyonu geliştirilmiştir. Bu amaçla, NaOH formülasyondan çıkarılmış ve negatif yük sağlamak amacıyla CMC kullanılarak nanoparçacık kaplaması yapılmıştır. Üretilmiş olan sselüloz nanoparçacıkları SEM, DLS/ZetaSizer ve FT-IR analizleri ile incelenmiştir. Hücre kültürü denemelerinde uygulanan nanoparçacık yönteminin ilacın

etkinliğinde bir farklılığa sebep olmadığını kanıtlamak için uygulanmış olan kimyasallar, ısı ve sonikasyon işlemleri selüloz olmayan koşullarda denenmiş ve canlılıkta bir değişim gözlemlenmemiştir. Ayrıca, 0,1-10 μM aralığında ilaçlı ve ilaçsız nanoparçacıklar LNCaP ve PNT1A hücre hatlarında bakteriyel selülaz enzim aktivitesinin olmadığı koşullarda incelenmiş ve iki farklı grup için de yaklaşık olarak %100'e yakın bir canlılık gözlemlenmiştir. Bu sonuçlar doğrultusunda üretilmiş olan selüloz nanoparçacıklarının Dox ile entegre edilmiş olsa dahi hücrede bir toksisiteye neden olmadığı ve nanoparçacık yapısına entegre edilmiş olan ilacın ise kontrolsüz bir salım gerçekleştirmediği ve etkinliğini kaybetmediği görülmüştür. Süreçte bakterinin doğrudan hücreler üzerinde kullanımı denenmiştir ancak yüksek kontaminasyon canlılık testi sonuçlarını anlmasız olacak şekilde etkilemiştirBu nedenle kısmi olarak izole edilen enzim kullanılmış ancak enzimin yeterli saflıkta olmaması ve enzim aktivasyonu için uygun koşulların sürekli olarak sağlanamamasından dolayı tüm denemelerde tutarlı sonuçlar elde edilememiştir. Kısmi olarak izole edilmiş olan enzim ile yapılan hücre kültürü denemeleri 3 tekrarlı olarak uygulandığı takdirde zamana bağlı olarak enzim aktivitesinde düşüş gözlemlenmiştir. İleriye dönük çalışmalarda daha yüksek safıktaki selülaz enzimi elde edilerek ve enzim aktivitesi daha iyi korunarak selüloz nanoparçacıklarından ilacın salınımının başarılı bir şekilde gerçekleştirilebileceği düşünülmektedir.

Anahtar Kelimeler: Selüloz Nanoparçacıkları, Doksorubisin, İlaç entegrasyonu, Hedefe yönelik kanser tedavisi,

1. INTRODUCTION

1.1. CELLULOSE

Cellulose is a natural material with a broad distribution in the biosphere, which is mainly synthesized in wood and plants. (Seddiqi et al. 2021; Orlando J. 2016). Cellulose constitutes nearly 50% of the dry biomass derived from plants and a large fraction of secondary biomass sources such as agricultural, industrial, and municipal wastes. Beyond that, this polymer hardly degrades in nature and causes environmental pollution (S. et al. 2002). Cellulose has a homo-biopolymer structure that includes linearized glucose monomers that are connected by covalent bonds called β-1,4 glycosidic bonds, which creates cellulose chains (Béguin & Aubert, 1994; Seddiqi et al., 2021). The discovery of the fibrous structure of this biomaterial was made by Anselme Payen in 1838, with chemical treatments of plant tissues, and he reported the molecular formula of cellulose as $C_6H_{10}O_5$ (Liu et al. 2021).

Cotton is the main component that is used in the clothing industry as a natural fibre, and the primary constituent of cotton is cellulose (95-99%). The production of textiles and garments generates significant quantities of cotton waste, which creates environmental pollution (Gülsu and Yüksektepe 2021). Nowadays, researchers are widely studying natural polymer-based technologies by using cellulose wastes, which supports the reduction of environmental pollution caused by cellulose (Sariboga and Sarioglu 2024a). Moreover, cellulose is an extremely abundant, renewable, sustainable, and biodegradable biomaterial, and applications with cellulose give properties like low toxicity, biocompatibility, hydrophilicity, and biodegradability (Manoukian et al. 2019; Morais and Curto 2022).

1.1.1. Cellulose: Structural Features and Dissolution

Cellulose, the major carbohydrate in plants, and formed by the linearized form of a homopolysaccharide that contains D-glucose monomers that are covalently linked via β-1,4-glycosidic linkages (Collard and Blin 2014) (Figure 1). Typically, cellulose is found in either crystalline or amorphous forms, with the crystalline form being predominant (Collard and Blin 2014).

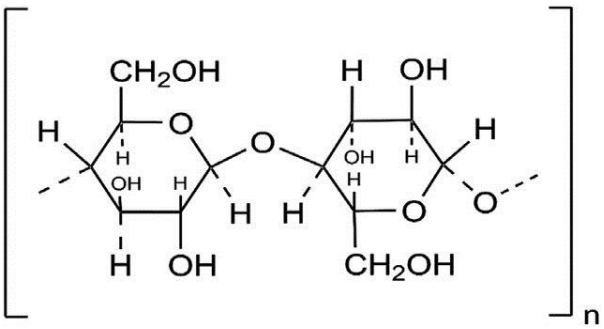

Figure 1. The general chemistry of cellulose is schematized with covalent linkages between glucose monomers via β-1,4-glycosidic bonds (Awais et al. 2021)

The amorphous structure of cellulose is mainly found at the microfibril surface, while the crystalline form is observed at the core of microfibrils (Bayer et al. 1998). In the amorphous form, hydrophilicity, reactivity, and enzymatic digestibility of the cellulose increase (Ioelovich 2021), while the crystalline form contains extensive non-covalent linkages such as hydrogen bonds and Van der Waals forces that cause non-degradable characteristics to cellulose (Figure 2) (Quiroz Castañeda and Folch-Mallol 2013).

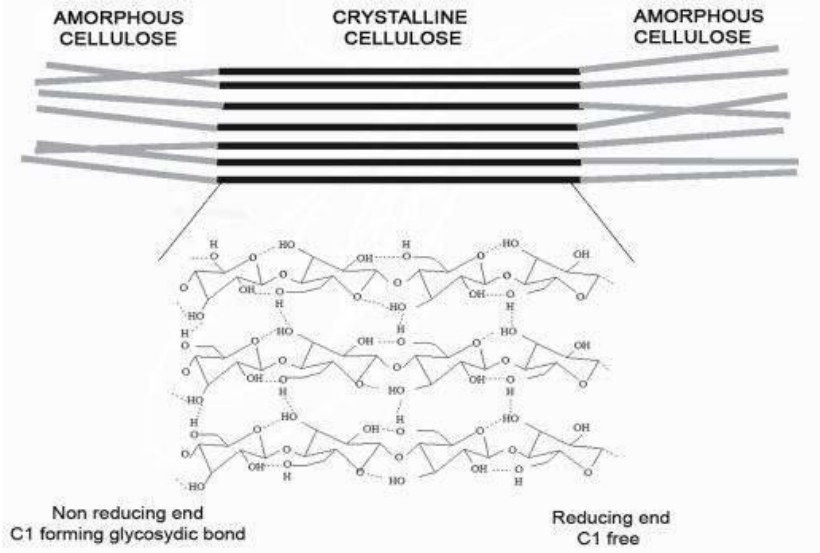

Figure 2. Basic scheme of amorphous and crystalline forms in cellulose. While amorphous structure has higher hydrophilicity, reactivity, and enzymatic digestibility, the crystalline form has less due to its non-covalent interactions (Quiroz Castañeda and Folch-Mallol 2013).

Cellulose is a hardly dissolving biomaterial that requires chemical, enzymatic, or microbial additives to be processed into its derivatives (Al Hakkak et al. 2019; Cao and Tan 2002; Jin, Zha, and Gu 2007; Zhu et al. 2006).

For chemical decomposition of cellulose, mostly ionic liquids (ILs) are used, such as BMIMCI, AMIMCI, or EMIMAc, etc. The crystalline cellulose structure features a high density of non-covalent linkages, which makes it hardly degradable, and ionic liquids for cellulose degradation are effective for the cleavage of hydrogen bonds between cellulose chains and separating cellulose into its derivatives (Zhu et al. 2006). ILs are mostly classified as 'Green' chemicals and eco-friendly compared to the conventional methods; however, the high costs of ILs limit large-scale investigations (Zhu et al. 2006; Shamsuri 2011).

Otherwise, several chemical solvent systems can dissolve the crystalline structure of the cellulose. Acidic (H_2SO_4 and HCl), alkali (NaOH, KOH, $Ca(OH)_2$, and NH_3), or organic compounds (Glycerol, ethylene glycol, or tetrahydrofurfuryl alcohol) are effective for cellulose dissolution (Ghasemi, Tsianou, and Alexandridis 2017). Similar to the ionic solvents, the chemical solvent must disrupt the strong intermolecular interactions in the crystalline regions of the cellulose (Ghasemi, Tsianou, and

Alexandridis 2017). Also, cellulose can be degraded with some combinations of solvent systems, such as combinations of NaOH, thiourea, and urea (Jin, Zha, and Gu 2007).

Biological dissolution of cellulose was thought to be done by the enzymatic degradation of microorganisms. Besides microorganisms, some other organisms can degrade cellulose enzymatically, such as some insects, mollusks, nematodes, and protozoa. Biological dissolution is provided by the cellulase enzyme, and it was believed to be carried out exclusively by microorganisms. However, some other organisms, such as certain insects, mollusks, nematodes, and protozoa, can also secrete cellulase enzymes and support cellulose degradation (Wilson 2011). Besides, cellulose is primarily used as an energy source by ruminants, shipworms, and termites. (Wilson 2011).

1.2. CELLULOSE BIOMATERIALS

Cellulose-based biomaterials are widely studied and applied across a broad range of fields owing to the abundance and chemical stability of cellulose. Innovations in nanotechnology have significantly expanded this field of study, and in recent years, cellulose-derived nanomaterials have attracted increasing attention (Sariboga and Sarioglu 2024a).

There are several different forms of cellulose structure marketed worldwide for biotechnological uses. Microcrystalline cellulose (MCC), carboxymethyl cellulose (CMC), Bacterial nanocellulose (BNC), nanofibrillated cellulose (CNF), microfibrillated cellulose (MFC), and cellulose nanocrystals (CNCs) are majorly utilized and marketed (Sariboga and Sarioglu 2024a).

Table 1. Biotechnological applications of cellulose-based materials and their corresponding cellulose types.

Biotechnological use	***Cellulose Types***	***Reference***
Antimicrobial material design	*CNC, BNC*	*(Juanjuan Li et al. 2018; Kaplan et al. 2014)*
Food Packaging	*CNC, CNF, MCC*	*(Moradi et al. 2019)*
Tissue engineering	*BNC, CNF*	(Hickey and Pelling 2019)
Drug Delivery and Targeting	*CNC, MCC, CMC, BNC*	(Ciolacu, Nicu, and Ciolacu 2020; Gülsu and Yüksektepe 2021)

Cellulose-based biomaterials are utilized in food packaging and preservation, wastewater treatments, antimicrobial material design, drug delivery and targeting, wound healing and skin applications, 3D bioprinting, tissue engineering, and so on (Sariboga and Sarioglu 2024a; Moradi et al. 2019; Ciolacu, Nicu, and Ciolacu 2020; Zhang et al. 2025; Hickey and Pelling 2019; Kaplan et al. 2014). Those examples are classified in Table 1.

1.2.1. Antimicrobial Material Design

Antimicrobial material design in biotechnology majorly targets slowing down or stopping microbial growth. After innovations in microbiology and the discovery of the first antibiotic, penicillin, several number of antibiotics were developed and overused. Overuse of antibiotics has resulted in antimicrobial resistance, which is now a global health issue (Juanjuan Li et al. 2018; Morrison and Zembower 2020). Consequently, the use of biotechnological innovation to build antimicrobial material designs gained great interest. In this field, due to their beneficial physical, chemical, and biological features, cellulose-based nanomaterials have received widespread attention (Sariboga and Sarioglu 2024a).

Antimicrobial material design can be generated with multiple methods, such as surface modifications like oxidation and esterification, and by combining nanocellulose with

antibiotics, metallic nanoparticles, polymers, or enzymes (Juanjuan Li et al. 2018; Kaplan et al. 2014).

1.2.2. Food Packaging

Appropriate packaging mechanisms in the food industry are fundamentally important in maintaining the freshness, safety, and quality of the food. Unfortunately, most of the commonly used packaging mechanisms include non-degradable material and cause pollution. Cellulose-based nanomaterials such as CNCs, CNFs, and BNCs are widely studied as an eco-friendly alternative packaging method.

Cellulose nanomaterials are also combined with various biodegradable polymers such as Polylactic acid (PLA), which results in enhanced mechanical durability and thermal resistance. In addition to structural improvements, a novel smart packaging system was developed (Figure 3). The packaging system was combined with a natural pigment, anthocyanins, which serve as visual indicators of food freshness by responding to pH changes. The usage of cellulose-based biodegradable biomaterials in packaging instead of petroleum-based plastic offers a sustainable alternative that minimizes environmental impact, supports circular economy practices, and addresses the growing concerns over plastic pollution (Moradi et al. 2019; Sariboga and Sarioglu 2024a).

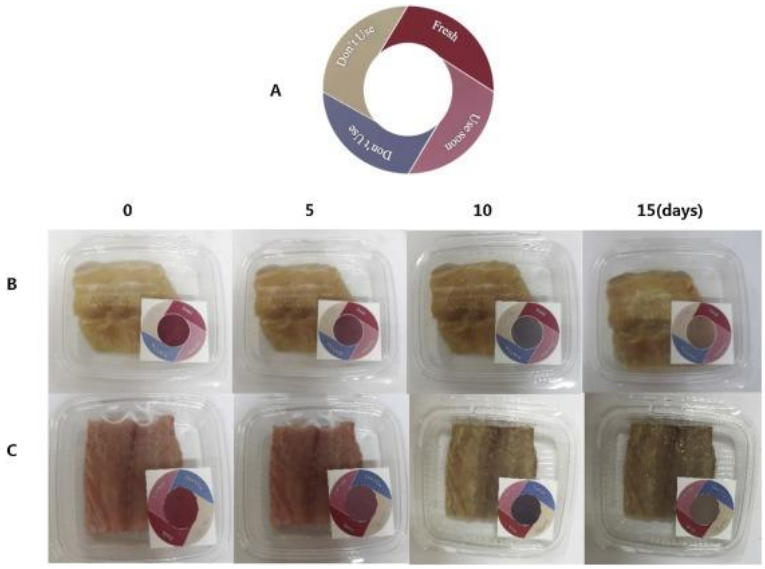

Figure 3. An example of a visual indicator for food freshness is indicated by pH changes (Moradi et al. 2019).

1.2.3. Tissue Engineering

In addition to being sustainable resources obtained from nature, cellulose-based biomaterials are prominent in tissue engineering with their features including biocompatibility, biodegradability, mechanical strength, and surface functionalization. These biopolymers contribute to the regeneration of various tissue types by providing an ideal environment for cell attachment, growth, and differentiation (Hickey and Pelling 2019).

In studies on different biological systems such as skin, bone, nerve, and vascular tissue, micro- and nanostructured forms of cellulose (e.g., nanofibril and nanocrystal structures) are widely investigated as scaffolding materials. These structures offer a convenient platform for supporting and guiding cells thanks to their physicochemical characteristics. Additionally, biological molecules are easily immobilized with modifications made on the surface of cellulose, and thus, cell behaviors can be shaped in a more controlled manner (Hickey and Pelling 2019).

The adjustable porosity levels of cellulose-based structures also facilitate the passage of oxygen and nutrients, which are critical for cell viability, thus supporting regenerative processes. These materials, which have both structural and biological

similarities to natural tissues, offer significant advantages over traditional synthetic materials in their of environmental sustainability (Hickey and Pelling 2019).

1.2.4. Drug Delivery and Targeting

Cellulose-based nanomaterials currently offer significant potential in drug delivery applications with different forms (e.g., nanoparticles, micelles, films, or sheets) as drug carrier systems, controlled release vehicles, and co-stabilizers. It has been reported that both hydrophilic and hydrophobic drugs can be transported by these systems using diverse routes such as oral, topical, or transdermal administration (Sariboga and Sarioglu 2024a).

Although the use of cellulose derivatives in the pharmaceutical industry is quite old, the development of cellulose-based nanocarrier systems is a relatively new approach. For example, while CNC (cellulose nanocrystals) can bind directly with some antibiotics (such as doxorubicin, tetracycline), when their surfaces are modified with CTAB, they can bind more effectively with hydrophobic chemotherapy agents (such as docetaxel, etoposide, and paclitaxel). Drug release rates of these systems vary depending on the type of modification, and controlled release can be achieved (Letchford et al. 2011).

In some studies, pH-sensitive release systems were developed, and high encapsulation efficiency and stable drug release were achieved thanks to the combination of CNC and sodium alginate microspheres. In addition, drug nanoparticles coated with CNF (cellulose nanofibrils) can remain stable for approximately one year, extending the shelf life of the formulation (Mohd Amin et al. 2012).

Bacterial cellulose (BC)-based membrane structures were also evaluated for oral drug delivery, and it was shown that these structures offer extended release properties. Again, in some systems, protein films placed on nanocellulose ensured direct binding of hydrophobic drugs to the surface, increasing the stability of drugs under physiological conditions. However, some disadvantages, such as interactions of natural nanocellulose with drugs and surface charges that may negatively affect pharmacological activity, have also been reported. For example, it was determined that

anionic CNF oxidized with TEMPO exhibited degradative effects on aspirin and accelerated drug degradation (Sariboga and Sarioglu 2024a).

In recent years, focus has been particularly on doxorubicin-loaded cellulose nanoparticles, and it has been observed that these structures provide both cellular uptake via endocytosis and a long-term release profile. For example, in one study, it was reported that these systems could achieve up to 97% drug release for 34 days and were effective on the A549 lung cancer cell line (Gülsu and Yüksektepe 2021).

These studies reveal that cellulose-based nanomaterials can be transformed into versatile and functional structures in drug delivery systems, and at the same time offer biocompatible and sustainable solutions.

1.3. RUMINANT MICROORGANISMS AND CELLULASE

Ruminant animals utilize cellulose as an energy source by generating a symbiotic relationship with ruminal microorganisms. Rumen is a rich environment that contains several bacterial species and provides an anaerobic environment. After improvements in anaerobic bacteria culturing methods, strictly anaerobic bacteria species from the rumen were analyzed and characterized by Robert Hungate (1950). He isolated key cellulolytic bacterial species and assigned them to *Bacteroides succinogenes*, *Ruminococcus albus*, and *Ruminococcus flavefaciens* (Russell, Muck, and Weimer 2009; Hungate 1950). Further, there are some other isolated bacterial species in the rumen; however, those three species are more common and important in the rumen microenvironment.

1.3.1. Endogenous Metabolism of Ruminant Bacteria

Majorly, bacteria from both gram classifications have the phosphotransferase system (PTS), which is the main sugar transport system that is important for the entry of carbohydrates (Plumbridge 2002). Bacteria with the PTS store phosphoenolpyruvate (PEP), and this system provides an energy source during starvation. However,

endogenous metabolism in cellulolytic ruminal bacteria is quite different; they do not have a PTS system. Instead, they use stored glycogen to stay alive during starvation. The endogenous metabolism uses 10 times less energy than normal maintenance, and this mechanism helps ruminant microorganisms to be more resilient and starvation resistant (Russell et al., 2009).

1.3.2. Microbial Turnover Through Lysis and Predation in the Rumen

For the growth and survival of ruminant cellulolytic bacteria, ammonia is the major nitrogen source, and they cannot efficiently absorb amino nitrogen. The nitrogen availability plays an essential role in the microbial dynamics within the rumen, which influences both bacterial lysis and protozoal predation. Limitations in nitrogen source cause autolysis due to failure to deactivate autolysins, and this self-degradation contributes to microbial turnover. Additionally, protozoal predation of bacteria is a significant pathway for microbial nitrogen cycling, even though protozoa themselves are prone to lysis. Eventually, both bacterial and protozoal lysis, as well as predation, are interconnected processes that facilitate nitrogen recycling within the rumen ecosystem (Russell, Muck, and Weimer 2009).

1.3.3. Microbial Rumen Fermentation

Fermentation occurs in the reticulo-rumen (Owens and Basalan 2016). Rumen itself has an acidic pH that ranges between 6.6 to 5.3, and during extensive fermentation, the pH level can even decrease to 5.0 (Kitkas et al. 2022). The ruminal fermentation mechanism allows for efficient absorption of acidic end-products such as volatile fatty acids (VFA) and nutrients produced by microorganisms, such as protein, vitamins, and minerals. Ruminal fermentation has a continuous and dynamic structure; the produced acids are taken up across the rumen wall and removed from the environment. This prevents the fermentation from stopping and ensures the continuity of the process. Rumen fermentation is different from the pauses due to acid accumulation seen in closed systems (e.g., silage production). Owing to this mechanism, ruminants can efficiently digest fibrous nutrients and use the metabolites produced by microorganisms by converting them into energy with minimal loss. This makes rumen

fermentation a very advantageous system in terms of both energy efficiency and nutrient conversion (Owens and Basalan 2016).

1.3.4. Cellulase

Ruminant bacterial species predominantly produce and secrete cellulase enzymes in the rumen, which play an essential role in the disruption of β-1,4-glycosidic bonds within the cellulose. Cellulase is an essential enzyme for the degradation of cellulose, located within the plant cell walls, and ingested by animals (Cao and Tan 2002; Yoon et al. 2014). Cellulase has a multi-enzyme system necessary for complete hydrolysis of the cellulose. The main enzymes involved are: β-1,4-endoglucanase, commonly called cellulase, which hydrolyzes β-1,4-D-glycosidic bonds; cellobiohydrolase (exoglucanase), which breaks these bonds from the non-reducing ends and releases cellobiose; and β-glucosidase (cellobiase), which decomposes cellobiose to release glucose (Figure 4). Cellobiase plays a crucial role in cellulose hydrolysis, as it inhibits both endo- and exo-glucanases (Fernandes 2018). In the food industry, cellulase enzyme is commonly used due to its improvements in the maceration process of wine and fruit juice production, aiding in the extraction of pigments, flavors, and fermentable sugars. On the other hand, cellulase is used in baking, which helps to break down gums in the dough, ensuring a more even rise, better flavor distribution, and improved dough texture (Fernandes 2018).

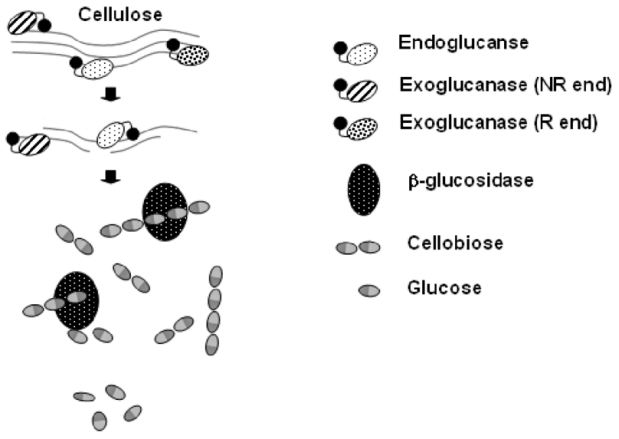

Figure 4. Enzymatic action of cellulase (Mathew et al. 2008).

1.4. CANCER

Even though there are broadly developed cancer therapies, cancer is still a significant health concern worldwide (Kiri and Ryba 2024). According to the Global Burden of Disease database, cancer represents the second primary cause of mortality, responsible for 14.6% of all fatalities. (Figure 5) (Kiri and Ryba 2024). Some cancer types can be caused by inherited factors, but mainly, they arise from environmental exposures (Blackadar 2016). This exposure may include some virus types such as HTLV, HIV, HBV, HCV, HPV, EBV, and HHV-8 are reported by IARC (International Agency for Research on Cancer), and there are also other factors reported by IARC such as UV light, smooking, pharmaceuticals, hormonal changes/treatments, alcohol consumption, parasitic organisms, fungal agents, bacterial species, preserved fish, wood dust exposure, and herbs. Otherwise, beta carotene intake, consumption of red and processed meats, insufficient dietary fiber, lack of breastfeeding, obesity, increased adult height, and inactivity were reported by the WCRF and AICR (Blackadar 2016).

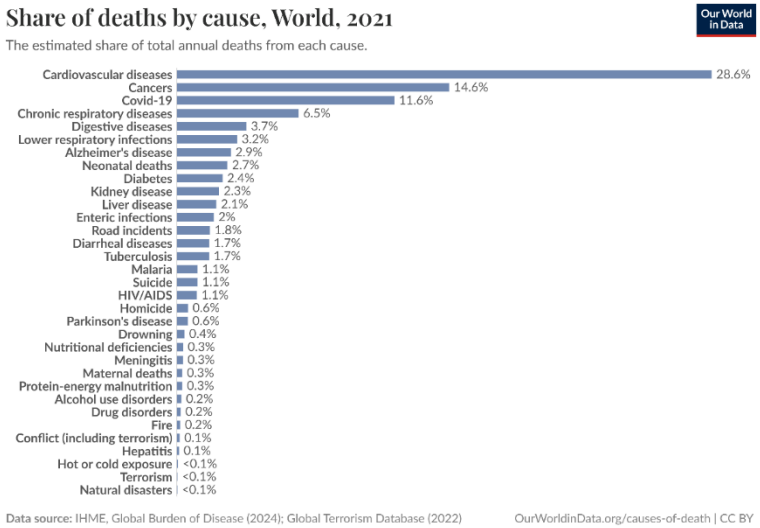

Figure 5. Global burden of diseases that cause death in the world in 2021 (Data source: IHME, Global Burden of Disease, 2024).

1.4.1. Hallmarks of Cancer

The functional features acquired by cancer cells during the process of differentiating from normal cells and transforming into malignant tumors have been defined as "Hallmarks of Cancer" (Figure 6). This concept was first put forward by Douglas Hanahan and Robert Weinberg and developed to describe the common biological abilities acquired by cells during the development of cancer. This approach provides a framework that helps understand the common phenotypic features of different tumor types.

In the beginning, they identified the six basic features: continuous production of division signals, escape from growth suppressors, resistance to cell death, unlimited proliferation capacity, angiogenesis (vessel formation), and invasion/metastasis ability (Hanahan and Weinberg 2000). Later, two more important features, such as escape from the immune system and reprogramming of cellular metabolism, were added to this list, and a total of eight basic features were identified. These features are thought to correspond to multi-step cancer formation processes (Hanahan 2022).

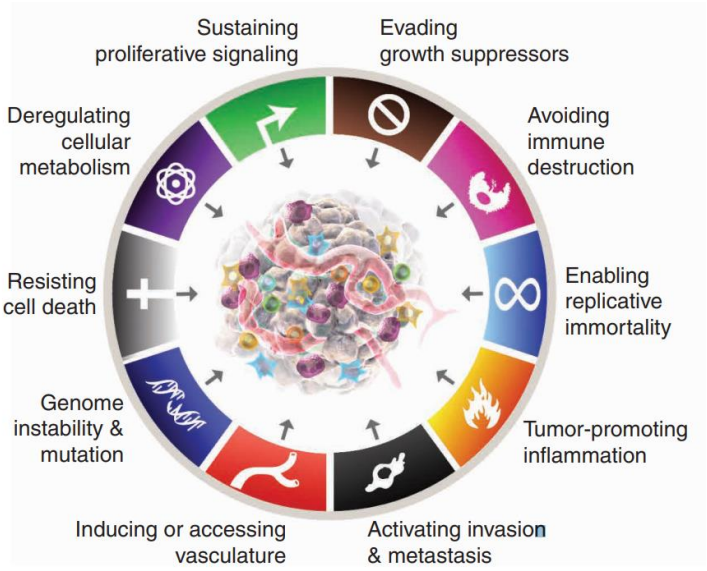

Figure 6. Hallmarks of Cancer (Hanahan 2022)

However, some enabling characteristics that facilitate the development of these features have also been identified. These are the mechanisms that enable cells to

acquire these basic features, such as genetic instability and tumor-supporting inflammation. In addition, the tumor microenvironment (TME), which surrounds tumor cells, also remarkably contributes to promoting tumor growth and progression. The TME is an interactive structure that contains cancer cells, cancer stem cells, and various stromal cell types (Hanahan 2022).

Recently, it has been suggested that some new titles should be added to this concept. New elements such as "revealing of phenotypic plasticity," "epigenetic reprogramming," "microbiota diversity," and "senescence (aged) cells" have the potential to be among the fundamental characteristics of cancer in the future. These elements are supported by current research that reveals how cancer cells adapt to environmental stimuli and how effective they can be in tumor development (Hanahan 2022).

1.4.2. Molecular and Cellular Mechanisms of Cancer

Although cancer is one of the most researched disease groups today, its cellular and molecular-level pathological mechanisms involved have yet to be fully elucidated. The numerous clinical appearances of different tumor types have raised the question of whether cancer can be considered a single disease. In this context, determining the common biological characteristics defining cancer has become important (Weber 2007).

The main factor in the formation of cancer is the dysfunction of oncogenes and tumor suppressor genes that control growth; however, uncontrolled cell division is not enough to define cancer. The senescence mechanisms that normally limit cells are disabled in cancer cells by means such as the enhancement of telomerase function. In addition, malignant cells can spread to different organs by expressing special genes that provide invasion and metastasis capabilities (Weber 2007). p53 gene is a well-known tumor suppressor gene that is responsible for both stopping the cell cycle and suppressing senescence (Demidenko et al. 2010).

Mainly, three genetic mechanisms cause activation of oncogenes, which are: mutations, gene amplifications, and chromosomal rearrangements (Pierotti and Della Porta 2022). Disorders in DNA repair and epigenetic control systems also pave the

way for the formation of permanent mutations in cells. This second line of defense is a key factor influencing cancer risk. The activation of oncogenes and metastasis genes together in precursor cells with low cellular differentiation levels can facilitate cancer development (Weber 2007).

Cancer does not only result from intracellular deterioration; the tumor microenvironment (such as host tissue, vascular system, immune and hormonal factors) is also a determinant in the progression of the disease. These environmental factors directly affect the growth, spread, and clinical symptoms of the tumor. While some genes are involved in tasks such as binding and migration of immune cells, they can assume different roles in different contexts.

Metastasis is defined as the development of secondary tumors in an organ distant from the site of the primary tumor. Metastasis is the main reason for the deaths related to cancer. Every day, high amounts of tumor cells are released into the blood circulation of cancer patients; however, *in vivo* studies indicate that only <0.1% of those tumor cells metastasize. For activation of metastasis, tumor cells must leave the primary site, survive in the bloodstream, resist intravascular pressure, adapt to the destinated microenvironment, and resist immune system assault (Fares et al. 2020). As defined by Hanahan and Weinberg, 'Activating invasion and metastasis' is a key characteristic of cancer (Hanahan and Weinberg 2000), and causes >90% of the related deaths (Fares et al. 2020).

Studies conducted within this framework explain the molecular mechanisms required for the emergence of invasive tumors under many headings, from cell cycle to DNA repair, from epigenetic regulation to immune response. These aspects of cancer biology shape not only treatment but also early diagnosis and prevention strategies (Weber 2007).

1.4.3. Types of Cancer

According to the NCBI Database, there are over 100 different types of cancer in the world. The most frequent cancer types among humans can be listed as: lung, breast, prostate, colorectal, gastric, and hepatic cancers, and so on (Mattiuzzi and Lippi 2019). There are numerous treatment methods developed for cancer in both traditional and

modern fields. Traditional treatments are mainly classified as surgery, radiotherapy, and chemotherapy (Abbas and Rehman 2018) While modern fields include stem cell-based therapy, gene editing therapy, nanoparticle therapies, therapies derived from natural products, and exosome therapies (Kaur, Bhardwaj, and Gupta 2023).

1.4.3.1. Prostate Cancer

The most common non-skin cancer in men around the world is prostate cancer, which is a heterogeneous disease that can grow slowly and be harmless, or it can be a fatal condition (Hall et al. 2024; G. Wang et al. 2018). Prostate diseases are mainly diagnosed in old men that including benign prostatic hyperplasia (BPH) and prostate cancer (Figure 7). BPH is characterized by an increased size of the prostate because of abnormal cell division in the transitional area surrounding the urinary tract. The incidence of this condition increases with age, occurring in 5–10% of men aged 40 and reaching 80% in the 70–80 age group. On the other hand, cancer-related mortality due to prostate cancer is the second highest in Western countries, and its incidence increases with age. Usually, prostate cancer is detected in men aged above 45; it is rare to occur at an earlier age (Cannarella et al. 2021).

Aging-related hormonal fluctuations are believed to play a role in the onset of prostatic diseases. Specifically, hormones such as sex steroids, insulin-like growth factor (IGF-1), thyroid hormones, cortisol, and insulin have been identified as influential factors affecting these conditions. Additionally, hyperinsulinemia, in particular, can trigger inflammation and hyperplasia in prostate tissue, but the exact mechanism behind this association remains unclear. (Cannarella et al. 2021).

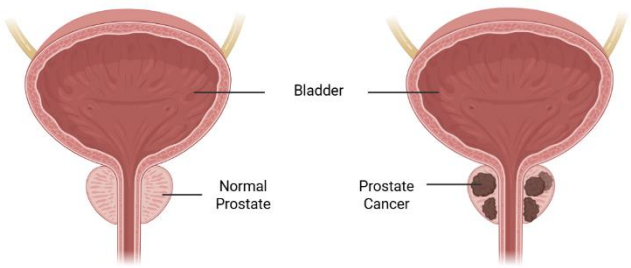

Figure 7. Prostate Cancer Physiology (Illustrated with BioRender.com)

One of the members of the nuclear receptor superfamily, called Androgen Receptor (AR), has structural similarities with receptors of some hormones such as estrogen, progesterone, glucocorticoid, and thyroid. The AR gene, mapped to the X chromosome's q11-12 locus, is made up of 8 exons and directs the synthesis of an 11 kDa protein. The AR protein has four main regions: N-terminal transactivation domain (NTD), DNA binding domain (DBD), a hinge region, and ligand binding domain (LBD) (Figure 8). The NTD region has multiple CAG (glutamine) repeats and varies between individuals that resulting in the variation of the amino acid sequence of AR. Eventually, shorter CAG repeats may cause an increase in AR activity that results in an increased risk of prostate cancer (Fujita and Nonomura 2019).

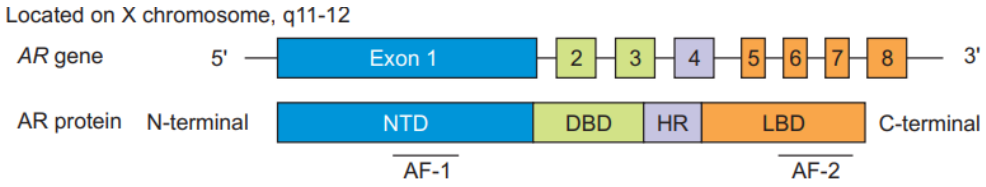

Figure 8. Illustration of mRNA and protein sequences of the androgen receptor (AR) (Fujita and Nonomura 2019)

In prostate cancer cells, androgen receptor activation by androgen steroids starts a cell-specific transcriptional program linked to oncogenesis (Fujita and Nonomura 2019). Prostate cancer cell survival and proliferation mainly depend on the testosterone hormone. In Figure 9A, testosterone is differentiated into an increased potency variant inside the cell, dihydrotestosterone (DHT). DHT binds to the androgen receptor (AR), activating it and transporting the AR to the nucleus. Consequently, genes involved in controlling the cell cycle and encouraging tumor cell growth become activated. Initially, administered androgen deprivation therapies (ADT) cause tumors to shrink; however, over prolonged exposure, some malignant cells adapt and lose responsiveness to the applied treatments. At this stage, the disease is named castration-resistant prostate cancer (CRPC). The androgen receptor gene in CRPC cells undergoes gene duplication or functional enhancement through mutations to adapt to the low DHT levels. Figure 9B represents that the use of AR signal transducers (ARSi),

such as enzalutamide or abiraterone, can cause some tumor cells to lose their differentiation and become AR-negative. In this case, transcriptional programs and chromatin structure are significantly altered. However, suppressed AR can be re-expressed by some external stimuli. Reactivation of AR may re-sensitize these cells to ARSi treatment (Formaggio, Rubin, and Theurillat 2021).

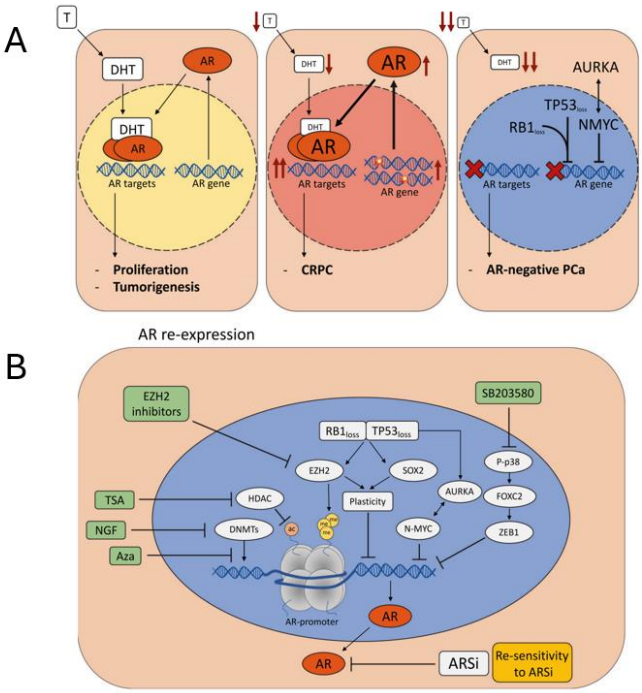

Figure 9. Representation of molecular pathways of androgen-positive and androgen-negative prostate cancer (Formaggio, Rubin, and Theurillat 2021).

1.4.3.2. Colorectal Cancer

Colorectal cancers rank third among the most commonly diagnosed cancer types globally. Colorectal cancer has several exogenous risk factors, but the most significant one was observed in the diet of patients (Labianca et al. 2010). Recently, the rate of CRC has decreased in individuals over 50 years of age, while it has increased in individuals under 50. Western-type nutrition, antibiotic use, stress, and changes in intestinal microbiota may play a role in this increase. In addition, 10–20% of patients have a family history, and up to 5% are associated with hereditary syndromes (Kwak and Chung 2007; Jiexi Li et al. 2021).

The clinical course of colorectal cancer and its response to treatment may vary based on the position of the tumor throughout the colon and rectum. Parameters such as different physiological activities of the intestinal segments, microbial composition, localized immune cell diversity, carcinogens taken with nutrition, the time of diagnosis of the disease, and embryological origin significantly contribute to the formation of this difference. In terms of embryonic development, the proximal colon originates from the midgut; the distal colon originates from the hindgut. This developmental difference causes changes in gene expression patterns throughout the colon (Jiexi Li et al. 2021).

Sporadic colon tumors located proximally are more prevalent in women and African-descended populations and are usually diagnosed at a more progressed stage. These tumors typically exhibit extensive CpG island methylator phenotype (CIMP), microsatellite instability (MSI), and deficiencies in the DNA mismatch repair (dMMR) system, along with frequent mutations in KRAS and BRAF genes, and the prognosis is generally worse. On the other hand, chromosomal instability (CIN) is predominant in distal tumors, and the survival rate of patients is higher (Jiexi Li et al. 2021).

Stem cells of the colon, positioned at the base of the epithelial crypts, carry markers such as LGR5 and OLFM4 and maintain their ability to self-renew within the "stem cell niche" with signals secreted by surrounding myofibroblasts. These cells transform into differentiated cells like enterocytes, goblet cells, and enteroendocrine cells, regulating intestinal functions. The long-lived and renewable structure of colonic stem cells may pave the way for the formation of cancer stem cells through genetic changes that accumulate over time. In this context, colorectal cancer is hypothesized to arise from a subset of stem cells that possess tumor-initiating potential. Animal models and cell transplantation studies have shown that only certain cells can form tumors and differentiate into various epithelial cell types (Jiexi Li et al. 2021; Zeki, Graham, and Wright 2011). Additionally, the chemoresistance exhibited by these cancer stem cells significantly contributes to both the relapse and advancement of the disease (Dallas et al. 2009; Jiexi Li et al. 2021). Therefore, recognizing the variations between normal and tumor stem cells is fundamental in designing more efficient treatments. (Jiexi Li et al. 2021).

1.5. DOXORUBICIN

Dox is an anthracycline antibiotic (Hanušová, Boušová, and Skálová 2011; Alam Khan and Jawaid Akhtar 2022) and originated from *Streptomyces peucetius var. Caesius* (Meredith and Dass 2016). Now, it is possible to synthesize it chemically (Varela-López et al. 2019). The name Doxorubicin was given to the drug in the early 1960s, which consists of aglyconic and sugar parts. The aglycone features a tetracyclic ring structure bearing adjacent quinone-hydroquinone groups, a methoxy substituent, and a short carbonyl-bearing side chain. This aglycone is linked via a glycosidic bond to a sugar moiety composed of a 3-amino-2,3,6-trideoxy-L-fucosyl unit (Figure 10) (Carvalho et al. 2009). Doxorubicin chemotherapy drug is mainly known for inhibiting DNA topoisomerase II and reducing DNA synthesis, which also increases the production of ROS that disrupts mitochondrial function (Figure 12) (Alhowail and Aldubayan 2023).

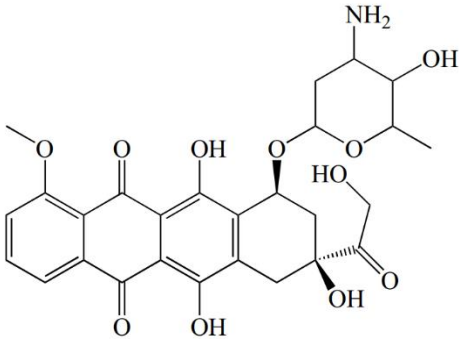

Figure 10. Chemical structure of the Doxorubicin chemotherapy drug (Carvalho et al. 2009).

Over the decades, Dox has been frequently utilized for both solid and hematologic tumor treatments, sometimes in combination with other drugs to fight many carcinoma types (Pugazhendhi et al. 2018; Varela-López et al. 2019). However, the utilization of this drug remarkably affects the non-cancerous part of the human body. The toxicity caused by Dox can be classified as acute (immediate) and chronic (long-term) toxicities (Hortobagyi et al. 1986; Varela-López et al. 2019). In 1986, National Cancer Institute reported that treatments with Dox are observed with immediate side effects like alopecia (98%), nausea (94%), vomiting (94%), severe (10%), Dox skin infiltration (6%), fever during neutropenia(6%), and microscopic hematuria (<1%)

(Hortobagyi et al. 1986). Additionally, Dox can cause myelosuppression and arrhythmia (Varela-López et al. 2019).

Otherwise, toxicity can be at a chronic (long-term) level, which includes toxic effects involving multiple organs observed in different patients (Pugazhendhi et al. 2018; Hortobagyi et al. 1986; Varela-López et al. 2019). The chronic side effects can last for weeks, months, or even years, which can cause damage to the heart, kidneys, liver, or brain. Among chronic side effects, cardiotoxicity is the most prominent effect that causes organ injury through cardiomyocyte damage, resulting in apoptotic and necrotic cell death. Even years after the treatment, long-term effects can still lead to impairment of the left ventricle, enlargement of the heart muscle (dilated cardiomyopathy), and congestive heart failure. Also, the drug can cause permanent changes in cognitive level that include memory/concentration loss or struggling to manage multiple tasks.

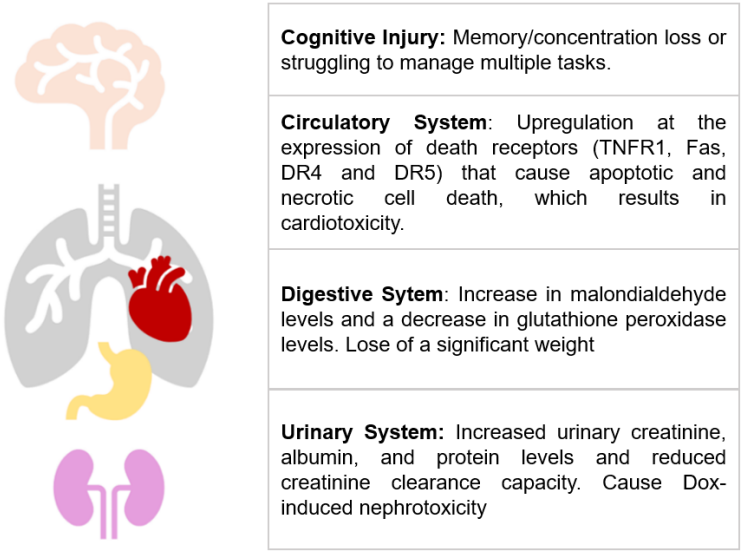

Figure 11. Schematic summary of injuries caused by Doxorubicin chemotherapy, including cognitive, circulatory, digestive, and urinary system injuries induced by the drug.

Due to its molecular mechanism, Doxorubicin causes excessive ROS production, which causes peroxidation of lipids, reduced synaptic plasticity, and mitochondrial impairment. Glutamate functions as a primary excitatory neurotransmitter on AMPA and NMDA receptors, and excessive activation of these receptors can lead to neuronal

toxicity, while inadequate activation can lead to cognitive impairment. The GluA1 subunit of AMPA and the NR1, NR2A/B/C subunits of NMDA are associated with synaptic plasticity. Increased Ca^{2+} influx via glutamate triggers processes such as oxidative stress, inflammation (NF-κB, COX-2, TNF-α), and apoptosis (Bax, caspase-3). These mechanisms are also involved in disorders such as Alzheimer's and Parkinson's. Recent studies show that DOX can cause cognitive decline by reducing long-term potential. Considering this, the outcomes of DOX on AMPA and NMDA receptor subunits, inflammatory and apoptosis markers were examined in female rats (Alhowail and Aldubayan 2023).

In the circulatory system, the cardiotoxicity induced by doxorubicin results from increased oxidative stress, inflammatory responses, and apoptosis (Pugazhendhi et al. 2018; Rawat et al. 2021). The Dox drug upregulates the upregulation of apoptotic receptors (TNFR1, Fas, DR4, and DR5), which results in apoptosis and necrosis. The cardiotoxicity due to Dox is mainly linked to oxidative stress, and this toxicity leads to irreversible heart damage. Numerous studies were conducted with suppression of oxidative stress and inhibition of ROS-mediated apoptosis to develop a cardioprotective mechanism (Pugazhendhi et al. 2018).

In vivo studies on rats during cardiotoxicity investigations, changes in liver parameters were also analyzed, causing a rise in malondialdehyde concentration and accompanied by a decline in glutathione peroxidase levels. Additionally, a higher death rate and considerable weight loss were recorded among 40 test mice of both sexes given intraperitoneal administration of Doxorubicin at 2.5 $mg.kg^{-1}$ relative to the control group. A notable elevation in plasma ALT (alanine aminotransferase) and AST (aspartate transaminase) levels was observed in doxorubicin-administered mice. It has been reported that oxidative stress, apoptosis, and necrosis mechanisms contribute to the formation of Dox-induced hepatotoxicity (Pugazhendhi et al. 2018).

In the urinary system, Doxorubicin resulted in increased urinary creatinine, albumin, and protein levels and reduced creatinine clearance capacity in *in vivo* studies. Creased urinary albumin and creatinine were evaluated as strong biomarkers in predicting advanced nephrotoxicity due to Dox treatment (glomerular impairment and secondary

tubular lesions). These parameters were found to be more sensitive than serum creatinine and BUN (Afsar et al. 2020).

1.5.1. Molecular Mechanisms of Doxorubicin

These severe toxicities and side effects happen due to the divergence of the molecular mechanisms of this chemotherapy drug. Cellular diffusion allows DOX to reach the cytoplasm, where it binds tightly to the 20S proteasome subunit, forming the DOX-proteasome complex. This complex passes through nuclear pores to reach the nucleus, where it interacts with DNA. DOX, which leaves the proteasome, damages DNA in the nucleus, leading to damage to cells and subsequent cell death. Regrettably, such effects occur in both cancerous and healthy cells, contributing to toxicity (Varela-López et al. 2019).

DOX stabilizes the topoisomerase II enzyme at DNA break sites, thus causing double-stranded DNA breaks to form. This condition impairs DNA repair mechanisms, causes cell cycle arrest at the G1 and G2 phases, and triggers apoptosis. The response to DNA damage is initiated through the ATM protein, which is involved in initiating the p53, which is a tumor suppressor. However, p53 is mutated in many types of cancer. It has also been reported that non-p53 pathways can be activated by DOX. Topoisomerase II levels have been shown to determine treatment efficacy. Additionally, DOX can also disrupt chromatin-related processes and affect DNA replication and transcription (Varela-López et al. 2019). In addition, trapping of topoisomerase IIβ in heart cells was related to cardiotoxicity (Vavrova et al. 2013). Otherwise, DOX can intercalate between DNA base pairs to form covalent DNA adducts. These adducts initiate the DNA damage response mechanisms and may lead to cell death independently of the topoisomerase II (Varela-López et al. 2019). Intercalation of DOX into DNA causes DNA relaxation, which disrupts the stability of nucleosomes. Increased nucleosome turnover has been described as a mechanism independent of p53 and ATM proteins. DOX also removes histones from chromatin, inhibiting DNA repair and triggering apoptosis. Torsional stress during RNA polymerase movement may make DNA more susceptible to agents such as ROS.

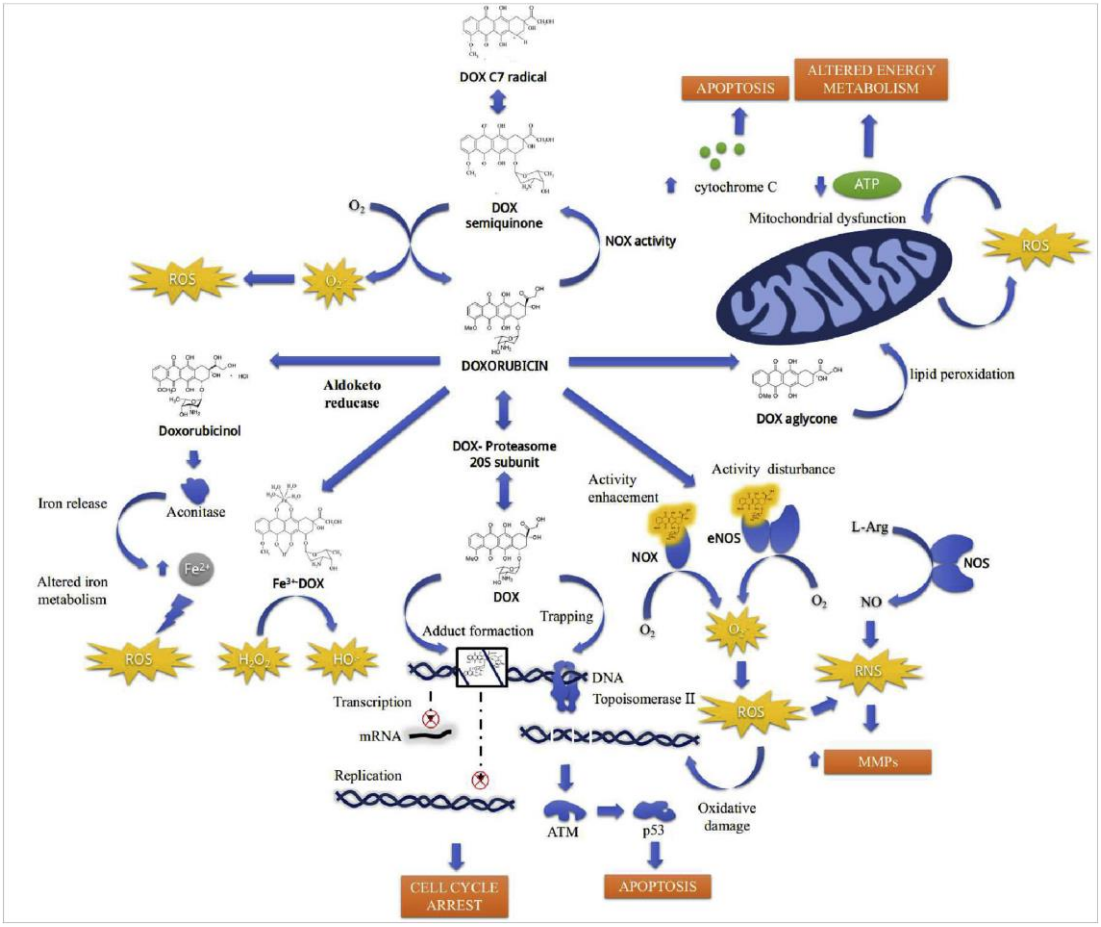

Figure 12. The molecular mechanisms of the Doxorubicin drug (Varela-López et al. 2019).

Ceramide is a lipid that is linked to cell growth arrest, programmed cell death, and aging (J. Wang 2007). It has been reported that ceramide levels increase after DOX application (Delpy 1999). It has also been determined that ceramide production differs between DOX-resistant and sensitive cells. Nevertheless, a complete understanding of the mechanism behind this process is still lacking.

DOX produces reactive oxygen species (ROS) and free radicals through different mechanisms. These molecules damage DNA, proteins and lipids, creating oxidative stress and contributing to cell death. Enzymes that undergo oxidative damage can disrupt chromatin structure. The quinone structure of DOX is reduced by NAD(P)H-oxidoreductases to form semiquinone radicals. These radicals react with oxygen to form superoxide anion and other ROS/RNS species. Thus, a continuous quinone-semiquinone cycle provides high amounts of free radical production. DOX increases

the production of free radicals that contribute to the apoptosis process in cardiac cells by activating NADPH oxidases (NOX). NOX activation also increases the production of peroxynitrite (ONOO−) and causes cardiac toxicity. DOX binds to the reductase site of the eNOS enzyme, causing superoxide production. This is additionally linked to systemic effects, including renal function and hypertension due to salt sensitivity. DOX is converted to a lipophilic aglycone derivative and enters the mitochondria, where it increases ROS production. The inner mitochondrial membrane is particularly vulnerable; cardiolipin peroxidation causes respiratory chain disruption and reduced ATP production. This can lead to increased proteotoxic load and cardiac damage, especially in cardiac muscle cells, with energy deficiency. In addition, mitochondrial membrane damage caused by DOX leads to the activation of the mitochondrial permeability transition pore (mPTP), which subsequently initiates apoptosis through cytochrome C release. The opening of these structures is also associated with necrotic cell death (Varela-López et al. 2019).

As a result of the therapeutic opportunities of Dox, it is an important chemotherapy agent that is still utilized for numerous carcinoma types; however, all those side effects caused by Dox on non-cancerous cells lead researchers to new strategies and to the use of targeted therapies.

1.6. TARGETED DRUG DELIVERY TECHNIQUES

Controlled cleavages of bonds between molecules are the main key point of newly designed targeted drug delivery and release technologies (Böhme and Beck- Sickinger 2015). Targeted drug delivery systems (DDS) are designed to improve therapeutic efficiency and reduce adverse effects by directing the drug specifically to the affected tissue. These systems, which were developed to address the shortcomings of traditional delivery approaches, enhance drug solubility, prolong tissue retention time, and increase overall bioavailability. In active targeting, drug carriers bind to particular receptors located on the cell membrane; in passive targeting, drug accumulation is achieved by utilizing permeable vascular structures in the tumor tissue. The use of DDS in methods such as photodynamic and photothermal therapy strengthens the

effect of cancer cell-specific therapy while reducing injuries in normal tissues (Ashique et al. 2021; Regenold et al. 2022).

Chemotherapy remains a standard intervention in cancer management, but as shown in the example of the Doxorubicin drug, several significant short-term and long-term side effects have been reported on healthy cells and organs, which need to be reduced (Sun et al. 2023; Pugazhendhi et al. 2018). Those severe side effects led researchers to look for a mechanism that only targets the tumor microenvironment and reduces the severity of the undesirable impacts on normal tissues and organs (Sun et al. 2023; Ashique et al. 2021; Regenold et al. 2022). The targeted drug release methods have two main classes: active targeting and passive targeting.

1.6.1. Active Targeting

Nanoparticle designs for active targeting drug delivery mechanisms are based on the principle of targeting biological changes specialized to cancer cells by adding a targeting structure, such as a ligand, antibody, or peptide, to the surface of the nanocarrier system. Relative to healthy cells, these biomarkers should be highly expressed in cancer cells. In this approach, nanoparticles recognize target cells and are taken into the cell by binding to them through ligand-receptor interactions; thus, drug release occurs directly inside the cell, and unwanted drug effects on surrounding tissues are reduced. One of the important advantages of active targeting is that it is directed to receptors that are excessively present in tumor cell membranes. For example, in more than half of breast cancer types, EGFR (epidermal growth factor) is observed with elevated expression levels, as well as in kidney, ovarian, colon, and non-small cell lung cancers. Therefore, targeting EGFR stands out as a promising strategy that allows more effective use of chemotherapeutic nanoparticle systems in various cancer types (Clemons et al. 2018).

1.6.2. EPR effect and Passive Targeting

Within the tumor microenvironment (TME), the EPR effect is recognized as a significant contributing mechanism (Vagena et al. 2025). EPR is the

pathophysiological phenomenon that was initially defined by Konno et al. in 1984 (Konno et al. 1984). This mechanism is especially observed in solid tumors in which passive accumulation of macromolecules like proteins, liposomes, micelles, and nanoparticles (>500 nm) occurs in tumor tissues. This phenomenon is a consequence of pathophysiological abnormalities in tumors, such as abnormal vasculature, inadequate lymphatic drainage, increased extracellular matrix stiffness, and high interstitial fluid pressure (Vagena et al. 2025).

Intense angiogenesis triggered by tumor cells causes the formation of vessels that are impaired in terms of structure and function. This situation causes wide gaps between endothelial cells, facilitating the passage of macromolecules out of the vessels, (Figure 13). In addition, due to the impaired lymphatic system, these molecules remain in this TME for a prolonged interval. The presence of mediators such as VEGF, bradykinin, and nitric oxide, which increase vascular permeability, also supports the maintenance of EPR (Vagena et al. 2025).

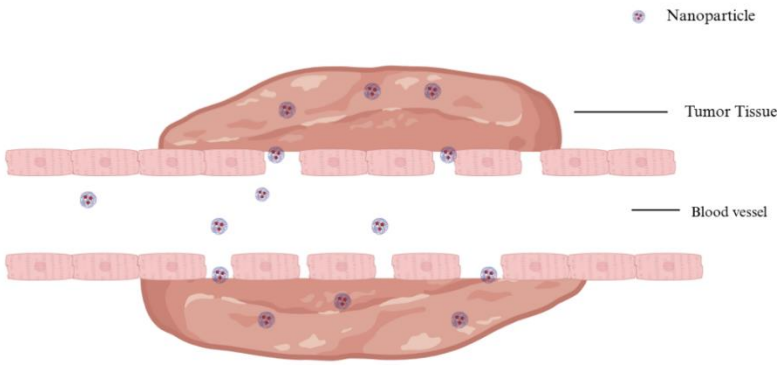

Figure 13. The EPR effect and the passive targeting model of nanoparticles in TME (Illustrated with BioRender.com).

Theoretically, the EPR phenomenon reduces systemic toxicity and increases treatment efficacy by ensuring that drugs accumulate at the tumor site. However, the effectiveness of this mechanism depends on some ideal conditions, and these conditions are not always provided in the real tumor microenvironment. Factors such as mass transfer, interstitial pressure, and drug distribution may limit the success of EPR. Although positive results have been obtained in preclinical studies, the clinical

success rate is low because most nanotherapeutic agents have shown low side effects but have not significantly changed the course of the disease (Vagena et al. 2025).

1.6.3. ThermoDOX

Liposomes tend to accumulate passively in tumor tissues as a result of the EPR effect, and for this characteristic, liposomes are a widely favored nanocarrier structure for chemotherapy agents in the tumor tissue (Besse et al. 2019; Regenold et al. 2022). Previously, DOXIL was produced as a liposomal nanoparticle that encapsulates the Doxorubicin drug, however, the slow diffusion of the Dox caused this treatment method to fail. Otherwise, ThermoDox treatment was developed with temperature-sensitive liposomes (TSL) and its combination of hyperthermia application in TME (Figure 14) (Regenold et al. 2022).

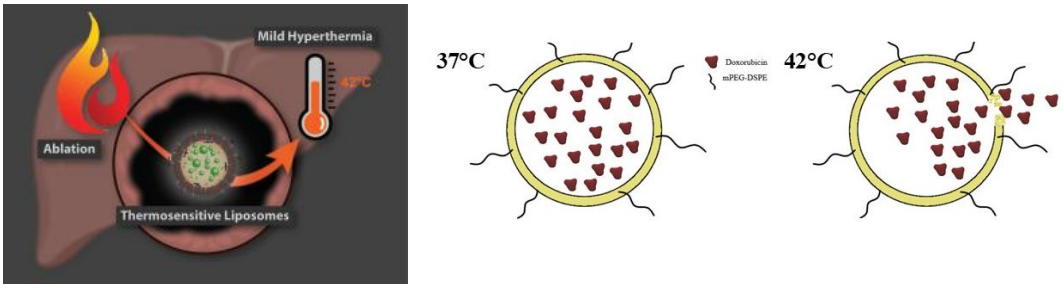

Figure 14. Thermodox treatment combines temperature-sensitive liposomal nanoparticles with radiofrequency ablation to generate a targeted drug release method in TME based on hyperthermia (Regenold et al. 2022).

Hyperthermia with radiofrequency ablation (RFA) is preferred among heat-based treatment methods due to its advantages, such as low invasiveness, ease of application, cost-effectiveness, and openness to technical development (Ni et al. 2005). RFA causes increased temperatures in the tumor tissue that lead to necrosis, and when combined with the ThermoDox nanoparticles, this combination therapy both helps to disrupt cells in the center of the tumor and triggers the Dox release from temperature-sensitive liposomal nanoparticles (ThermoDox) (Regenold et al. 2022).

2. MATERIALS & METHODS

2.1. ISOLATION AND IDENTIFICATION OF CELLULOSE DIGESTIVE BACTERIA FROM THE RUMEN

2.1.1. Collection of Samples From the Cattle Rumen Fluid

For isolation of rumen-originated cellulolytic bacteria, rumen fluid was collected from the rumen. Sample collection was performed by adding $_{dd}H_2O$ to the three different places on the surface of the rumen and pipetting back the water with a micropipette. Then, serial dilutions were prepared for each sample to observe microbial growth in further steps (Sari et al. 2017).

2.1.2. Isolation of Cellulose-Digesting Bacteria

A selective medium was prepared to culture cellulolytic bacteria from the samples, including Bushnell-Haas salt, 1% CMC, and 2% agar. Bacteria cultivation from the diluted samples was generated on the prepared selective agar media, and samples were underwent incubation at 39˚C for 4 days (Sari et al. 2017).

2.1.3. Cellulase Enzyme Activity Analysis with Congo Red Assay

Isolated bacteria species were inoculated on Yeast Extract (YE) agar media by the streaking method, and the first check of cellulase enzyme activity was performed with the Congo red assay. Preparation of a 0.3% Congo red dye was carried out by mixing 150 mg of Congo red powder and 50 mL of $_{dd}H_2O$, and further addition of 50 mL of 98% EtOH. Then, bacteria samples on solid agar medium were exposed to the prepared Congo red dye for 20 minutes, and incubated at room temperature, which is followed

by washing with $_{dd}H_2O$ for 10 seconds. Then, plates were rinsed with 1 M NaCl solvent for about 5 minutes of incubation twice (Sari et al. 2017). Finally, samples were rinsed with 5% acetic acid to clarify the zones observed around the colonies. The bacterial strain with higher cellulase activity was isolated and grown in a Yeast extract medium for faster growth.

2.2. DNS ENZYME ACTIVITY ASSAY

2.2.1. Partial Isolation of Cellulase Enzyme

The isolated ROBY strain was grown in 1% Yeast extract and 1% CMC media overnight. Since cellulase is a soluble enzyme type and expected to be secreted to the extracellular space, partial isolation of cellulase was done from the supernatant (Topuz et al. 2007). Centrifugation of the liquid bacterial culture was performed at 6000 rpm and 0˚C for 20 minutes to separate the supernatant. Then, 70% of EtOH was added to the supernatant to generate an EtOH precipitation, and the sample was incubated at -20˚C for 24 hours, and the process followed with centrifugation at 6000 rpm and 0˚C for 20 minutes, and the pellet was dissolved with phosphate buffer with 20% glycerol at pH 6.5.

Otherwise, since *A. pittii ROBY strain* is a gram-negative bacterial species, and does not tend to secrete enzymes. Thus, intracellular enzyme isolation was also generated. Samely, bacteria were grown in 1% YE and 1% CMC media overnight. The next day, the bacteria were centrifuged at 7000 g, the supernatant discarded, and the bacteria were rinsed with the addition of 1X PBS buffer. Then, the bacteria were recentrifuged a 7000 g for 15 minutes. Then, cells were treated with 5 mL of acetone and incubated on ice for 10 minutes and centrifuged at 7000 g for 20 minutes, and the supernatant was discarded and left to air dry (Bhaduri and Demchick 1983). Then, the bacterial pellet was treated with lysis buffer (includes 50 mM Tris.HCl, 150 mM NaCl, and 0.3% Tween 85) and cells were left for ultrasonication for 15 minutes with breaks on ice. The sample was next centrifuged at 15,000 g for 20 minutes at 4˚C, after which the supernatant was harvested and treated with 70% ethanol for a duration of 24 hours

at -22˚C, and then centrifuged back at 0˚C. Finally, the pellet that contains intracellular soluble enzymes was dissolved in phosphate buffer with 20% glycerol at pH 6.5.

2.2.2. Preparation of DNS Solvent

Cellulase enzyme activity at various pH levels was evaluated using the 3,5-dinitrosalicylic acid (DNS) assay. The DNS solvent was formulated by dissolution of 0.5 g of DNS with 15 g of potassium sodium tartrate in 35 mL of $_{dd}H_2O$. Separately, 0.8 g of NaOH was dissolved in 10 mL of $_{dd}H_2O$ in a different beaker. Then, both solvents were mixed, and the total volume was arranged to 50 ml.

2.2.3. DNS Enzyme Activity Assay

A substrate solvent was prepared in which 1% carboxymethyl cellulose (CMC) was dissolved in 1X PBS buffer, and 5 different pH levels were arranged (pH: 5, 6, 7, 8, and 9). Then, each substrate solvent was mixed with the enzyme solvent in a 1:1 ratio (1 ml), and, by the way, the enzyme activity was analyzed at divergent pH levels. Further, samples were left for incubation at 37˚C for 30 min. The reaction was terminated by adding 2 mL of DNS reagent, and samples were heated in boiling water for 5 minutes, and then transferred the ice. Afterward, colorimetric measurement of samples was accomplished at 600 nm (with a microplate reader). Ahead of the enzyme activity assay, a standard curve was set up with various glucose concentrations (2-8 mg/ml) (Figure S1).

2.2.4. gDNA Isolation from the Newly Isolated Bacteria

After the cellulolytic activity was highly observed in the ROBY strain, genomic DNA isolation was performed for species identification with the NucleoSpin® DNA Purification Kit. Approximately 30 mg of the pellet was suspended with 100 µL of Elution buffer, and the sample was transferred to the MN tube type B. 40 µL of Buffer MG and 10 µL of liquid proteinase K were added, and the tubes were sonicated with an ultrasonic cleaner for 15 minutes. Tubes were centrifuged at 11,000 x g for 1 min. Next, 600 µL of Buffer MG was added, and solutions were vortexed for a few seconds and centrifuged at 11,000 x g for 1 min. The supernatant was transferred onto the

NucleoSpin® Microbial DNA column, placed in a 2 mL collection tube, and centrifuged at 11,000 x g for 1 min. Then, the collection tube was removed, and the column was put into a new collection tube. The column was further rinsed with buffer BW and buffer B5 with centrifugation at 11,000 x g for 1 min in each wash, and for drying, the column was centrifuged at 11,000 x g for 1 min. Finally, the column was transferred to a microcentrifuge tube, 100 µL of Elution buffer was added, and µ centrifuged at 11,000 x g for 1 min to transfer purified DNA into a centrifuge tube. Furthermore, A_{260}/A_{280} ratio analysis was performed by using a UV-Vis Spectrophotometer (DeNovix DS-11). All samples displayed absorbance levels spanning from 1.6 to 2.0

2.2.5. Sequencing 16S rRNA for Species Identification

The isolated gDNA from the ROBY strain was utilized as a template for amplifying 16S rRNA, and this amplification was maintained by using these universal forward and reverse primers which are; 27F (5′-AGAGTTTGATCCTGGCTCAG-3′) and 1492R (5′-TACGGYTACCTTGTTACGACTT-3′) were used, and those primers span the almost total sequence of the 16S rRNA (~1400 bp).

2.2.6. Scanning Electron Microscopy for Bacteria

To analyze the isolated bacteria species with a scanning electron microscope (SEM), the bacterial strain was fixed by placing it on a small piece of conductive aluminum foil; this procedure was carried out similarly to the protocol described by Czerwińska (Czerwińska-Główka and Krukiewicz 2021). Firstly, aluminium was sterilized with 70% EtOH and cut into small pieces with scissors. To ensure sterilization, foil pieces were additionally sterilized with 30 min UV-C on both sides. Then, foil pieces were incubated in liquid medium for the duration of bacterial growth and attachment to the surface. After the bacteria attached to the surface, the liquid medium was discarded, and a 3% glutaraldehyde solution was poured in and left for 24 hours of fixation. Then, the samples were rinsed three times by using distilled water ($_{dd}H_2$ O) and gradually dehydrated with increasing ethanol concentrations from 30% to 99%. Finally, samples were left for fry overnight at 50 °C, and analyzed with SEM.

2.3. GROWTH AND ENZYMATIC ANALYSIS OF THE *RUMINOCOCCUS FLAVEFACIENS* BACTERIA

2.3.1. Preparing An Anaerobic Growth Media

In the experimental process, the main aim was the utilization of an anaerobic cellulolytic bacterial species. Therefore, cellulose-including anaerobic media types were prepared. Media 1 includes 1% Yeast Extract (YE), 1% carboxymethylcellulose (CMC), and 3.2 mM L-cysteine; media 2 includes Bushnell-Haas salt, 1% CMC, and 3.2 mM L-cysteine; media 3 includes 1.6% agar, 1% Yeast Extract (YE), 1% carboxymethylcellulose (CMC), and 3.2 mM L-cysteine; media 4 includes 1.6% agar Bushnell-Haas salt, 1% CMC, and 3.2 mM L-cysteine.

2.3.2. Growth of *Ruminococcus Flavefaciens* Bacteria

The bacterial strain *Ruminococcus flavefaciens* Sijpesteijn 1948 was purchased from the Leibniz Institute DSMZ. *R. flavefaciens* is a ruminant and an anaerobic bacterium that requires a slightly acidic and strict anaerobic environment to grow and survive. For this purpose, an anaerobic growth medium and an anaerobic environment should be arranged. The bacterial species was grown with both liquid and solid media. Since *R. flavefaciens* is an anaerobic species, an anaerobic growth condition was required. A jar was utilized to create a basic anaerobic environment, and for consumption of the oxygen inside the jar, a candle was added and lit before closing the jar lid. Also, against the possibility of oxygen leakage, a heat pad that heats up in the presence of oxygen was added. With the help of this mechanism, *R. flavefaciens* bacteria were grown in both liquid and solid culture media.

2.3.3. Cellulase Enzyme Activity Analysis with Congo Red Assay

A similar protocol for Congo red (CR) assay was utilized. *R. flavefaciens* bacterium was inoculated on Yeast Extract (YE) agar media by the streaking method, and cellulase enzyme analysis was performed with the Congo red assay. Samples were exposed to the prepared CR dye for 20 min and gently rinsed with $_{dd}H_2O$. Further,

plates were rinsed with 1 M NaCl for 5 minutes of incubation twice (Sari et al. 2017). Finally, samples were rinsed with 5% acetic acid to clarify the zones observed around the colonies.

2.4. CELLULASE ENZYME ACTIVITY ANALYSIS AT DIFFERENT PH LEVELS WITH DNS ENZYME ACTIVITY ASSAY

2.4.1. Partial Isolation of Cellulase Enzyme

The isolated ROBY strain was grown in anaerobic growth conditions, which media includes 1% Yeast extract, 1% CMC, and 3.2 mM L-cysteine. Since cellulase is a soluble enzyme type and expected to be secreted to the extracellular space, partial isolation of the cellulase enzyme was done from the supernatant (Topuz et al. 2007). The bacterial liquid culture was centrifuged at 6000 rpm and 0°C for 20 minutes to separate the supernatant. Further, 70% ethanol was added to the supernatant, and the mixture was incubated at −20°C for 24 hours. Following incubation, the mixture underwent centrifugation at 6000 rpm and 4°C for 30 minutes, and the final pellet was dissolved in phosphate buffer containing 20% glycerol at pH 6.5.

2.4.2. DNS Enzyme Activity Assay

A substrate solvent was prepared in which 1% carboxymethyl cellulose (CMC) was dissolved in 1X PBS buffer, and 5 different pH levels were arranged (pH: 5, 6, 7, 8, and 9). Then, each substrate solvent was mixed with the enzyme solvent in a 1:1 ratio (1 ml), and, by the way, the enzyme activity was analyzed at divergent pH levels. Further, samples were incubated at 37˚C for 30 minutes. To stop the reaction, 2 ml of DNS solvent was added, and samples were heated at 100˚C for 5 minutes. Afterward, colorimetric measurement of samples was accomplished at 600 nm (by using a microplate reader), and relative enzyme activity was calculated with the results.

2.5. PRODUCTION AND CHARACTERIZATION OF DOXORUBICIN ENTEGRETED SPHERICAL CELLULOSE NANOPARTICLES

2.5.1. Preparation of Doxorubicin

Doxorubicin was purchased from Sigma Aldrich and has 98% purity. The solubility of Dox drug in $_{dd}H_2O$ is 10 mg/mL. Further, the drug was diluted and measured at 480 nm (from 0.1 μM to 5 mM), and a Dox standard curve was arranged (Figure S2). On the other hand, 10 mg/mL Dox drug was heated up to different temperatures between 25 to 55°C, and absorbance changes were analyzed with measurements at 480 nm.

2.5.2. Cellulose Nanoparticle Production with Ionic Solvent

Cellulose is in a hardly degrading structure, however, chemicals like ionic solvents can help the degradation of cellulose into much smaller particles. Therefore, an ionic solvent, EMIMAc, was utilized for the dissolution of cellulose. As a cellulose substance, microcrystalline cellulose (MCC), and the ionic solvent EMIMAc were purchased from Sigma Aldrich. Before usage, the ionic solvent was incubated at 68˚C for 24 hours to generate a drying and ensure the solvent's purity. Then, the amount of ionic solvent was heated to 80˚C in a baker on a magnetic stirrer and mixed with 1% MCC. The dissolution process of cellulose took about 48 hours. On the other hand, the chemotherapy drug, Doxorubicin (Dox), was aimed to be encapsulated within cellulose and produce cellulose nanoparticles. Doxorubicin hydrochloride (10mg) was dissolved in 1 mL of $_{dd}H_2O$, and the free Dox concentration was maintained at 10 mg/mL. Further, the nanoparticle solvent was cooled down to 55˚C, at which temperature the Doxorubicin drug does not lose its activity. The drug was inserted into the nanoparticle solvent in a 1:10 ratio, and the solvent was mixed by using a magnetic stirrer that was set at 55˚C for 4 hours to maintain integration between cellulose particles and the chemotherapy drug. Then, acetone and diethyl ether were maintained as non-solvent chemicals to cellulose, EMIMAc, and doxorubicin for washing steps. The first wash was maintained with acetone, which was added to the solvent at 97% and vortexed. With centrifugation at 6000 rpm for 2 minutes, the non-soluble part was removed via phase separation of acetone and nanoparticle solvent. In this part, the

supernatant was separated for the calculation of non-capsulated Doxorubicin. For this calculation, a standard curve of the Doxorubicin drug was generated with measurements at 480 nm with divergent concentrations (Figure S2). With non-capsulated Dox concentration, loading capacity, and encapsulation efficiency calculations were performed.

2.5.3. Cellulose Nanoparticle Production with Alkali Mixture

Beyond ionic solvents, cellulose can also be degraded via alkali solvents. Jin et al. described a way to dissolve cellulose directly, and a similar methodology was utilized to dissolve cellulose (Jin, Zha, and Gu 2007). Here, microcrystalline cellulose (MCC) was dissolved in a solvent system consisting of NaOH, Thiourea (CH_4N_2S), and urea ($CO(NH_2)_2$). The research shows that combinations of NaOH-Urea or NaOH-Thiourea can break down the cellulose structure. However, none of those components can dissolve cellulose by itself. The best concentrations of those materials for better dissolution of cellulose were analyzed as NaOH (8%), Thiourea (6.5%), and urea (8%) by Jin et al., 2007. Therefore, concentrations for the alkali solvent system were determined according to this research, and cellulose was dissolved at high temperatures. Later, there was a great need for the neutralization of pH, since the product would be utilized in cell culture experiments. The pH was neutralized to 7 with HCl (37%). By the way, a highly saline mixture was obtained, and to get rid of the saline, the solvent was centrifuged at 0˚C, 6000 rpm for 30 min twice to ensure lowering the saline concentrations. Further, the solvent was reheated to 55 °C, and the amount of nanoparticle solution was mixed with Doxorubicin chemotherapy drug (10 mg/mL). In this step, the solvent underwent sonication at 55°C for 10 minutes, and then was left on ice for 10 minutes. This step was performed multiple times to provide integration of the drug with cellulose particles. At the third repeat of this step, CMC was added as 0.5% to support the stability of the produced nanoparticles, and the process was replicated a few times more with the addition of vortex steps. Afterwards, the mixture was rinsed with acetone once to get rid of the remaining salt, and then finally rinsed with diethyl ether. To collect nanoparticles appropriate for the EPR effect, the mixture was filtered by using a syringe filter (0.22 μm).

2.5.4. Nanoparticle Production with Thiourea & Urea

During nanoparticle formation using an alkaline solvent, a significant amount of salt was generated as a byproduct during the neutralization step. Although cold centrifugation helped to remove some of this salt, a considerable amount of NaCl remained in the solution. This residual salt interacted with the drug during encapsulation, leading to aggregation. To eliminate this issue, NaOH was removed from the method, and nanoparticle production was attempted using only thiourea and urea. As a result, drug aggregation was reduced, and a higher drug loading efficiency was achieved. However, the produced nanoparticles were observed to have poor stability due to their zeta potential being close to neutral. To improve stability by imparting a negative surface charge, various strategies were explored. It was found that adding carboxymethyl cellulose (CMC) at concentrations of around 0.5–1% could render the particles negatively charged. Therefore, 1% CMC was added to the nanoparticle suspension to enhance stability and achieve a suitable zeta potential.

2.5.5. Characterization of Cellulose Nanoparticles with TEM

Transmission electron microscopy (TEM) views of CNP and Dox-CNP were analyzed through a service procurement from İstanbul Medeniyet University. The device

2.5.6. Characterization of Cellulose Nanoparticles with DLS/Zeta Sizer

Samples were diluted in a 1:100 ratio and analyzed with a DLS/Zeta Sizer Malvern Zetasizer Pro device at the Boğaziçi University Institute of Biomedical Engineering.

2.5.7. Characterization of Cellulose Nanoparticles with FT-IR

Samples were diluted in a 1:100 ratio and analyzed with the FT-IR Shimadzu QATR-S device at the Boğaziçi University Institute of Biomedical Engineering.

2.6. BACTERIAL CAPACITY FOR CNP DEGRADATION AND DRUG RELEASE

2.6.1. Use of Cellulose Nanoparticles as a Carbon Source in Bacterial Culture

In this study, the degradability of cellulose nanoparticles by bacteria and the release of Doxorubicin were investigated. Both plain cellulose nanoparticles and Doxorubicin-loaded nanoparticles were added in equal amounts to Bushnell-Haas liquid medium, which lacks a carbon source. The experiments were conducted in triplicate, with pH adjusted between 6.0, 6.5, and 7.0. The bacterial culture used (A. pittii) was sampled at 1, 3, 4, and 24 hours in the liquid medium. The collected samples were diluted and subjected to CFU (Colony Forming Unit) counting, and OD600 values were also measured. Meanwhile, the released Dox Concentration in the bacterial medium was examined using spectrophotometric measurements.

2.6.2. Investigation of Doxorubicin Release

Doxorubicin release was monitored based on an initial concentration of approximately 13.30 µg/ml. The effect of both the bacteria and the extracellular cellulase enzyme on Doxorubicin release was evaluated. It was observed that as the bacteria began actively degrading the cellulose nanoparticles, the released Doxorubicin started to damage bacterial cells and negatively affect their viability. After 24 hours, the concentration of free Doxorubicin reached around 8 µg/ml. These results indicate that drug release from the nanoparticles occurs in parallel with bacterial degradation.

2.6.3. Release Test and Washing Method for Cellulose Nanoparticles

In the release experiments, the released Dox (%) was calculated compared to the initial drug concentration and to the amount detected after a washing step using diethyl ether. The amount of free Doxorubicin was quantified after washing, and it was observed that in the absence of bacteria, Doxorubicin release was significantly lower. It was determined that the breakdown of cellulose nanoparticles by bacteria, particularly during cell death and lysis, led to drug release and a corresponding decrease in bacterial viability.

2.7. IN VITRO TRIALS ON LNCaP, CaCo-2, and PNT1A CELL LINES

2.7.1. Cell Lines

In this research, two cancer and one healthy cell line were utilized.

PNT1A: The PNT1A cell line is an immortalized human cell line that represents healthy prostate epithelial cells.

CaCo-2: The Caco-2 cell line is a model derived from human colon adenocarcinoma that exhibits properties similar to intestinal epithelial cells

LNCaP: The LNCaP cell line is a hormone-sensitive cancer cell line that originated from human prostate adenocarcinoma

2.7.2. Cell Culturing, Counting, and Seeding

Media preparation: In this project, the PNT1A healthy prostate cell line, the LNCaP androgen-positive prostate cancer cell line, and the CaCo-2 colon cancer cell line were utilized, and throughout the project, those cell lines were repeatedly grown, passaged, seeded, and frozen. To support their growth, PNT1A and LNCaP cells were incubated in RPMI-1640 medium (Gibco, Grand Island, NY), while CaCo-2 cells were cultured in DMEM, both media containing 10% FBS and 1% penicillin-streptomycin. Also, PBS 10X stock was diluted with $_{dd}H_2O$ to 1X to be used in washing steps.

Starting Cell Culture: Cell lines were taken from the stocks in the -80 freezer and centrifuged at 1250 rpm for 5 min to get rid of the toxic material, DMSO (Dimethyl sulfoxide), which is used to freeze cells. Further, the pellet was dissolved with the suitable media that was prepared, RPMI for LNCaP and PNT1A, and DMEM for CaCo-2 cell lines. CaCo-2 and PNT1A cell lines were grown in 10 cm^2 petri dishes, and the LNCaP cell line was grown in a T25 flask. After cells were grown and spanned approximately 75-80% of the plate surface, the cell lines were passaged.

Passaging: The passaging process is the dilution of cells from the plate's surface. In this method, the media on the cells were soaked, and the The cells were treated with PBS for washing and subsequently exposed to 0.05% Trypsin-EDTA (1 mL for T25 plates, and 2.5 mL for 10 mL petri dishes) and cell lines were put into the incubator with 37˚C and 5% CO_2 properties for 5 minutes to remove cells from the surface and to dissociate the cells into single-cell suspensions. Further, the trypsin process was stopped with the addition of an appropriate medium (DMEM or RPMI) in twice the amount of the trypsin added before. Further, the solvent was put into a 15 mL falcon tube, and the mixture was homogenized as much as possible. Finally, the number of cells was reseeded on the plate (T25 or 10 cm^3 petri dish) according to the cell type, and the appropriate media was added as much as the culture plate medium (5 mL for T25 plate, and 10 mL for the petri dish). Afterward, the rest of the cells at the bottom of the falcon were frozen.

Freezing Cells: Constantly, newly opened cell lines are frozen after their first passage. The rest of the cells at the bottom of the falcon were centrifuged at 1250 rpm for 5 minutes. The cell pellet was suspended with the appropriate medium, and for freezing, DMSO (Dimethyl sulfoxide) was added as 5-10% according to the cell type. Majorly, the LNCaP cell line is more sensitive, so the LNCaP cell line is frozen with 5% DMSO, whereas PNT1A and CaCo-2 cell lines are frozen with 10% DMSO.

Cell Seeding: Further, cells were regrown and passaged, and after passage was completed, the remaining cells were counted with the help of the Neubauer slide, and a cell count per 1 mL calculation was done. For 96-well plates, counted cells were arranged as follows: 10.000 cells for the CaCo-2, 15.000 cells for the PNT1A, and 15.000 cells for the LNCaP per well, and all wells should be maximized with the appropriate medium and seeded on a 96-well plate.

Treatment: After cell seeding, the cell lines were incubated for a day and attached to the bottom of the plate. Further, treatment conditions were prepared as will be given 20µL in each well and will be designed according to conditions in Table 2.

Table 2. Cell culture planning conditions

Conditions	***CNP***	***Dox-CNP***	***Free Dox***	***Enzyme***
1	+	-	-	-
2	-	+	-	-
3	-	-	+	-
4	-	-	-	+
5	+	-	-	+
6	-	+	-	+

2.7.3. Viability Test with Crystal Violet

For in vitro experiments, CaCo-2 (colon cancer), LNCaP (prostate cancer), and PNT1A (healthy prostate epithelial cells – used as a control) cell lines were used. The newly developed cellulose nanoparticles (CNP and Dox-CNP) were applied to these cell lines, and changes in cell viability following experimental treatment were observed. For the assay, 15,000 LNCaP cells, 10,000 CaCo-2 cells, and 15,000 PNT1A cells per well were seeded. The observed toxicity in CNPs, insufficient drug encapsulation, and high toxicity associated with the enzyme slowed down the progression of these experiments, and cell culture optimization took longer than expected.

In preliminary viability assays, 0.5% crystal violet (dissolved in ethanol) was used. For this assay, the cell culture medium was initially aspirated, and the treated wells in the 96-well plate were rinsed with 1X PBS. Each well was then stained with pre-prepared crystal violet solution and incubated on a tabletop shaker for 20 minutes. After the incubation period, the dye solution was removed, and the wells were initially rinsed with 1X PBS, followed by three rinses with distilled water. Once the plate dried, the retained dye in each well was dissolved using 200 µL of methanol and incubated

again on a shaker for 20 minutes. Finally, absorbance values of each well are analyzed at 590 nm, and viability (%) is determined.

After optimizing the nanoparticles and enzyme concentrations, treatments were applied to all the control groups defined in the project. These groups included: untreated control, CNP, Dox-CNP, CNP+Enzyme, Dox-CNP+Enzyme, free Doxorubicin, and enzyme-only treatments.

2.7.4. WST-8/CCK8 Viability Test

Similar to the crystal violet assay, cells were plated into 96-well plates and treated with the optimized therapeutic formulations. Although the WST-8 assay is more costly than the crystal violet method, it provides more accurate and reliable results; therefore, this step was considered the most definitive part of the experimental evaluation. After applying the appropriate treatment conditions, the samples were incubated for 72 hours. Followingly, WST-8 solution was added to each well at a volume equal to 10% of the medium. The plate was placed in an incubator at 37°C with 5% CO_2 for approximately 3 to 4 hours, after which A450 measurements were carried out to determine changes in viability.

2.7.5. IC50 Calculation For LNCaP, CaCo-2, and PNT1A Cell Lines

LNCaP, CaCo-2, and PNT1A cell lines were plated in a 96-well plate with different Dox concentrations for further IC50 calculation. Then, the CCK-8 assay was applied for viability results, and the experiment was carried out with 3 replicates. Further, results were analyzed with GraphPad Prism 8.

2.7.6. Conducting a Preliminary Study to Determine the Values at Which Enzyme and CNPs Can Be Applied Before the Experimental Treatment Method

To observe usable quantities and concentrations of cellulose nanoparticles and isolated intracellular and extracellular enzymes were analyzed. As a viability test, the crystal violet viability test was utilized.

2.7.7. Exposure of Bacteria-Treated Cell Lines to Empty and Doxorubicin-Containing Cellulose Nanoparticles

At the beginning of the project, cellulolytic bacteria were planned; however, during the cell culture experiment, bacteria caused serious contamination. The experiment was repeated three times, and each experiment resulted similarly. For the viability test, both CCK-8 assay and Crystal violet viability test were utilized, however, increased bacteria population was a manipulated result. Eventually, the experimental process was carried out with an enzyme that is partially isolated from the *R. flavefaciens* and *A. pittii*.

2.7.8. Cellular Uptake Assays

For the cellular uptake assays, cells were seeded into 6-well plates and treated with the predetermined Dox, Dox-CNP, CNP, and enzyme concentrations. After a 72-hour incubation period, nuclei were stained with DAPI. Using the fluorescent property of Doxorubicin, cellular uptake was observed under a fluorescence microscope.

3. RESULTS

3.1. ISOLATION & IDENTIFICATION OF CELLULOSE DIGESTIVE BACTERIA

At the beginning of this study, the main aim was to isolate a bacterial species with cellulolytic characteristics from a bovine rumen, and multiple trials were generated to estimate cellulase enzyme activity. Firstly, samples were taken from various parts of the rumen and seeded on agar plates (BH+CMC) in various dilutions. Further, a bacterial species sample was collected, and its enzymatic activity was analyzed through the Congo Red assay and DNS enzyme activity assay (Figures 15-16).

3.1.1. Congo Red Assay

Isolated bacterial samples were inoculated on a fresh agar (BH +CMC) with the streaking method and incubated for bacterial growth in appropriate conditions. Then, grown bacterial colonies were stained with Congo Red. In Figure 15, the area surrounding the bacterial colony indicates cellulase enzyme secretion and reflects cellulolytic activity.

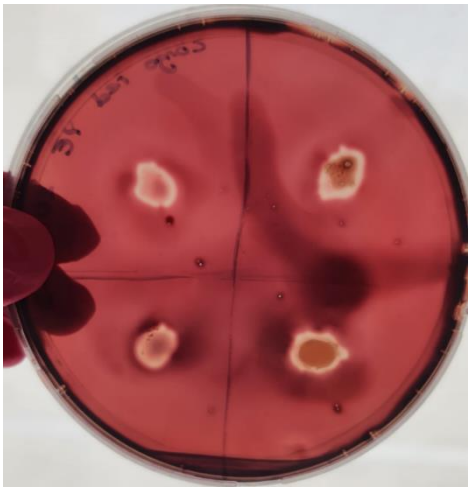

Figure 15. Congo red assay result of the isolated cellulolytic bacteria from the rumen liquid. Zones around colonies result from the breaking of β-glycosidic linkages in the chemical structure of cellulose by the secreted cellulase enzyme from the isolated cellulolytic bacteria (All colonies are replicates of the ROBY strain)

3.1.2. DNS Enzyme Activity Assay

The DNS enzyme activity assay is used for measurements of glucose concentrations. To analyze cellulase enzyme activity at different pH levels (5-9), the extracellular cellulase enzyme was partially isolated. As substrate solution, 1X PBS with 1% CMC (Carboxymethyl cellulose) was prepared with different pH levels ranging from 5 to 9, and enzyme and substrate solvents were mixed in a 1:1 ratio and incubated. Here, the capacity of isolated cellulase enzymes for breaking of cellulose structure at different pH levels was analyzed. Eventually, in Figure 16, slightly acidic environments were observed with higher enzymatic activity of cellulase.

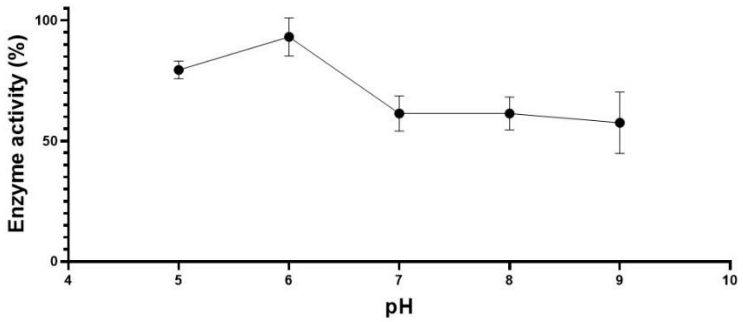

Figure 16. Relative enzyme activity analysis for the partially isolated cellulase enzyme from *A. pittii* was analyzed concerning different pH levels via the DNS enzyme activity assay.

3.1.3. Phylogenetic Analysis with MEGA Software

The isolated bacterial strain was named as *ROBY*. For the species identification, gDNA isolation was accomplished and used for sequencing of the 16S rRNA sequence. The isolated bacteria strain is identified as *Acinetobacter pittii*, and the phylogenetic tree was illustrated with MEGA (Molecular Evolutionary Genetics Analysis) software (Figure 17).

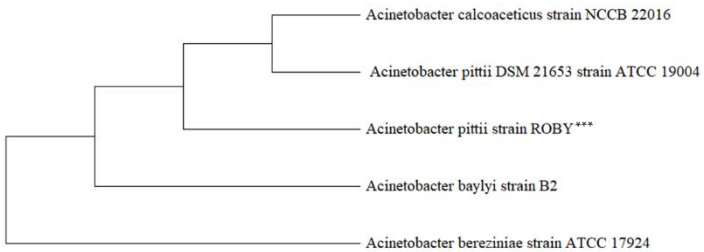

Figure 17. The phylogenetic tree of the isolated cellulolytic bacteria, *Acinetobacter pittii ROBY* strain (Figure was illustrated with MEGA-Molecular Evolutionary Genetics Analysis Software).

3.1.4. Analysis of *ROBY* Strain on SEM

Identification and Characterization of the isolated cellulolytic bacteria, *A. pittii* ROBY strain, was finalized by analysis with a scanning electron microscope (SEM). In this step, the bacteria species were fixed to a conductive surface and analyzed with the THERMOSCIENTIFIC Model: QUATTRO S SEM device at the Boğaziçi University Institute of Biomedical Engineering. In Figure 18, *A. pittii* is shaped like a short rod and has cilia extensions.

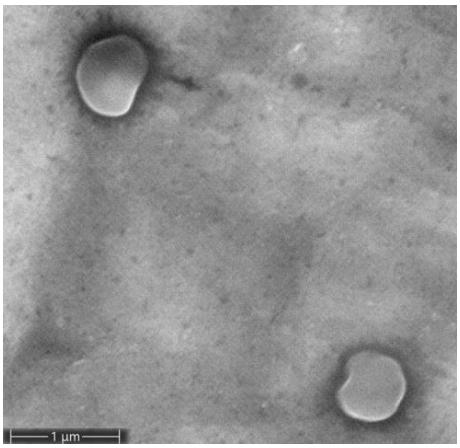

Figure 18. Scanning electron microscope view of the *Acinetobacter pittii* ROBY Strain.

3.2. CELLULOLYTIC ACTIVITY OF ANAEROBIC *RUMINOCOCCUS FLAVEFACIENS* BACTERIA

At the beginning of this study, the usage of a gram-positive anaerobic cellulolytic bacteria was aimed; thus, a cellulolytic anaerobic gram-positive ruminant bacteria species, *Ruminococcus flavefaciens* Sijpesteijn 1948 bacteria strain, was purchased. Similar cellulolytic activity assays were applied as similar to *A. pittii* ROBY strain.

3.2.1. Congo Red Assay

Ruminococcus flavefaciens Sijpesteijn 1948 strain is a strictly anaerobic bacterial species with high cellulolytic activity that originates from the Rumen. The bacteria were grown in an anaerobic environment on agar plates that included 1% Yeast Extract, Bushnell-Haas salt, and 1% CMC. Similar to the results with *A. pittii* ROBY strain, this bacterium was also observed with the secretion of cellulase enzyme, according to the zones around colonies (Figure 19).

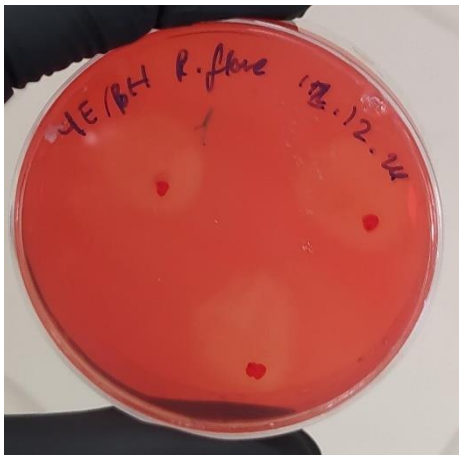

Figure 19. Congo red assay results of *Ruminococcus flavefaciens* Sijpesteijn 1948 strain visualized with zones around colonies, which represent secretion of cellulase enzyme and existence of cellulolytic activity.

3.2.2. DNS Enzyme Activity Assay

To analyze enzymatic activity at different pH levels, the DNS enzyme activity assay was performed similarly to the *A. pittii* ROBY strain. Differently, bacteria were grown in anaerobic liquid media and an anaerobic environment. Partial isolation of extracellular cellulase was performed. Same as the protocol in *A. pittii*, the activity of cellulas was analyzed at various pH values ranging from 5 to 9 (Figure 20). Accordingly, cellulase enzyme activity was higher in slightly acidic environments.

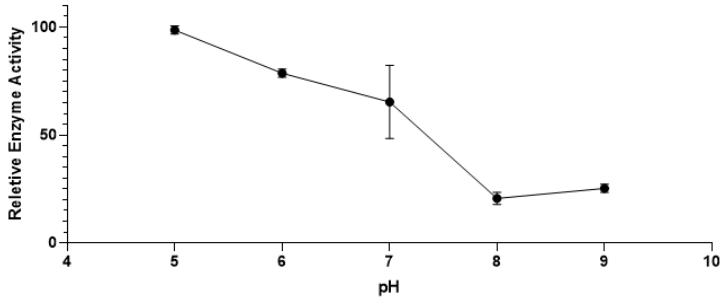

Figure 20. Relative enzyme activity analysis for partially isolated cellulase enzyme from *R. flavefaciens* was analyzed concerning different pH levels via the DNS enzyme activity assay.

3.3. CELLULOSE NANOPARTICLES

3.3.1. Preparation of the Doxorubicin (Dox)

Doxorubicin hydrochloride (579.98 g/mol) was purchased from Sigma-Aldrich with 98% purity and dissolved in a 10 mg/mL concentration with $_{dd}H_2O$. Then, the drug was heated between 25-55˚C and the absorbance spectra at these temperatures were examined with a UV-Vis spectrophotometer in the range of 300-600 nm. In Figure 21, the absorbance of the drug did not show any notable change when examined up to 55˚C. Then, a standard curve of Dox was analyzed at 480 nm with the UV-Vis spectrophotometer at 480 nm in concentrations between 0.1μM and to 5mM (Figure S2).

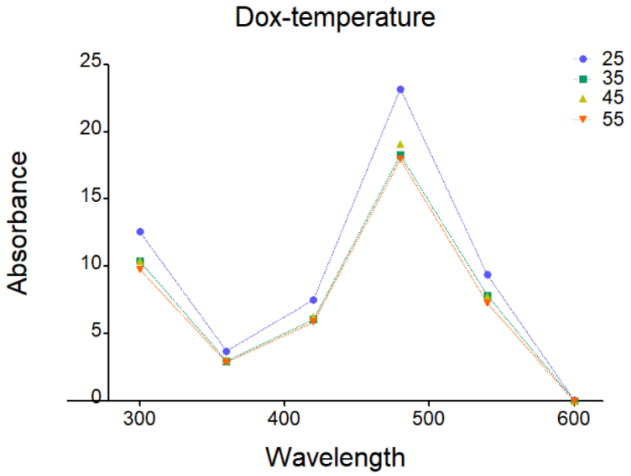

Figure 21. Absorbance value changes of the Doxorubicin drug under conditions of exposure to different temperatures.

3.3.2. Production of CNP by EMIMAc Method

EMIMAc is an ionic solvent, was utilized for the dissolution of the MCC for the production of cellulose nanoparticles (CNP), and entegration of those nanoparticles with Doxorubicin (Dox) chemotherapy drug (Dox-CNP). The produced CNPs (Figure 22A) and Dox-CNP (Figure 22B) with EMIMAc were first analyzed with transmission electron microscopy (TEM) and observed with spherical shapes and a size lower than 500 nm.

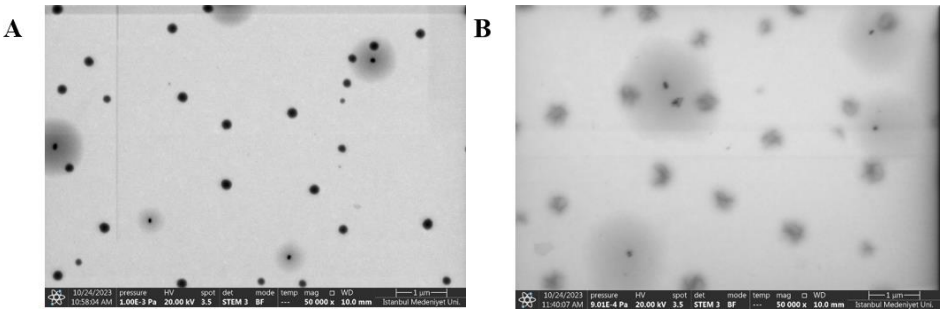

Figure 22. TEM views of (A) free cellulose nanoparticles (CNPs) and (B) Doxorubicin integrated cellulose nanoparticles (Dox-CNP) produced by EMIMAc.

To maintain stability, Tween 85 was added to the nanoparticle solvent. Then, for the size distribution measurement, samples were analyzed with DLS/Zeta sizer at the Boğaziçi University Institute of Biomedical Engineering. In measurements, the refractive index of EMIMAc ($n_{(\ 2\ 0}$ /$D_{)}$ = 1.50) was utilized. In Figure 23A and B, the average size was measured as 2,648 nm for CNP and 2,802 nm for Dox-CNP, and in Figure 23 C and D, the Zeta potential of CNP is measured as 9,661, and the Dox-CNP was measured as 10,31, which shows that nanoparticles produced have in low cationic characteristic.

A) CNP-Dox

Name	Mean	Standard Deviation	RSD	Minimum	Maximum
Z-Average (nm)	2,802	0,05297	1,891	2,741	2,841
Polydispersity Index (PI)	0,2042	0,01325	6,489	0,1889	0,2125
Derived Mean Count Rate (kcps)	204,5	1,344	0,6571	203	205,5
Run Retention (%)	96,11	3,469	3,61	93,33	100

B) CNP-Free

Name	Mean	Standard Deviation	RSD	Minimum	Maximum
Z-Average (nm)	2,648	0,0746	2,817	2,563	2,701
Polydispersity Index (PI)	0,1982	0,02146	10,83	0,1744	0,2159
Derived Mean Count Rate (kcps)	178,3	1,045	0,5864	177,1	179,1
Run Retention (%)	95,67	4,041	4,225	92	100

C) CNP-Dox Zeta

Name	Mean	Standard Deviation	RSD	Minimum	Maximum
Zeta Potential (mV)	10,31	2,846	27,61	7,07	12,42
Zeta Deviation (mV)	21	2,317	11,04	19,6	23,67
Conductivity (mS/cm)	0,3714	0	0	0,3714	0,3714
Quality Factor	0,9305	0,2334	25,08	0,6691	1,118
Number Of Zeta Runs	12	0	0	12	12
Mean Count Rate (kcps)	517,5	0	0	517,5	517,5
Reference Beam Count Rate (kcps)	2326	0	0	2326	2326
Effective Voltage (V)	149,1	0,002374	0,001592	149,1	149,1
Measured Current (mA)	0,8556	0,002	0,2338	0,8535	0,8574
Wall Zeta Potential (mV)	4,719	1,303	27,61	3,242	5,705
Attenuator	8	0	0	8	8

D) CNP-Free Zeta

Name	Mean	Standard Deviation	RSD	Minimum	Maximum
Zeta Potential (mV)	9,661	0,7092	7,34	9,084	10,45
Zeta Deviation (mV)	26,48	2,882	10,88	24,32	29,76
Conductivity (mS/cm)	0,641	0	0	0,641	0,641
Quality Factor	0,7173	0,359	50,05	0,3402	1,055
Number Of Zeta Runs	12	0	0	12	12
Mean Count Rate (kcps)	14,27	0	0	14,27	14,27
Reference Beam Count Rate (kcps)	2386	0	0	2386	2386
Effective Voltage (V)	149,1	0,0006424	0,0004309	149,1	149,1
Measured Current (mA)	1,503	0,005066	0,337	1,499	1,509
Wall Zeta Potential (mV)	3,085	1,21	39,23	1,688	3,801
Attenuator	11	0	0	11	11

Figure 23. DLS/ZetaSizer results of (A) Dox-CNP and (B) CNP, and Zeta potential results of (C) Dox-CNP and (D) CNP produced with EMIMAc.

Further, nanoparticles were analyzed with FT-IR spectroscopy at Boğaziçi University Institute of Biomedical Engineering to observe the integration of Doxorubicin drug

into the cellulose nanoparticle. Both CNP and Dox-CNP were analyzed with FT-IR in Figure 24. The main aim in the measurements with FT-IR spectroscopy is to visualize significant peaks for the Dox drug if non-capsulated or non-integrated Dox exists. In Figure 24, there is no significant peak that shows the existence of free Dox.

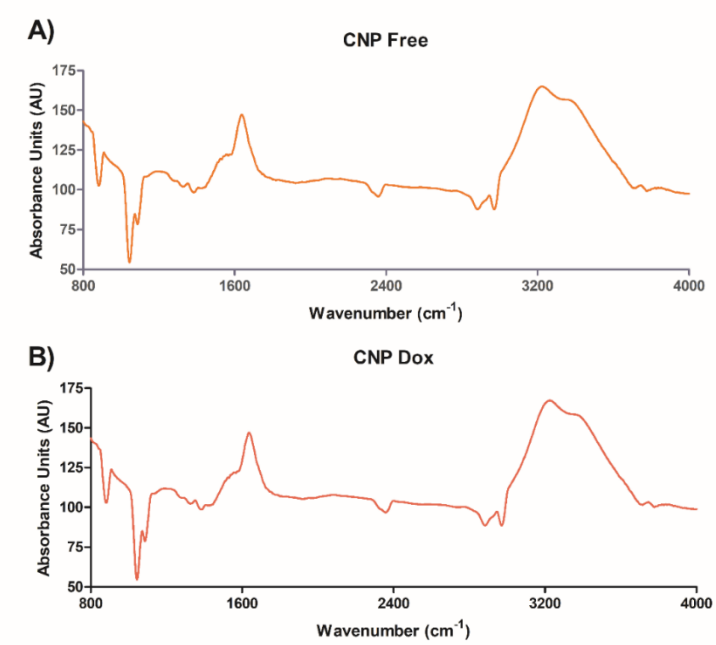

Figure 24. FT-IR spectroscopy results of (A) CNP and (B) Dox-CNP.

3.3.3. Production of CNP by Alkali Solvent Mixture

CNP produced with the EMIMAc method is obtained at a high cost and high toxicity; thus, a new method was generated for CNP production. Here, an alkali solvent mixture that includes 8% NaOH, 6.5% thiourea, and 8% urea was utilized for the decomposition of MCC in the production of cellulose nanoparticles (CNP). Firstly, the size and the morphology of nanoparticles were analyzed through TEM images (Figure 25). According to the collected TEM pictures of nanoparticles, the average size of CNP was calculated as approximately 280 nm.

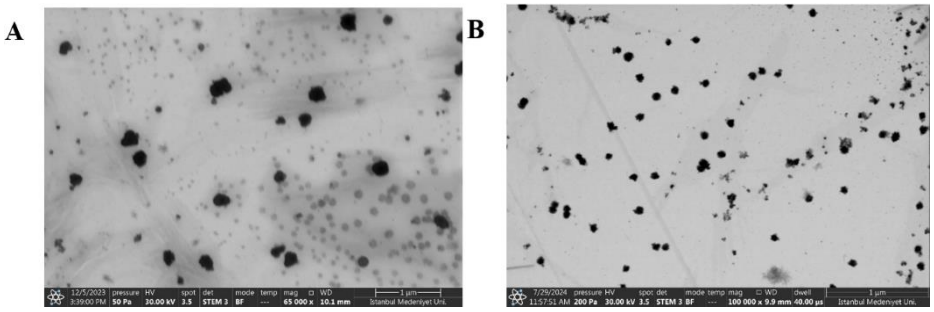

Figure 25. TEM views of (A) CNP and (B) Dox-CNP produced with the Alkali solvent system (NaOH, Thiourea, and Urea). The average CNP size is calculated as 280 nm.

Characterization analysis of the produced nanoparticles was carried out at the Boğaziçi University Institute of Biomedical Engineering. In DLS/ZetaSizer measurements refractive index of salt water was utilized, because, during the CNP production with alkali solvent, there was also a neutralization step that makes the CNP solvent salty. In Figure 26, the size results of the CNP with alkali solvent show that the measured average size of CNP is 836,4 nm and Dox-CNP is 674,2 nm, and the zeta potential of CNP is -0,0151 mV and Dox-CNP is -6,13 mV. Eventually, CNPs produced with Alkali solvents show a slightly anionic or neutral zeta potential.

A

Name	Mean	Standard Deviation	RSD	Minimum	Maximum
Z-Average (nm)	674,2	411,9	61,1	331,2	1131
Polydispersity Index (PI)	0,6927	0,2257	32,58	0,5185	0,9476
Mean Count Rate (kcps)	33,65	1,71	5,082	32,31	35,57

B

Name	Mean	Standard Deviation	RSD	Minimum	Maximum
Z-Average (nm)	836,4	130,4	15,59	729,5	981,6
Polydispersity Index (PI)	0,7727	0,2164	28	0,5469	0,9782
Mean Count Rate (kcps)	31,77	1,856	5,843	30,52	33,9

C

Name	Mean	Standard Deviation	RSD	Minimum	Maximum
Zeta Potential (mV)	-0,0151	0,6129	4060	-0,4144	0,6906
Zeta Deviation (mV)	3,886	1,866	48,01	2,652	6,032
Conductivity (mS/cm)	0,0005893	0	0	0,0005893	0,0005893
Quality Factor	0,251	0,05372	21,4	0,2023	0,3086
Number Of Zeta Runs	12	0	0	12	12
Mean Count Rate (kcps)	53,59	0	0	53,59	53,59
Reference Beam Count Rate (kcps)	2382	0	0	2382	2382
Effective Voltage (V)	149,1	0,001207	0,0008098	149,1	149,1
Measured Current (mA)	-4,237E-05	9,276E-06	21,89	-4,875E-05	-3,173E-05
Wall Zeta Potential (mV)	0,2281	0,9142	400,9	-0,7718	1,021
Attenuator	11	0	0	11	11

D

Name	Mean	Standard Deviation	RSD	Minimum	Maximum
Zeta Potential (mV)	-6,13	0,7106	11,59	-6,899	-5,498
Zeta Deviation (mV)	7,209	3,547	49,2	4,298	11,16
Conductivity (mS/cm)	0,9854	0	0	0,9854	0,9854
Quality Factor	0,8422	0,3317	39,39	0,4606	1,061
Number Of Zeta Runs	12	0	0	12	12
Mean Count Rate (kcps)	5,773	0	0	5,773	5,773
Reference Beam Count Rate (kcps)	2281	0	0	2281	2281
Effective Voltage (V)	149,1	0,001577	0,001058	149,1	149,1
Measured Current (mA)	2,479	0,05785	2,333	2,413	2,518
Wall Zeta Potential (mV)	-5,353	1,698	31,72	-6,381	-3,393
Attenuator	11	0	0	11	11

Figure 26. DLS/ZetaSizer results of (A) Dox-CNP and (B) CNP, and Zeta potential results of (C) Dox-CNP and (D) CNP produced with Alkali solvent.

On the other hand, similar to the EMIMAc method, FT-IR analysis was initiated. Differently, in this trial, free Dox was also added in the same concentration to observe signals belonging to the Doxorubicin drug. In Figure 27, distinct peaks are seen at wave numbers 1100 and 2900 for free Dox; these peak images belonging to doxorubicin are not present in the CNP and DOX-CNP spectra.

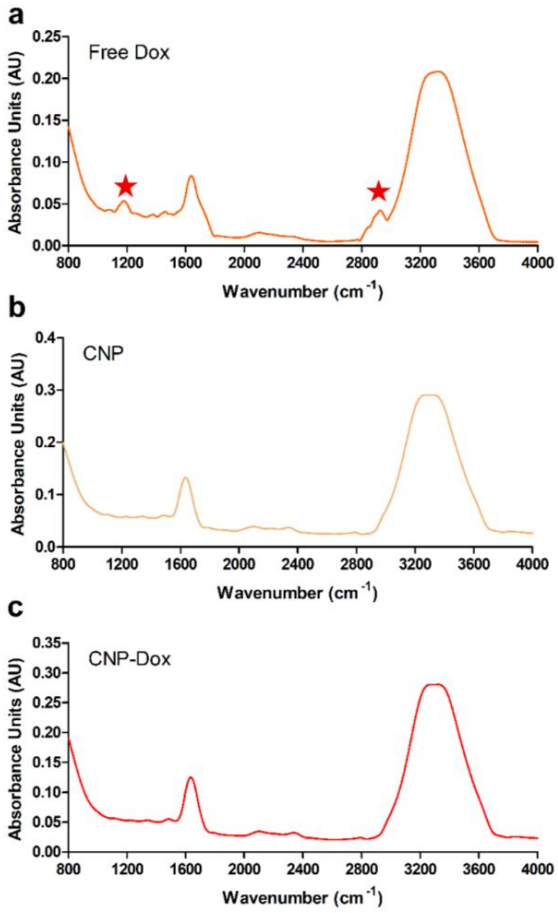

Figure 27. FT-IR results of (A) free Dox, (B) CNP, and (C) Dox-CNP.

3.3.4. Production of Cellulose Nanoparticles with Urea/Thiourea

There was a high salt problem in the method with alkali solvent; the drug was constantly precipitated in the nanoparticle solvent, and the zeta potential was neutral, and stability was not good enough. Thus, a novel nanoparticle production method was accomplished by removing NaOH from the formula and adding a coating layer with CMC to produce anionic cellulose nanoparticles. For this nanoparticle, only characterization analysis was done with TEM (Figure 28). Size of nanoparticles observed below 500 nm in spherical shape, and the background of these nanoparticles was analyzed clearly, unlike the alkali method.

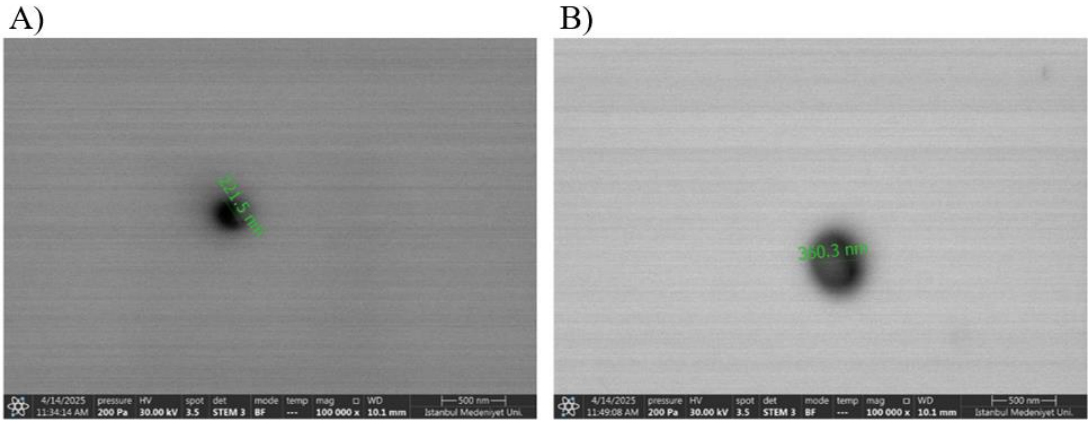

Figure 28. TEM views of (A) CNP and (B) Dox-CNP produced with thiourea and urea and stabilized with CMC.

3.3.5. Comparison of CNP Production Methods

EMIMAc is an ionic solvent that can degrade cellulose; however, it has a high cost. In Table 3, the comparison of EMIMAc and Alkali methods is listed. The newly developed CNP production method is observed with 10 times lower cost than the EMIMAc method. Beyond this, loading capacity, encapsulation efficiency, time to produce nanoparticles, and average size measurements done with SEM were compared for both EMIMAc and Alkali methods and numerically noted in the table. The comparison revealed no significant differences between the two CNP production methods, except for cost.

Table 3. Comparison of cellulose nanoparticles produced with EMIMAc ve Alkali solvents

	EMIMAc	***Alkali***
Cost	37.83$ per mL	3.56$ per mL
Loading Capacity	19.57%	19.38%
Encapsulation Efficiency	97.87%	96.94%
Time	1 week	1 week
Average size	~250 nm	~280 nm

3.4. BACTERIAL CAPACITY TO DEGRADE CNP AND DRUG RELEASE

After isolation and characterization of cellulose-digesting bacterial species, and production of cellulose nanoparticles efficiently, the bacterial capacity to degrade CNP and trigger drug release is analyzed. To investigate the degradation of cellulose nanoparticles by the isolated bacteria (*A. pittii*) and the simultaneous release of Doxorubicin drug, CNP or Dox-CNP (Produced with the Alkali method) were added to Bushnell Haas fluid as a carbon source for the bacteria. The experiment was carried out with 3 repetitions and examined at different pH (6, 6.5, and 7) ranges. The best results were obtained at pH 7.0. Samples were taken from the liquid culture at the end of 1, 3, 4, and 24 hours, diluted, and CFU (Colony forming unit) values were examined by inoculation on agar plates containing 1% YE and 1.6% Agar (VCC assay). As seen in Figure 29, CNP (empty cellulose nanoparticles), DOX-CNP (Doxorubicin-loaded cellulose nanoparticles), and Bushnell Haas growth medium containing the same amount of bacteria and no carbon source were used as a control in the experimental process. When the living cell test is examined in the samples with CNP, an increase in bacterial viability is constantly observed; the samples with Dox-CNP show an increase for a while, but after 3 hours, the viability is reduced; and the control group did not change (Figure 29).

Further, the drug release capacity of enzymes isolated from *A. pittii* and *R. flavefaciens* was analyzed in Figure 30. Enzymatic activity facilitated the release of Dox from the nanoparticles, almost 100% after 24 hours, while there was no significant change in the Dox-CNP without the enzyme. On the other hand, the cumulative release is also analyzed for 24 hours (Figure 31).

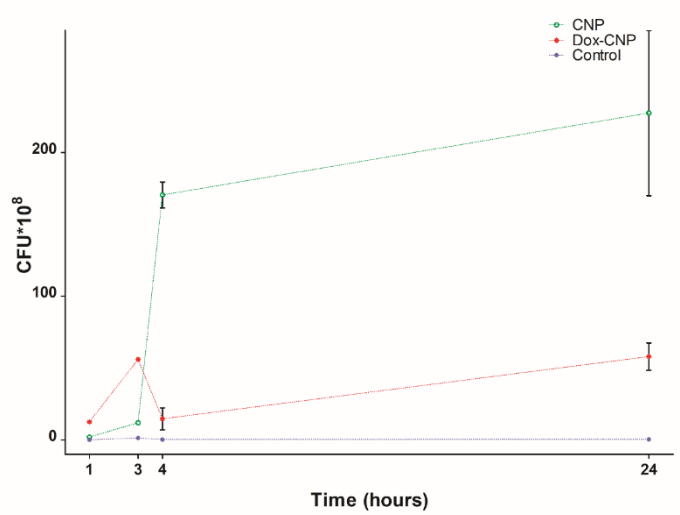

Figure 29. Bacterial capacity for degradation of cellulose nanoparticles is examined in the presence of CNPs and Dox-CNPs with VCC (Viable cell counting assay) by calculating CFU (colony forming units) per mL over time.

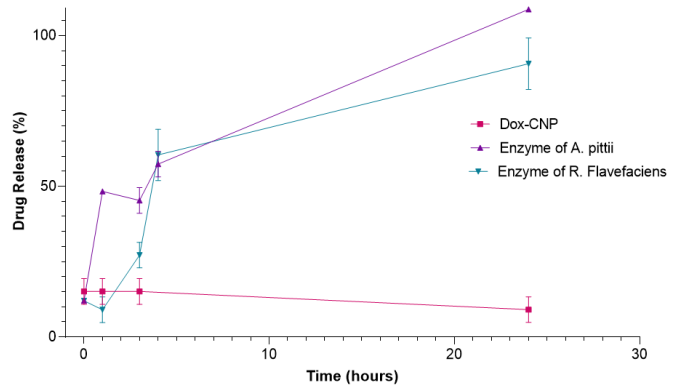

Figure 30. Illustration of the percentage of drug release in the presence of partially isolated enzymes from *A. pittii* and *R. flavefaciens*, compared to the control group containing only Dox-CNP.

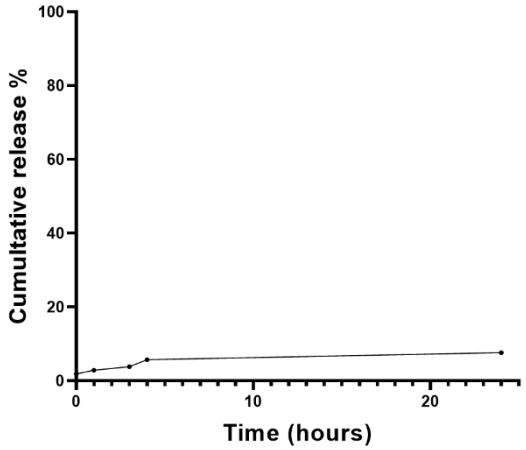

Figure 31. Illustration of the percentage of cumulative release of Dox from the cellulose nanoparticles without an enzyme-triggered mechanism at 37˚C.

3.5. CELL CULTURE

In the cell culture part of the project, the main aim is to apply the newly designed novel targeted drug release method within *in vitro* conditions by using PNT1A (a non-tumorigenic prostate epithelial cell line), LNCaP (a prostate adenocarcinoma epithelial cell line), and Caco-2 (a colorectal adenocarcinoma epithelial cell line). The primary objective of this experimental process is to establish appropriate concentrations for the enzyme and cellulose nanoparticles to carry out this targeted drug release method properly.

3.5.1. Conducting a Preliminary Study to Determine the Values at Which Enzyme and Nanoparticle Can Be Applied Before the Experimental Treatment Method

To determine the appropriate concentration for the treatment with Doxorubicin chemotherapy drug, IC50 analysis was carried out with PNT1A, LNCaP, and CaC0-2 cell lines. For IC50, concentrations between 0.1-1μM were applied, and results were analyzed with the CCK-8 viability assay. In Figure 32, IC50 calculations were illustrated by using GraphPad Prism 8, and IC50 was calculated as 0.07475 μM

(R2=0.9994) for the PNT1A cell line, 0.1784 µM (R2=0.9996) for the CaCo-2 cell line, and 0.1226 µM (R2=0.9945) for the LNCaP cell line.

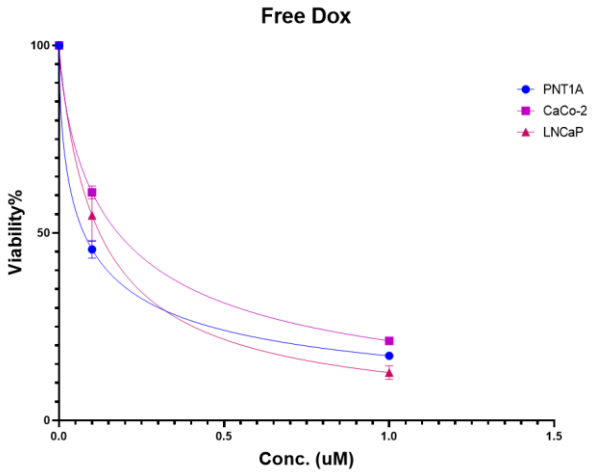

Figure 32. IC50 values for all three cell lines were determined using the CCK-8 viability test in duplicate. This value was calculated as 0.07475 µM (R^2=0.9994) for the PNT1A cell line, 0.1784 µM (R^2=0.9996) for the CaCo-2 cell line, and 0.1226 µM (R^2=0.9945) for the LNCaP cell line.

The intracellular and extracellular enzymes that are isolated from both *A. pittii* and *R. flavefaciens* bacteria were treated on the LNCaP cell line in Figure 33. While the extracellular enzyme isolated from *A. pittii* is observed with high toxicity (~60%), both intracellular and extracellular enzymes isolated from *R. flavefaciens* are observed with much higher viability (>80%).

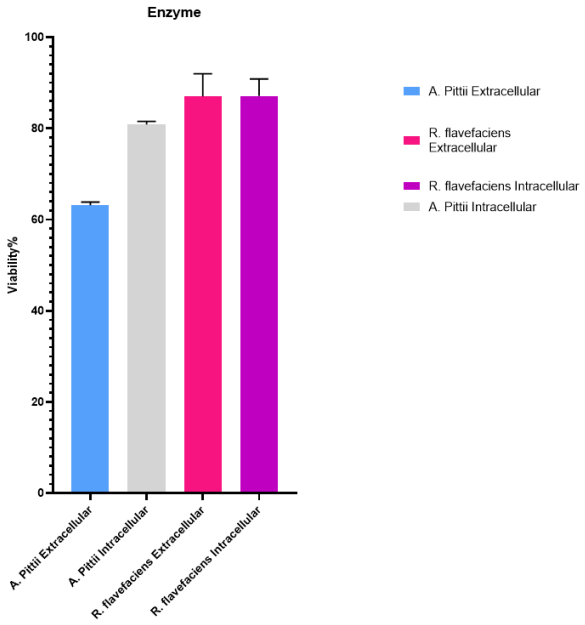

Figure 33. Crystal violet viability assay results of enzymes isolated intracellularly and extracellularly from the *A. pittii* and *R. flavefaciens* bacteria species are illustrated, and the LNCaP cell line was utilized for the viability analysis.

Empty and Doxorubicin-loaded cellulose nanoparticles (CNP and Dox-CNP) produced by Thiourea & Urea solvent are analyzed for their toxicity effect on the LNCaP cell line, and the crystal violet viability assay was utilized. As shown in Figure 34, the viability is significantly reduced in a dose-dependent manner. Further, a coating layer was added to the produced nanoparticle structure as 0.5% of CMC (Carboxymethyl cellulose), which is an anionic structure and is planned to reduce the uptake of nanoparticles by cells. Therefore, in Figure 35, both empty and Dox-loaded cellulose nanoparticles were observed with high cell viability near to 100%.

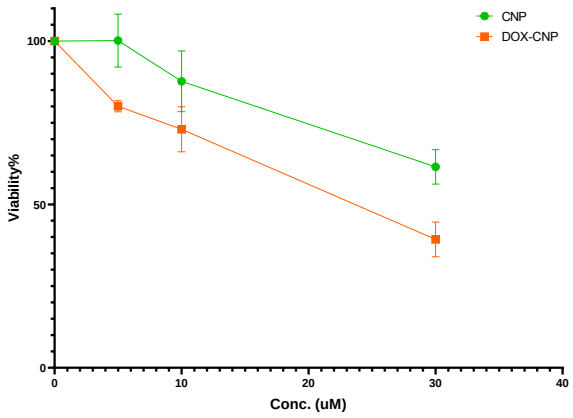

Figure 34. Crystal violet viability assay results of CNP and Dox-CNP without CMC coating, LNCaP cell line.

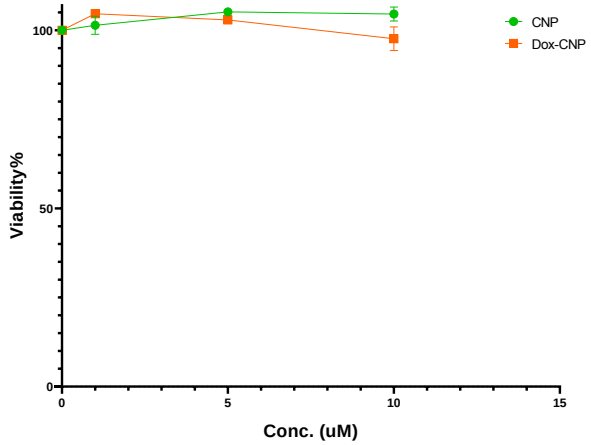

Figure 35. Crystal violet viability assay results of CNP and Dox-CNP with 0.5% CMC coating, LNCaP cell line.

The nanoparticle process is quite long and causes exposure of Dox to chemicals, heat, and sonication that may cause to stop the activity of the Dox. Therefore, TU (Thiourea & Urea)+Dox+heat+ultrasonication combination, Dox+heat+ultrasonication combination, and free Dox were examined at different concentrations for analysis of the drug activity of Dox in the nanoparticle production process. In Figure 36, the usage of chemicals, heat, or ultrasonication does not cause a notable difference in the activity of Dox.

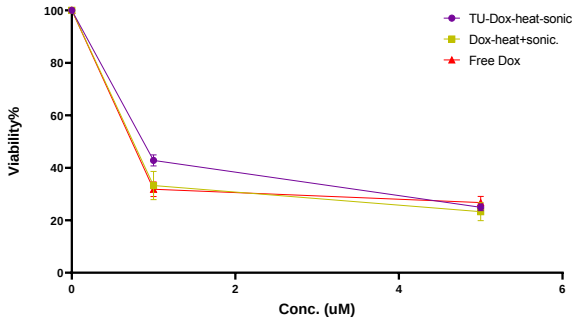

Figure 36. Crystal violet viability test results of treatment with TU (Thiourea & Urea) +Dox+heat+ultrasonication combination, Dox+heat+ultrasonication combination, and free Dox are illustrated. Therefore, chemicals, heat, or ultrasonication in the nanoparticle production process do not change the drug's effectiveness on the LNCaP cell line.

The main experimental treatment aim was to combine cellulose nanoparticles with cellulase enzyme and reveal an enzyme-triggered drug release method for cancer therapy. For this reason, combinations of the intracellularly isolated cellase enzyme from *A. pittii* and cellulose nanoparticles were analyzed with the CCK-8 assay. CNP and enzyme (CE), Dox-CNP and enzyme (DCE), and Dox-CNP and enzyme combination that is incubated for 2 hours before treatment (DCE 2h) were analyzed (Figure 37). However, results do not indicate a significant viability reduction due to the triggered release of the chemotherapy drug. When the partially isolated intracellular enzyme was fresh (Figure S3), a dramatic decrease in viability was observed dose-dependently. However, following replicates of this experiment resulted in insufficient release and high standard deviation between replicates.

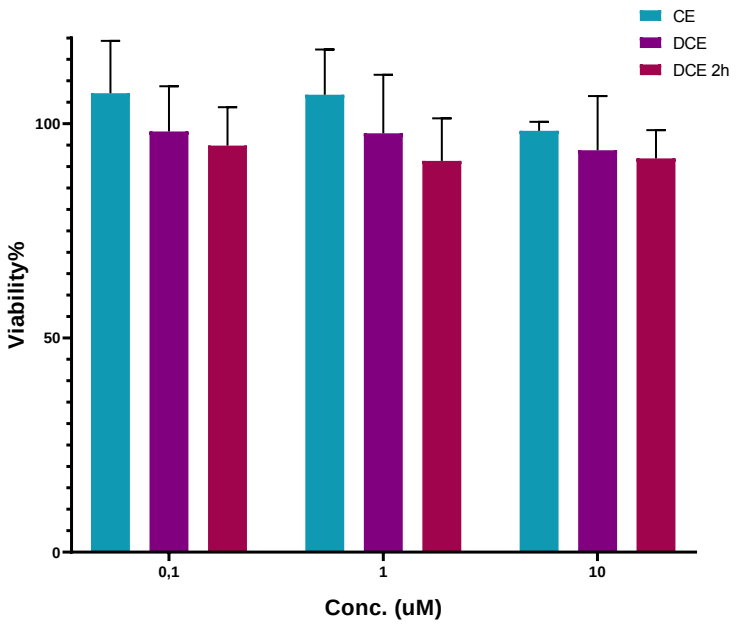

Figure 37. Combinations of the intracellularly isolated cellulase enzyme from *A. pittii* and cellulose nanoparticles were analyzed with the CCK-8 assay. CNP and enzyme (CE), Dox-CNP and enzyme (DCE), and Dox-CNP and enzyme combination that is incubated for 2 hours before treatment (DCE 2h) are analyzed on the LNCaP cell line.

Further, cell uptake of the assay and DAPI staining was performed for the four groups on the CaCo-2 cell line, which are: Control, Free Dox, Dox-CNP, and enzyme (DCE), and fluorescent analysis was generated for DAPI and Dox (Figure 38). DAPI exhibited fluorescence upon binding to DNA, and all groups were visualized in the DAPI. On the other hand, only the Free Dox group exhibited fluorescence in Dox. This experiment also showed that the targeted drug release by the cellulase enzyme was not efficiently carried out.

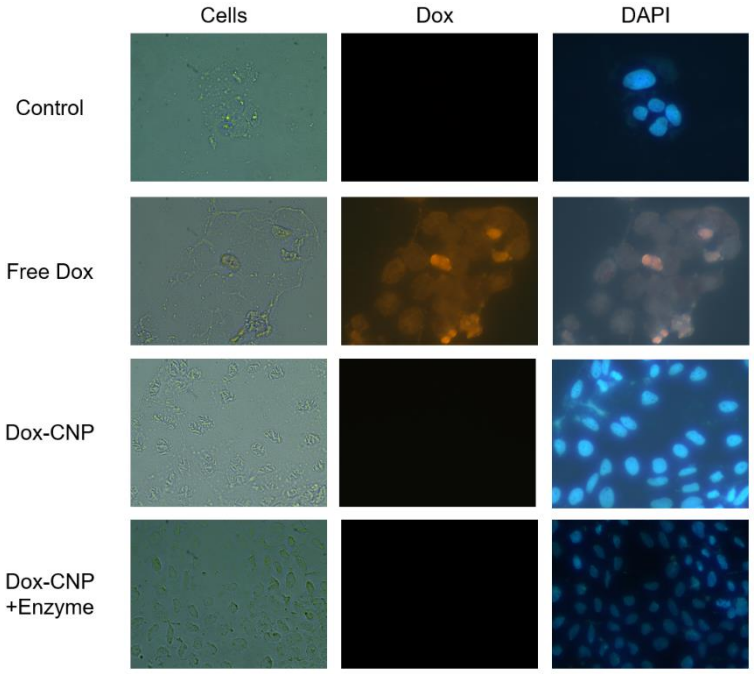

Figure 38. DAPI staining and Dox drug uptake into the cell are analyzed with Fluorescent microscopy with four groups: Control, Free Dox, Dox-CNP, and enzyme (DCE).

4. DISCUSSION

As the predominant biopolymer in nature, cellulose is abundantly found throughout the biosphere and is hardly degraded due to its chemical structure. This biopolymer produces a lot of waste in landfills, especially due to the textile waste, and requires processing on a large scale (Platnieks et al. 2023; Varnaitė-Žuravliova and Baltušnikaitė-Guzaitienė 2024). Thus, the production of cellulose-based biomaterials has gained increasing attention in biotechnology. On account of its low/lack of toxicity and biocompatibility features, cellulose is widely studied in nanotechnological investigations for drug delivery methods (Roman et al. 2010), especially with chemotherapy drugs that have high toxicity (Gülsu and Yüksektepe 2021). Doxorubicin (Dox) chemotherapy drug has an efficient anticancer characteristic, however, it causes serious long-term and short-term multi-organ toxicities. Thus, Dox is the most studied chemotherapy drug with targeted drug delivery systems. For instance, DOXIL and ThermoDox nanoparticles are liposomal nanoparticles encapsulated with Dox. DOXIL uses PEG-coated liposome technology to keep cancer drugs in circulation longer and reduce toxicity in healthy tissues. However, drug release is passive, and access to the tumor depends solely on vascular permeability. ThermoDox is a heat-sensitive liposomal form that provides controlled, rapid drug release by local hyperthermia application. This way, the drug is deposited in high concentration directly at the tumor site, thus increasing efficacy and reducing systemic side effects (Regenold et al. 2022). However, DOXIL nanoparticles use passive targeting, which results in the slow release of the drug, and the released drug concentration might be insufficient in TME. Otherwise, ThermoDox nanoparticles must be combined with local hyperthermia, and most of the clinical trials failed due to the insufficient distribution of heat in the tumor tissue (Dou, Hynynen, and Allen 2017).

Another important innovation in cancer treatment methodology aims to reactivate the immune response. The TME has an immunosuppressive characteristic. In most cancer treatments, after radiotherapy or chemotherapy, antigens are released into the tumor tissue, but they mostly fail to activate an immune response. Direct usage of modified bacteria (such as a genetically weakened *Salmonella* strain) was directly injected into a TME, and increased the antigen content and elevated interactions of tumor antigens and dendritic cells (W. Wang et al. 2022). Other than direct usage, bacteria-based components are also effective for activation of the immune response in TME (M. Zhou et al. 2023).

In this study, the main goal is to generate a targeted drug release therapy by using cellulose nanoparticles (CNP), integrated with Doxorubicin drug, and degradation of CNP by cellulase enzyme secreted by cellulolytic bacteria in cancer cells that is partially isolated from a celluolytic bacteria, and to achieve targeted drug release that is triggered by bacterial enzyme.

For isolation of the cellulolytic bacteria, samples from a bovine rumen were collected from different parts, and samples were inoculated on a specific agar that contains CMC as a carbon source. Further, the grown cellulolytic bacteria are analyzed for their capability to secrete cellulase enzyme; for this reason, the Congo Red assay was utilized. Congo Red mainly binds to the β-glucosidic bonds in the chemical structure of cellulose and helps to degrade cellulose into glucose monomers (Sariboga and Sarioglu 2024b). In Figure 15, the isolated bacterial species called ROBY strain was observed with zones around colonies after staining with Congo Red dye. Therefore, this result shows that the isolated bacteria can degrade cellulose and can secrete the cellulase enzyme, and degrade the cellulose structure.

Further, the enzymatic activity of the cellulase in the ROBY strain was analyzed with the 3,5-dinitrosalicylic acid (DNS) enzyme activity assay. The DNS dye is mainly used for the analysis of the enzymatic activation of cellulase or xylanase (Sinegani and Emtiazi 2006; Bailey, Biely, and Poutanen 1992). The DNS enzyme activity assay is a common method used for colorimetric measurements of reducing sugars, and cellulase enzyme results in reducing sugar by breaking β-glycosidic bonds in the cellulose structure. By using this mechanism, cellulase enzyme activity at different pH

levels was analyzed, and in Figure 16, slightly acidic pH levels resulted in higher enzymatic activities.

After observations in the enzyme activity assay, the isolated bacteria species were identified with the sequencing of 16S rRNA and species identification. Then, the bacteria were identified as *Acinetobacter pittii* species in genus *Acinetobacter*, and is a gram gram-positive, strict anaerobes, short-rod shaped, oxidase-negative, catalase-positive, and non-motile bacteria (Sariboga and Sarioglu 2024b). Also, *A. pittii* is an opportunistic pathogen that can cause infection, especially in immunocompromised individuals, assessed within the scope of Biosafety Level 2. It is frequently seen in hospital-acquired isolates and is known for its resistance to multiple antibiotics and disinfectants (Tierney et al. 2022). Thus, this bacterium is not a good option for cancer therapy methods for *in vitro* or *in vivo* studies in the future. Therefore, we decided to partially isolate the enzyme from the bacteria and use it for the treatments. However, there is still a risk for toxicity due to the toxic outcomes of this bacterium extracellularly.

For this reason, another bacterial species that originates from the rumen, *Ruminococcus flavefaciens* Sijpesteijn 1948 strain, was obtained from the Leibniz Institute DSMZ-German Collection of Microorganisms and Cell Cultures GmbH. In Figures 19 and 20, the enzyme activity assays, Congo Red and DNS enzyme activity assay, were applied for *R. flavefaciens*, and the bacteria were observed with an appropriate enzymatic activity. In Figure 9, the Congo Red assay result indicates the secretion of the cellulase enzyme extracellularly and degrades cellulose, and in Figure 20, the enzymatic activity was observed to be higher in slightly acidic conditions. Since TME has a slightly acidic environment, we expect to observe better drug release in TME.

Another important part of this project is to produce cellulose nanoparticles (CNP) with microcrystalline cellulose (MCC). For this reason, a CNP model was produced by using an ionic liquid, 1-Ethyl-3-methylimidazolium acetate (EMIMAc), with a similar method of Al Hakkak et al. (2019) (Al Hakkak et al. 2019). With EMIMAc, both empty (CNP) and Dox-loaded (Dox-CNP) cellulose nanoparticles were produced, and their characterizations were done with TEM, FT-IR, and DLS/ZetaSizer. According to the

size and morphology analysis of CNPs with TEM showed that CNPs were produced in spherical shape and have an average size is ~250 nm. On the other hand, size and zeta potential results showed that the size average of CNP is 2,802 nm. Before the measurement of the average size of CNPs, Tween 85 was added to the nanoparticle solvent to provide nanoparticle stability (Gülsu and Yüksektepe 2021). However, this addition changed the nanoparticle solvent into a blurred color, and during measurements, the refractive index of EMIMAc was utilized, which probably led to inaccurate measurements. Also, the zeta potential results are measured in low anionic characteristic ($Zeta_{Dox\text{-}CNP}$: 10,31 and ZetaCNP: 9,661). Mammalian cells have an anionic cell surface, and to prevent non-specific uptake of CNPs into the cells, the produced nanoparticle should have a much anionic characteristic (Verma and Stellacci 2010).

Further, nanoparticles were analyzed with FT-IR to analyze the efficiency of the integration of Dox in the nanoparticles. In Figure 24, FT-IR spectroscopy results of empty (CNP) and doxorubicin-loaded (CNP-Dox) cellulose nanoparticles are included. According to the literature, distinct peaks specific to doxorubicin are expected to be observed in the wavenumber range of 800–4000 cm^{-1}, and some prominent peaks observed commonly at FT-IR measurements of Dox, which are; at 3331 cm^{-1} (N–H stretching), 3525cm^{-1} (O–H stretching), 2935 cm^{-1} and 2897 cm^{-1} (C–H stretching), and 1729 cm^{-1} (C = O stretching) (Sariboga and Sarioglu 2024b; Bansal, Singh, and Kaur 2021). In Figure 24, measurements were graphed using GraphPad Prism 5 software, and appropriate curve fitting operations were performed on the spectra. Consequently, there is no significant peak that belongs to the Dox, which probably shows that the Dox was successfully integrated into the cellulose structure and does not exist freely in the nanoparticle solution. Further, those nanoparticles were tried on cell culture, and observed with high toxicity, and a different CNP production method was developed.

The produced nanoparticle with the EMIMAc method had a high cost (37.83$ per mL), cationic potential, and high toxicity on cells (tried on Ca-Co-2 cell line). Therefore, a new method was developed by the dissolution of MCC with an alkali solvent (NaOH/Thiourea/Urea) with the support of heat and ultrasonication. Firstly, nanoparticles were examined with TEM views as shown in Figure 25, thus, first

measurements were initiated on the TEM figures, and the average size of nanoparticles was calculated as ~280 nm. Further, cells were analyzed with DLS/ZetaSizer. In Figure 26, zeta potentials of nanoparticles were observed as near neutral, which shows that nanoparticles stability is not good enough. Due to their unstable form, the nanoparticles showed agglomeration, and their average size was measured at more than 500 nm, which is not appropriate. In this study, we want to use the enhanced permeability and retention (EPR) effect in the TME for passive targeting and accumulation of cellulose nanoparticles in the tumor microenvironment. Therefore, the stability must be improved. Also, FT-IR analysis results are observed in Figure 27, which shows results for free Dox, CNP, and Dox-CNP. In free Dox, two significant peaks are analyzed and marked with the red star, the first one observed at around 1200 cm^{-1}, which probably indicates signals for C–O–C stretch, and the other signal is around 2900 cm^{-1}, which probably represents C–H stretching signals for Dox (Bansal, Singh, and Kaur 2021). On the other hand, there are no visible peaks in the Dox-CNP that belong to Dox, and signals from both CNP and Dox-CNP are observed to be similar to each other. Consequently, we estimated that the drug was successfully integrated into the nanoparticles with the Alkali method.

Then, two nanoparticle production methods were compared with each other in Table 3. In cost, Alkali solvent was produced for 3.56$ per mL and EMIMAc solvent was produced for 37.83$ per mL; thus, the Alkali method gives a 10 times cheaper method for nanoparticle production. Otherwise, their loading capacity (LC_{EMIMAc}: 19.57% and LC_{Alkali}: 19.38%), encapsulation efficiency (E_{EMIMAc}: 97.87% and E_{Alkali}: 96.94%), process time (1 week for both), and average size (S_{EMIMAc}: ~250 nm and S_{Alkali}: ~280 nm) were not observed with significant changes. However, the Alkali method showed lower toxicity than EMIMAc on bacteria; thus, CNP and Dox-CNP with the Alkali method were utilized for bacterial capacity to degrade CNPs.

Bacterial and/or enzymatic degradation of cellulose nanoparticles and drug release is another important concept in our study. *R. flavefaciens* is a slow-growing anaerobic bacterium and not easy to handle; also, the isolated cellulolytic bacterium *A. pittii* is an aerobic bacterium that grows fastly and is much easier to handle. Thus, *A. pittii* ROBY strain was utilized for the analysis of bacterial capacity to digest CNP and release of Dox drug. The experiment was carried out with 3 repetitions and examined

at different pH (6, 6.5, and 7) ranges. In the experimental process, BH salt was used as a medium, however, only carbon source addition was generated with either CNP or Dox-CNP. The best results were obtained at pH 7.0, and results and the other replicates of the experiment were carried out at pH 7. Samples were taken from the liquid culture at the end of 1, 3, 4, and 24 hours, diluted, and a Viable Cell Counting (VCC) assay was performed by examination of CFU (Colony forming unit) values, and results were illustrated with GraphPad Prism 8. In Figure 29, the graphic shows VCC results of CNP, Dox-CNP, and control. In the first hours, both CNP and Dox-CNP included bacteria samples showed an increase in their viability, and after 3rd hour, bacterial viability of the sample with Dox-CNP was significantly reduced. Here, the constant increase in viability in CNP shows that bacteria can utilize CNP as a carbon source to indicating that these bacteria can disrupt cellulose in CNP. Otherwise, the sample with Dox-CNP is observed with reduced viability after the 3rd hour, indicating that the bacteria can disrupt and degrade CNP and release Doxorubicin drug, and owing to the antibacterial characteristic of Doxorubicin, the viability of bacteria significantly decreases.

Otherwise, partially isolated enzymes from both bacterial strains were also combined with Dox-CNP to analyze targeted release of the drug from nanoparticles. In this concept, a 24-hour study was conducted on Dox-CNP as control, Dox-CNP+ Enzyme of *A. pittii*, and Dox-CNP+ Enzyme of *R. flavefaciens*, to examine drug release in a time-dependent manner. In Figure 30, results were illustrated by using GraphPad Prism 8. Releasing % of Dox-CNP remained constant in the absence of enzymes, and in the presence of enzymes (at pH 6.5) of both bacterial strains, almost 100% of drug release was initiated. Also, in Figure 31, the cumulative release of Dox is analyzed at 37˚C. The cumulative release was detected in minimal percentages.

CNP produced by Alkali solvent was much better than the one with EMIMAc; however, over time, Dox precipitated in the Alkali solvent and showed toxicity in cell culture studies. In the alkali solvent system, there are 8% NaOH, 6.5% Thiourea, and 8% urea exist, and after dissolution of MCC with alkali solvent, the mixture was neutralized with HCl, which causes high concentrations of salt in the solvent, and this salt concentration was reduced by applying a cold centrifuge. However, there is still salt in the solvent that causes aggregation of the drug. Therefore, we tried a new

method by reducing the percentages of thiourea and urea to 4% and removing NaOH from the formula, and generated the finalized nanoparticle production method, TU-CNPs. In Figure 28, TEM views of TU-CNP showed a much clearer background than the Alkali one (Figure 25), and the nanoparticles were successfully produced in spherical shapes, and for negative coating layer, 0.5% CMC was utilized in the nanoparticle production and this method reduced uptake of CNP by cells and diminished its toxicity thanks to newly synthesized CNP.

The cell culture is the most important part of the project that examines the targeted drug release method under *in vitro* conditions. Cell culture studies were started with IC50 analysis of Doxorubicin at different concentrations, in order to decide appropriate drug concentrations before the targeted therapy method trials. In order to get results with higher accuracy, IC50 analysis was performed with CCK-8 viability assay, and results were calculated with GraphPad Prism 8; as 0.07475 μM (R^2=0.9994) for the PNT1A cell line, 0.1784 μM (R^2=0.9996) for the CaCo-2 cell line, and 0.1226 μM (R^2=0.9945) for the LNCaP cell line (Figure 32). Also, *A. pittii* bacteria was tried for three times, however, each experiment resulted in high toxicity on mammalian cell and overgrowth of the bacteria, further, mammalian culture media, high glucose DMEM, was replaced with low glucose DMEM, but did not stop the overgrowth of bacteria and toxicity due to the bacteria. Unfortunately, bacteria were also visualized in the viability assays (Both CCK-8 and Crystal Violet viability assays were experienced) and led to inaccurate readings in cell viability assays. Thus, results for bacterial usage could not be included.

On the other hand, *in vitro* methods were not appropriate for the growth, survival, or activity of the *R. flavefaciens*, because *R. flavefaciens* is a strict anaerobic bacterium and can not survive in the presence of oxygen, and *in vitro* conditions of LNCaP, CaCo-2, or PNT1A cell lines can not be arranged anaerobically, which could cause nonspecific death of the mammalian cells. Thus, only a partially isolated enzyme was utilized from this bacterium; however, because of the slow growth rate of the bacteria, the enzyme isolation could not be carried out appropriately. Otherwise, it is known that the tumor microenvironment has an anaerobic condition, and *in vivo* studies may be promising since the bacterium can be given through the tumor microenvironment of colorectal cancer and prostate cancer, and show a better enzymatic activity (W.

Wang et al. 2022). Owing to the slow growth of *R. flavefaciens*, it would not survive and cause infection in the TME, and the drug (Dox) that is released with secreted enzymes by the bacteria has a great antibiotic characteristic that would also kill the bacteria and reduce the infection risk. However, we believe that this experiment's purpose would be achieved only if the treatment were carried out with *in vivo* studies.

Enzymes from both bacterial strains are partially isolated either intracellularly or extracellularly, and the viability test results of those enzymes are illustrated as a barr graph with GraphPad Prism 8, in Figure 33, and enzymes from *R. flavefaciens* are observed with higher viability compared to the enzymes of *A. pittii*, however, due to the slow growth of *R. flavefaciens*, enzyme isolation was limited and in Figure 30, drug release capacity of *A. pittii* was observed quite higher than enzyme of *R. flavefaciens*. Thus, combinations of CNP and enzymes are initiated with partially and intracellularly isolated cellulase enzymes of *A. pittii*.

Before the combination of cellulase enzyme and CNPs in cell culture, preliminary analysis was conducted at different concentrations of CNP produced by TU solvent. In Figure 34, both CNP and Dox-CNP cause a dose-dependent reduction in the viability. This mechanism is probably due to a similar problem that we faced in nanoparticles with Alkali solvents, which was due to the inappropriate zeta potential of the nanoparticles. After this estimation, an anionic coating method for nanoparticles was searched, and 0.5% CMC was added to the CNP formula of TU-CNP (L. Zhou et al. 2014). Eventually, in Figure 35, the toxicity was improved with the addition of a CMC coating layer. Further, several combination studies were conducted with nanoparticle and enzyme combinations, however, the targeted drug release was not successfully carried out. Since the CNP production method includes exposure to chemicals, heating, and ultrasonication, which may cause deficiencies in the activity of the integrated drug. Thus, chemicals (TU), heat, and ultrasonication (sonic) in the CNP production method were arranged with Dox and without CNP on the LNCaP cell line. In Figure 36, there is no significant difference in the viability of those control groups when compared to the free Dox, which indicates that the CNP production method does not cause problems in the drug release process.

Further, combinations of CNP and enzyme (CE), Dox-CNP and enzyme (DCE), and Dox-CNP and enzyme combination that is incubated for 2 hours before treatment

(DCE 2h) are analyzed on the LNCaP cell line to observe whether pretreatment supports the release of Dox or not, and results are illustrated in Figure 37. However, the targeted release of Doxorubicin was not successfully achieved under *in vitro* conditions. When the partially isolated intracellular enzyme was fresh (Figure S3), a dramatic decrease in viability was observed dose-dependently. However, subsequent replicates of this experiment showed insufficient release and a high standard deviation among replicates, which is likely due to a decline in enzyme activity over time (Figure 37). Also, Figure 38 shows cellular uptake results of Dox with DAPI staining; however, we could not observe a targeted drug release that is triggered by enzymatic activity. Since no issues were observed during the nanoparticle production process (Figure 36), it is considered that the failure related to targeted release may be attributed to the partially isolated enzyme. Firstly, the isolation process of the enzyme was conducted partially, with really low purity, and since cellulase enzyme production is not the main mechanism of *A. pittii*, we estimate that cellulase enzyme production by this enzyme is limited, and in low quantities. Therefore, the major problem may be the enzyme isolated in low purity. Secondly, the DNS enzyme activity assays for both bacterial strains (Figure 16 and Figure 20) are observed in higher activity in an acidic environment; however, in cell culture conditions, cells mostly have neutral pH levels. Thus, the usage of enzymatic activity under *in vivo* conditions would give better results since the tumor microenvironments show acidic pH, which can increase enzymatic activity (Justus, Dong, and Yang 2013).

To conclude, this study presents an innovative cancer treatment approach that combines cellulolytic activity with cellulose-based nanoparticles for targeted drug delivery within the tumor microenvironment. The use of bacteria or bacterial substances in cancer treatments sounds challenging to many people. The main problem in cancer treatment failure is the exhausted immune system of humans, and several investigations use bacteria directly in the TME to reactivate the immune system at TME (S. Li et al. 2022). Thus, the usage of bacteria and/or bacterial substances, such as enzymes, can increase immune response in TME. In our study, we planned a microbial degradation of nanoparticles specifically in the tumor microenvironment. For this purpose, we isolated a bacterium with cellulolytic characteristics. Then, a brand-new cellulose nanoparticle production method was developed, and the

Doxorubicin chemotherapy drug was integrated within the nanoparticles. The isolated bacteria and the partially isolated cellulase enzyme from the bacteria were analyzed, with their nanoparticle degradation and drug release performance were analyzed, and successfully carried out. Otherwise, when the same conditions were tested under *in vitro* conditions, the targeted release could not be carried out successfully. The main problem in the failure of the cell culture part is estimated to be the low purity of the cellulase enzyme, and the requirement for acidic environments for higher activity of the cellulase enzyme.

5. REFERENCES:

Abbas, Zaigham, and Sakina Rehman. 2018. “An Overview of Cancer Treatment Modalities.” *Neoplasm* 1: 139–57.

Afsar, Tayyaba, Suhail Razak, Ali Almajwal, and Dara Al-Disi. 2020. “Doxorubicin-Induced Alterations in Kidney Functioning, Oxidative Stress, DNA Damage, and Renal Tissue Morphology; Improvement by Acacia Hydaspica Tannin-Rich Ethyl Acetate Fraction.” *Saudi Journal of Biological Sciences* 27 (9): 2251–60. doi:10.1016/j.sjbs.2020.07.011.

Alam Khan, Shah, and Md Jawaid Akhtar. 2022. “Structural Modification and Strategies for the Enhanced Doxorubicin Drug Delivery.” *Bioorganic Chemistry* 120 (March): 105599. doi:10.1016/j.bioorg.2022.105599.

Alhowail, Ahmad H., and Maha A. Aldubayan. 2023. “Doxorubicin Impairs Cognitive Function by Upregulating AMPAR and NMDAR Subunit Expression and Increasing Neuroinflammation, Oxidative Stress, and Apoptosis in the Brain.” *Frontiers in Pharmacology* 14 (November). doi:10.3389/fphar.2023.1251917.

Ashique, Sumel, Navjot Kaur Sandhu, Viney Chawla, and Pooja A. Chawla. 2021. “Targeted Drug Delivery: Trends and Perspectives.” *Current Drug Delivery* 18 (10): 1435–55. doi:10.2174/1567201818666210609161301.

Awais, Habib, Yasir Nawab, Adnan Amjad, A. Anjang, Hazizan Md Akil, and M. Shukur Zainol Abidin. 2021. “Environmental Benign Natural Fibre Reinforced Thermoplastic Composites: A Review.” *Composites Part C: Open Access* 4 (March): 100082. doi:10.1016/j.jcomc.2020.100082.

BÃ©guin, Pierre, and Jean-Paul Aubert. 1994. “The Biological Degradation of Cellulose.” *FEMS Microbiology Reviews* 13 (1): 25–58. doi:10.1111/j.1574-6976.1994.tb00033.x.

Bailey, Michael J., Peter Biely, and Kaisa Poutanen. 1992. “Interlaboratory Testing of Methods for Assay of Xylanase Activity.” *Journal of Biotechnology* 23 (3): 257–70. doi:10.1016/0168-1656(92)90074-J.

Bansal, Ranju, Ranjit Singh, and Khushpal Kaur. 2021. “Quantitative Analysis of Doxorubicin Hydrochloride and Arterolane Maleate by Mid IR Spectroscopy Using Transmission and Reflectance Modes.” *BMC Chemistry* 15 (1): 27. doi:10.1186/s13065-021-00752-3.

Bayer, Edward A, Henri Chanzy, Raphael Lamed, and Yuval Shoham. 1998. "Cellulose, Cellulases and Cellulosomes." *Current Opinion in Structural Biology* 8 (5): 548–57. doi:10.1016/S0959-440X(98)80143-7.

Besse, Helena, Angelique Barten-van Rijbroek, Kim van der Wurff-Jacobs, Clemens Bos, Chrit Moonen, and Roel Deckers. 2019. "Tumor Drug Distribution after Local Drug Delivery by Hyperthermia, In Vivo." *Cancers* 11 (10): 1512. doi:10.3390/cancers11101512.

Bhaduri, S, and P H Demchick. 1983. "Simple and Rapid Method for Disruption of Bacteria for Protein Studies." *Applied and Environmental Microbiology* 46 (4): 941–43. doi:10.1128/aem.46.4.941-943.1983.

Blackadar, Clarke Brian. 2016. "Historical Review of the Causes of Cancer." *World Journal of Clinical Oncology* 7 (1): 54. doi:10.5306/wjco.v7.i1.54.

Böhme, David, and Annette G. Beck- Sickinger. 2015. "Drug Delivery and Release Systems for Targeted Tumor Therapy." *Journal of Peptide Science* 21 (3): 186–200. doi:10.1002/psc.2753.

Cannarella, Rossella, Rosita A. Condorelli, Federica Barbagallo, Sandro La Vignera, and Aldo E. Calogero. 2021. "Endocrinology of the Aging Prostate: Current Concepts." *Frontiers in Endocrinology* 12 (February). doi:10.3389/fendo.2021.554078.

Cao, Yu, and Huimin Tan. 2002. "Effects of Cellulase on the Modification of Cellulose." *Carbohydrate Research* 337 (14): 1291–96. doi:10.1016/S0008-6215(02)00134-9.

Carvalho, Cristina, Renato Santos, Susana Cardoso, Sonia Correia, Paulo Oliveira, Maria Santos, and Paula Moreira. 2009. "Doxorubicin: The Good, the Bad and the Ugly Effect." *Current Medicinal Chemistry* 16 (25): 3267–85. doi:10.2174/092986709788803312.

Ciolacu, Diana Elena, Raluca Nicu, and Florin Ciolacu. 2020. "Cellulose-Based Hydrogels as Sustained Drug-Delivery Systems." *Materials* 13 (22): 5270. doi:10.3390/ma13225270.

Clemons, Tristan D., Ruhani Singh, Anabel Sorolla, Nutan Chaudhari, Alysia Hubbard, and K. Swaminatha Iyer. 2018. "Distinction Between Active and Passive Targeting of Nanoparticles Dictate Their Overall Therapeutic Efficacy." *Langmuir* 34 (50): 15343–49. doi:10.1021/acs.langmuir.8b02946.

Collard, François-Xavier, and Joël Blin. 2014. "A Review on Pyrolysis of Biomass Constituents: Mechanisms and Composition of the Products Obtained from the Conversion of Cellulose, Hemicelluloses and Lignin." *Renewable and Sustainable Energy Reviews* 38 (October): 594–608. doi:10.1016/j.rser.2014.06.013.

Czerwińska-Główka, Dominika, and Katarzyna Krukiewicz. 2021. “Guidelines for a Morphometric Analysis of Prokaryotic and Eukaryotic Cells by Scanning Electron Microscopy.” *Cells* 10 (12): 3304. doi:10.3390/cells10123304.

Dallas, Nikolaos A., Ling Xia, Fan Fan, Michael J. Gray, Puja Gaur, George van Buren, Shaija Samuel, Michael P. Kim, Sherry J. Lim, and Lee M. Ellis. 2009. “Chemoresistant Colorectal Cancer Cells, the Cancer Stem Cell Phenotype, and Increased Sensitivity to Insulin-like Growth Factor-I Receptor Inhibition.” *Cancer Research* 69 (5): 1951–57. doi:10.1158/0008-5472.CAN-08-2023.

Delpy, E. 1999. “Doxorubicin Induces Slow Ceramide Accumulation and Late Apoptosis in Cultured Adult Rat Ventricular Myocytes.” *Cardiovascular Research* 43 (2): 398–407. doi:10.1016/S0008-6363(99)00142-X.

Demidenko, Zoya N., Lioubov G. Korotchkina, Andrei V. Gudkov, and Mikhail V. Blagosklonny. 2010. “Paradoxical Suppression of Cellular Senescence by P53.” *Proceedings of the National Academy of Sciences* 107 (21): 9660–64. doi:10.1073/pnas.1002298107.

Dou, Yannan, Kullervo Hynynen, and Christine Allen. 2017. “To Heat or Not to Heat: Challenges with Clinical Translation of Thermosensitive Liposomes.” *Journal of Controlled Release* 249 (March): 63–73. doi:10.1016/j.jconrel.2017.01.025.

Fares, Jawad, Mohamad Y. Fares, Hussein H. Khachfe, Hamza A. Salhab, and Youssef Fares. 2020. “Molecular Principles of Metastasis: A Hallmark of Cancer Revisited.” *Signal Transduction and Targeted Therapy* 5 (1): 28. doi:10.1038/s41392-020-0134-x.

Fernandes, Pedro. 2018. “Enzymatic Processing in the Food Industry.” In *Reference Module in Food Science*. Elsevier. doi:10.1016/B978-0-08-100596-5.22341-X.

Formaggio, Nicolò, Mark A. Rubin, and Jean-Philippe Theurillat. 2021. “Loss and Revival of Androgen Receptor Signaling in Advanced Prostate Cancer.” *Oncogene* 40 (7): 1205–16. doi:10.1038/s41388-020-01598-0.

Fujita, Kazutoshi, and Norio Nonomura. 2019. “Role of Androgen Receptor in Prostate Cancer: A Review.” *The World Journal of Men’s Health* 37 (3): 288. doi:10.5534/wjmh.180040.

Ghasemi, Mohammad, Marina Tsianou, and Paschalis Alexandridis. 2017. “Assessment of Solvents for Cellulose Dissolution.” *Bioresource Technology* 228 (March): 330–38. doi:10.1016/j.biortech.2016.12.049.

Gülsu, Aydan, and Ecem Yüksektepe. 2021. “Preparation of Spherical Cellulose Nanoparticles from Recycled Waste Cotton for Anticancer Drug Delivery.” *ChemistrySelect* 6 (22): 5419–25. doi:10.1002/slct.202101683.

Hakkak, Jafar Al, Warren J. Grigsby, Kalyani Kathirgamanathan, and Neil R. Edmonds. 2019. “Generation of Spherical Cellulose Nanoparticles from Ionic Liquid Processing via Novel Nonsolvent Addition and Drying.” *Advances in*

Materials Science and Engineering 2019 (February): 1–6. doi:10.1155/2019/2081027.

Hall, Rose, Elizabeth Bancroft, Nora Pashayan, Zsofia Kote-Jarai, and Rosalind A Eeles. 2024. "Genetics of Prostate Cancer: A Review of Latest Evidence." *Journal of Medical Genetics* 61 (10): 915–26. doi:10.1136/jmg-2024-109845.

Hanahan, Douglas. 2022. "Hallmarks of Cancer: New Dimensions." *Cancer Discovery* 12 (1): 31–46. doi:10.1158/2159-8290.CD-21-1059.

Hanahan, Douglas, and Robert A Weinberg. 2000. "The Hallmarks of Cancer." *Cell* 100 (1). Elsevier: 57–70. doi:10.1016/S0092-8674(00)81683-9.

Hanušová, Veronika, Iva Boušová, and Lenka Skálová. 2011. "Possibilities to Increase the Effectiveness of Doxorubicin in Cancer Cells Killing." *Drug Metabolism Reviews* 43 (4): 540–57. doi:10.3109/03602532.2011.609174.

Hickey, Ryan J., and Andrew E. Pelling. 2019. "Cellulose Biomaterials for Tissue Engineering." *Frontiers in Bioengineering and Biotechnology* 7 (March). doi:10.3389/fbioe.2019.00045.

Hortobagyi, G. N., A. U. Buzdar, C. E. Marcus, and T. L. Smith. 1986. "Immediate and Long-Term Toxicity of Adjuvant Chemotherapy Regimens Containing Doxorubicin in Trials at MD Anderson Hospital and Tumor Institute." In *NCI Monographs: A Publication of the National Cancer Institute*, 105–9.

Hungate, R. E. 1950. "THE ANAEROBIC MESOPHILIC CELLULOLYTIC BACTERIA." *Bacteriological Reviews* 14 (1): 1–49. doi:10.1128/br.14.1.1-49.1950.

Ioelovich, Michael. 2021. "Preparation, Characterization and Application of Amorphized Cellulose—A Review." *Polymers* 13 (24): 4313. doi:10.3390/polym13244313.

Jin, Huajin, Chunxi Zha, and Lixia Gu. 2007. "Direct Dissolution of Cellulose in NaOH/Thiourea/Urea Aqueous Solution." *Carbohydrate Research* 342 (6): 851–58. doi:10.1016/j.carres.2006.12.023.

Justus, Calvin R., Lixue Dong, and Li V. Yang. 2013. "Acidic Tumor Microenvironment and PH-Sensing G Protein-Coupled Receptors." *Frontiers in Physiology* 4. doi:10.3389/fphys.2013.00354.

Kaplan, Engin, Tuncay Ince, Esma Yorulmaz, Fadile Yener, Ersan Harputlu, and Nelisa Türkoğlu Laçin. 2014. "Controlled Delivery of Ampicillin and Gentamycin from Cellulose Hydrogels and Their Antibacterial Efficiency." *Journal of Biomaterials and Tissue Engineering* 4 (7): 543–49. doi:10.1166/jbt.2014.1198.

Kaur, Rasanpreet, Alok Bhardwaj, and Saurabh Gupta. 2023. “Cancer Treatment Therapies: Traditional to Modern Approaches to Combat Cancers.” *Molecular Biology Reports* 50 (11): 9663–76. doi:10.1007/s11033-023-08809-3.

Kiri, Saurav, and Tyrone Ryba. 2024. “Cancer, Metastasis, and the Epigenome.” *Molecular Cancer* 23 (1): 154. doi:10.1186/s12943-024-02069-w.

Kitkas, Georgios C., Georgios E. Valergakis, Maria Kritsepi-Konstantinou, Athanasios I. Gelasakis, Panagiotis D. Katsoulos, Emmanouil Kalaitzakis, and Nikolaos K. Panousis. 2022. “Association between Ruminal PH and Rumen Fatty Acids Concentrations of Holstein Cows during the First Half of Lactation.” *Ruminants* 2 (4): 382–89. doi:10.3390/ruminants2040026.

Konno, T, H Maeda, K Iwai, S Maki, S Tashiro, M Uchida, and Y Miyauchi. 1984. “Selective Targeting of Anti-Cancer Drug and Simultaneous Image Enhancement in Solid Tumors by Arterially Administered Lipid Contrast Medium.” *Cancer* 54 (11): 2367–74. doi:10.1002/1097-0142(19841201)54:11<2367::aid-cncr2820541111>3.0.co;2-f.

Kwak, Eunice L., and Daniel C. Chung. 2007. “Hereditary Colorectal Cancer Syndromes: An Overview.” *Clinical Colorectal Cancer* 6 (5): 340–44. doi:10.3816/CCC.2007.n.002.

Labianca, Roberto, Giordano D. Beretta, Basem Kildani, Laura Milesi, Federica Merlin, Stefania Mosconi, M. Adelaide Pessi, et al. 2010. “Colon Cancer.” *Critical Reviews in Oncology/Hematology* 74 (2): 106–33. doi:10.1016/j.critrevonc.2010.01.010.

Letchford, Jackson, Ben Wasserman, Ye, Wadood Hamad, and Helen Burt. 2011. “The Use of Nanocrystalline Cellulose for the Binding and Controlled Release of Drugs.” *International Journal of Nanomedicine*, February, 321. doi:10.2147/IJN.S16749.

Li, Jiexi, Xingdi Ma, Deepavali Chakravarti, Shabnam Shalapour, and Ronald A. DePinho. 2021. “Genetic and Biological Hallmarks of Colorectal Cancer.” *Genes & Development* 35 (11–12): 787–820. doi:10.1101/gad.348226.120.

Li, Juanjuan, Ruitao Cha, Kaiwen Mou, Xiaohui Zhao, Keying Long, Huize Luo, Fengshan Zhou, and Xingyu Jiang. 2018. “Nanocellulose- Based Antibacterial Materials.” *Advanced Healthcare Materials* 7 (20). doi:10.1002/adhm.201800334.

Li, Shuping, Hua Yue, Shuang Wang, Xin Li, Xiaojun Wang, Peilin Guo, Guanghui Ma, and Wei Wei. 2022. “Advances of Bacteria-Based Delivery Systems for Modulating Tumor Microenvironment.” *Advanced Drug Delivery Reviews* 188 (September): 114444. doi:10.1016/j.addr.2022.114444.

Liu, Lirui, Wen-Cong Huang, Yang Liu, and Meng Li. 2021. “Diversity of Cellulolytic Microorganisms and Microbial Cellulases.” *International Biodeterioration & Biodegradation* 163 (September): 105277. doi:10.1016/j.ibiod.2021.105277.

Manoukian, Ohan S., Naseem Sardashti, Teagen Stedman, Katie Gailiunas, Anurag Ojha, Aura Penalosa, Christopher Mancuso, Michelle Hobert, and Sangamesh G. Kumbar. 2019. “Biomaterials for Tissue Engineering and Regenerative Medicine.” In *Encyclopedia of Biomedical Engineering*, 462–82. Elsevier. doi:10.1016/B978-0-12-801238-3.64098-9.

Mathew, Gincy, Rajeev Sukumaran, Reeta Singhania, and Ashok Pandey. 2008. “Progress in Research on Fungal Cellulases for Lignocellulose Degradation.” *Journal of Scientific and Industrial Research* 67 (November): 898–907.

Mattiuzzi, Camilla, and Giuseppe Lippi. 2019. “Current Cancer Epidemiology.” *Journal of Epidemiology and Global Health* 9 (4): 217. doi:10.2991/jegh.k.191008.001.

Meredith, Ann-Marie, and Crispin R Dass. 2016. “Increasing Role of the Cancer Chemotherapeutic Doxorubicin in Cellular Metabolism.” *Journal of Pharmacy and Pharmacology* 68 (6): 729–41. doi:10.1111/jphp.12539.

Mohd Amin, Mohd Cairul Iqbal, Abadi Abadi, Naveed Ahmad, Haliza Katas, and J Jamal. 2012. “Bacterial Cellulose Film Coating as Drug Delivery System: Physicochemical, Thermal and Drug Release Properties.” *Sains Malaysiana* 41 (May): 561–68.

Moradi, Mehran, Hossein Tajik, Hadi Almasi, Mehrdad Forough, and Parya Ezati. 2019. “A Novel PH-Sensing Indicator Based on Bacterial Cellulose Nanofibers and Black Carrot Anthocyanins for Monitoring Fish Freshness.” *Carbohydrate Polymers* 222 (October): 115030. doi:10.1016/j.carbpol.2019.115030.

Morais, Flávia P., and Joana M. R. Curto. 2022. “Design and Engineering of Natural Cellulose Fiber-Based Biomaterials with Eucalyptus Essential Oil Retention to Replace Non-Biodegradable Delivery Systems.” *Polymers* 14 (17): 3621. doi:10.3390/polym14173621.

Morrison, Lindsay, and Teresa R. Zembower. 2020. “Antimicrobial Resistance.” *Gastrointestinal Endoscopy Clinics of North America* 30 (4): 619–35. doi:10.1016/j.giec.2020.06.004.

Ni, Y., S. Mulier, Y. Miao, L. Michel, and G. Marchal. 2005. “A Review of the General Aspects of Radiofrequency Ablation.” *Abdominal Imaging* 30 (4): 381–400. doi:10.1007/s00261-004-0253-9.

Orlando J., Rojas. 2016. *Cellulose Chemistry and Properties: Fibers, Nanocelluloses and Advanced Materials*. *Springer*. Vol. 271.

Owens, Fredric N., and Mehmet Basalan. 2016. “Ruminal Fermentation.” In *Rumenology*, 63–102. Cham: Springer International Publishing. doi:10.1007/978-3-319-30533-2_3.

Pierotti, Marco A, and Giuseppe Della Porta. 2022. “Mechanisms of Oncogene Activation.” *Advances in Oncology*. Routledge, 3–12.

Platnieks, Oskars, Sergejs Beluns, Sabine Briede, Maksims Jurinovs, and Sergejs Gaidukovs. 2023. “Cellulose Synergetic Interactions with Biopolymers: Functionalization for Sustainable and Green Material Design.” *Industrial Crops and Products* 204 (November): 117310. doi:10.1016/j.indcrop.2023.117310.

Plumbridge, J. 2002. “Regulation of Gene Expression in the PTS in Escherichia Coli: The Role and Interactions of Mlc.” *Current Opinion in Microbiology* 5 (2): 187–93. doi:10.1016/S1369-5274(02)00296-5.

Pugazhendhi, Arivalagan, Thomas Nesakumar Jebakumar Immanuel Edison, Bharath Kumar Velmurugan, Joe Antony Jacob, and Indira Karuppusamy. 2018. “Toxicity of Doxorubicin (Dox) to Different Experimental Organ Systems.” *Life Sciences* 200 (May): 26–30. doi:10.1016/j.lfs.2018.03.023.

Quiroz Castañeda, Rosa, and Jorge Folch-Mallol. 2013. “Degradation of Lignocellulosic Biomass - Techniques, Applications and Commercialization Sustainable Degradation of Lignocellulosic Biomass - Techniques, Applications and Commercialization.” In , 275.

Rawat, Pushkar Singh, Aiswarya Jaiswal, Amit Khurana, Jasvinder Singh Bhatti, and Umashanker Navik. 2021. “Doxorubicin-Induced Cardiotoxicity: An Update on the Molecular Mechanism and Novel Therapeutic Strategies for Effective Management.” *Biomedicine & Pharmacotherapy* 139 (July): 111708. doi:10.1016/j.biopha.2021.111708.

Regenold, Maximilian, Pauric Bannigan, James C. Evans, Adam Waspe, Michael J. Temple, and Christine Allen. 2022. “Turning down the Heat: The Case for Mild Hyperthermia and Thermosensitive Liposomes.” *Nanomedicine: Nanotechnology, Biology and Medicine* 40 (February): 102484. doi:10.1016/j.nano.2021.102484.

Roman, Maren, Shuping Dong, Anjali Hirani, and Yong Woo Lee. 2010. “Cellulose Nanocrystals for Drug Delivery.” In , 81–91. doi:10.1021/bk-2009-1017.ch004.

Russell, James B., Richard E. Muck, and Paul J. Weimer. 2009. “Quantitative Analysis of Cellulose Degradation and Growth of Cellulolytic Bacteria in the Rumen.” *FEMS Microbiology Ecology* 67 (2): 183–97. doi:10.1111/j.1574-6941.2008.00633.x.

S., Haruta, Cui Z., Huang Z., Li M., Ishii M., and Igarashi Y. 2002. “Construction of a Stable Microbial Community with High Cellulose-Degradation Ability.”

Applied Microbiology and Biotechnology 59 (4–5): 529–34. doi:10.1007/s00253-002-1026-4.

Sari, Wenny Novita, Safika, Darmawi, and Yudha Fahrimal. 2017. "Isolation and Identification of a Cellulolytic Enterobacter from Rumen of Aceh Cattle." *Veterinary World* 10 (12): 1515–20. doi:10.14202/vetworld.2017.1515-1520.

Sariboga, Ruken, and Omer Faruk Sarioglu. 2024a. "Applications of Cellulose- Based Nanomaterials for Sustainability and Therapeutics: A Review." *ChemBioEng Reviews* 11 (4). doi:10.1002/cben.202300069.

———. 2024b. "Cellulolytic Characterization of the Rumen-Isolated Acinetobacter Pittii ROBY and Design of a Potential Controlled-Release Drug Delivery System." *Engineering Microbiology* 4 (3): 100164. doi:10.1016/j.engmic.2024.100164.

Seddiqi, Hadi, Erfan Oliaei, Hengameh Honarkar, Jianfeng Jin, Lester C. Geonzon, Rommel G. Bacabac, and Jenneke Klein-Nulend. 2021. "Cellulose and Its Derivatives: Towards Biomedical Applications." *Cellulose*. doi:10.1007/s10570-020-03674-w.

Shamsuri, Ahmad Adlie. 2011. "IONIC LIQUIDS: PREPARATIONS AND LIMITATIONS." *MAKARA of Science Series* 14 (2). doi:10.7454/mss.v14i2.677.

Sinegani, Ali Akbar Safari, and Giti Emtiazi. 2006. "The Relative Effects of Some Elements on the DNS Method in Cellulase Assay." *Journal of Applied Sciences and Environmental Management* 10 (3). doi:10.4314/jasem.v10i3.17326.

Sun, Leming, Hongmei Liu, Yanqi Ye, Yang Lei, Rehmat Islam, Sumin Tan, Rongsheng Tong, Yang-Bao Miao, and Lulu Cai. 2023. "Smart Nanoparticles for Cancer Therapy." *Signal Transduction and Targeted Therapy* 8 (1): 418. doi:10.1038/s41392-023-01642-x.

Tierney, Braden T., Nitin K. Singh, Anna C. Simpson, Andrea M. Hujer, Robert A. Bonomo, Christopher E. Mason, and Kasthuri Venkateswaran. 2022. "Multidrug-Resistant Acinetobacter Pittii Is Adapting to and Exhibiting Potential Succession Aboard the International Space Station." *Microbiome* 10 (1): 210. doi:10.1186/s40168-022-01358-0.

Topuz, Ural, Özlem Eren Kiran, Uğur ÇÖMLEKÇİOĞLU Kahramanmaraş Sütçü İmam Üniversitesi, Fen Edebiyat Fakültesi, and Biyoloji Bölümü. 2007. "Selülaz Üreticisi Bacillus Suşlarının Enzimatik Özelliklerinin Araştırılması." *KSU Journal of Science and Engineering*. Vol. 10.

Vagena, Ioanna-Aglaia, Christina Malapani, Maria-Anna Gatou, Nefeli Lagopati, and Evangelia A. Pavlatou. 2025. "Enhancement of EPR Effect for Passive Tumor Targeting: Current Status and Future Perspectives." *Applied Sciences* 15 (6): 3189. doi:10.3390/app15063189.

Varela-López, Alfonso, Maurizio Battino, María D. Navarro-Hortal, Francesca Giampieri, Tamara Y. Forbes-Hernández, José M. Romero-Márquez, Ricardo Collado, and José L. Quiles. 2019. "An Update on the Mechanisms Related to Cell Death and Toxicity of Doxorubicin and the Protective Role of Nutrients." *Food and Chemical Toxicology* 134 (December): 110834. doi:10.1016/j.fct.2019.110834.

Varnaitė-Žuravliova, Sandra, and Julija Baltušnikaitė-Guzaitienė. 2024. "Properties, Production, and Recycling of Regenerated Cellulose Fibers: Special Medical Applications." *Journal of Functional Biomaterials* 15 (11): 348. doi:10.3390/jfb15110348.

Vavrova, Anna, Hana Jansova, Eliska Mackova, Miloslav Machacek, Pavlina Haskova, Lucie Tichotova, Martin Sterba, and Tomas Simunek. 2013. "Catalytic Inhibitors of Topoisomerase II Differently Modulate the Toxicity of Anthracyclines in Cardiac and Cancer Cells." *PLoS ONE* 8 (10): e76676. doi:10.1371/journal.pone.0076676.

Verma, Ayush, and Francesco Stellacci. 2010. "Effect of Surface Properties on Nanoparticle–Cell Interactions." *Small* 6 (1): 12–21. doi:10.1002/smll.200901158.

Wang, Guocan, Di Zhao, Denise J. Spring, and Ronald A. DePinho. 2018. "Genetics and Biology of Prostate Cancer." *Genes & Development* 32 (17–18): 1105–40. doi:10.1101/gad.315739.118.

Wang, Jing. 2007. "Mechanisms Involved in Ceramide-Induced Cell Cycle Arrest in Human Hepatocarcinoma Cells." *World Journal of Gastroenterology* 13 (7): 1129. doi:10.3748/wjg.v13.i7.1129.

Wang, Wenguang, Haiheng Xu, Qingsong Ye, Feng Tao, Ian Wheeldon, Ahu Yuan, Yiqiao Hu, and Jinhui Wu. 2022. "Systemic Immune Responses to Irradiated Tumours via the Transport of Antigens to the Tumour Periphery by Injected Flagellate Bacteria." *Nature Biomedical Engineering* 6 (1): 44–53. doi:10.1038/s41551-021-00834-6.

Weber, Georg F. 2007. *Molecular Mechanisms of Cancer*. Dordrecht: Springer Netherlands. doi:10.1007/978-1-4020-6016-8.

Wilson, David B. 2011. "Microbial Diversity of Cellulose Hydrolysis." *Current Opinion in Microbiology* 14 (3): 259–63. doi:10.1016/j.mib.2011.04.004.

Yoon, Li Wan, Teck Nam Ang, Gek Cheng Ngoh, and Adeline Seak May Chua. 2014. "Fungal Solid-State Fermentation and Various Methods of Enhancement in Cellulase Production." *Biomass and Bioenergy* 67 (August): 319–38. doi:10.1016/j.biombioe.2014.05.013.

Zeki, Sebastian S., Trevor A. Graham, and Nicholas A. Wright. 2011. “Stem Cells and Their Implications for Colorectal Cancer.” *Nature Reviews Gastroenterology & Hepatology* 8 (2): 90–100. doi:10.1038/nrgastro.2010.211.

Zhang, Ziao, Yujie Lu, Shoujian Gao, and Shuping Wu. 2025. “Sustainable and Efficient Wastewater Treatment Using Cellulose-Based Hydrogels: A Review of Heavy Metal, Dye, and Micropollutant Removal Applications.” *Separations* 12 (3): 72. doi:10.3390/separations12030072.

Zhou, Lei, Thao Le Thanh, Jianyu Gong, Jae-Hwan Kim, Eun-Ju Kim, and Yoon-Seok Chang. 2014. “Carboxymethyl Cellulose Coating Decreases Toxicity and Oxidizing Capacity of Nanoscale Zerovalent Iron.” *Chemosphere* 104 (June): 155–61. doi:10.1016/j.chemosphere.2013.10.085.

Zhou, Min, Yucheng Tang, Wenjie Xu, Xinyan Hao, Yongjiang Li, Si Huang, Daxiong Xiang, and Junyong Wu. 2023. “Bacteria-Based Immunotherapy for Cancer: A Systematic Review of Preclinical Studies.” *Frontiers in Immunology* 14: 1140463. doi:10.3389/fimmu.2023.1140463.

Zhu, Shengdong, Yuanxin Wu, Qiming Chen, Ziniu Yu, Cunwen Wang, Shiwei Jin, Yigang Ding, and Gang Wu. 2006. “Dissolution of Cellulose with Ionic Liquids and Its Application: A Mini-Review.” *Green Chemistry* 8 (4): 325. doi:10.1039/b601395c.

6. SUPPLEMENTARY DATA

Table S1. List of instruments that are utilized.

Device Type	**Brand**	**Model**
-86˚C ULT Freezer	Haier	DW-86L486E
Autoclave	Nüve	OT 90L
Cell Culture Cabinet	Labconco	A2
Centrifuge (Cold)	Beckman Coulter	
Centrifuge (Cold)	Eppendorf	Centrifuge 5418 R
Centrifuge	Electro-mag	M 815 E
Centrifuge	Beckman Coulter	Allegra X-15R Centrifuge
CO2 Incubator	Heraeus Instruments	CO2 incubator Function line BB16
CO_2 Incubator	Binder	C150
DLS/Zeta Sizer	Malvern	Zetasizer Pro
Fluorescence Microscope	Zeiss	
FT-IR	Shimadzu	QATR-S
Incubator	Electro-mag	M3025P
Light Microscope	Nikon	Eclipse-TS100
Magnetic Stirrer	Four E'S Scientific	MI0102003
Microcentrifuge	Weightlab instruments	WN-CMV6000 microcentrifuge
Micropipette 1 ml	Four E'S Scientific	Precipette
Micropipette 20 uL	Four E'S Scientific	Precipette

Micropipette 200 uL	Four E'S Scientific	Precipette
Microplate Spectrophotometer	Thermo Fisher	Multiskan GO
pH Meter	Vio Labs	XS 201 T pH Electrode
Precision scale	Dikomsan	FHB-300
Rocking Shaker	Lab Companion	CRS-350
Shaking incubator	Nükleon	NCI55
Spectrophotometer	DeNovix	DS-11+Spectrophotometer
Spectrophotometer	INESA	INESA 722N Vis Spectrophotometer
Transmission electron microscope (TEM)	Thermo Scientific	QUATTRO S
Ultra-Low Temperature Freezer	Haier Biomedical	Haier DW86L388
Ultra-pure water Purification System	Merck	Milli-Q
Ultrasonic Cleaner	Weightlab instruments	WF-UD2
Vortex	Four E'S Scientific	MI0101002
Waterbath	Nüve	VWB 18

Table S2. List of chemicals that are utilized.

Name	**Brand**	**Catalog**
3,5-Dinitrosalicilic acid	Sigma Aldrich	
Acetone	TEKKİM	TK.010050
Agar	Merck Milipore	1016141000
Ammonium Nitrate	Sigma Aldrich	221244

Calcium chloride dihydrate	TEKKİM	TK.800201
Carboxymethyl cellulose (CMC)	Sigma Aldrich	
Cell Counting Kit-8	MedChemExpress	HY-K0301-5mL
Congo Red	Sigma Aldrich	C6767
Dextrose (Glucose)	-	-
Diethyl ether	Sigma Aldrich	673811
Di-Potassium Hydrogen Phosphate	TEKKİM	TK.930147
Di-sodium hydrogen Phosphate (Dodekahidrat)	TEKKİM	TK.802300
DMEM	Gibco	11965092
DNA, RNA, and Protein purification kit	NucleoSpin	740966.50
Dox.HCl	Sigma Aldrich	D1515-10MG
EMIMAc	Sigma Aldrich	689483-5G
FBS		
Glutaraldehyde 50%	TEKKİM	TK.090251
Glycerine (Glycerol)	ERLAB	-
Glycine (Glisin)	TEKKİM	TK.930135
HCl 37%	TEKKİM	TK.911011
Iron (III) Chloride (anhydrous)	TEKKİM	TK.200690
Magnesium Sulfate Heptahydrate	TEKKİM	TK.120310

Microcrystalline Cellulose	ZAG Kimya	-
pH 10 buffer	Norateks	-
Potassium Chloride	TEKKİM	TK.150440
Potassium Dihydrogen Phosphate	TEKKİM	TK.200990
Potassium Sodium Tartarate	Sigma Aldrich	217255
RPMI	Gibco	11875093
Sodium Carboxymethyl Cellulose	Sigma Aldrich	419338
Sodium Chloride (NaCl)	TEKKİM	
Sodium Hydroxide (NaOH)	TEKKİM	
Teksoll (95%)	TEKKİM	
Thiourea (99%)	-	-
Tri-Sodium Phosphate	TEKKİM	TK.200650
Trypsin 0.05% EDTA	Gibco	25300054
Tween 85	Sigma Aldrich	P4634
Urea	TEKKİM	TK.190610
Yeast Extract	Biolife	-

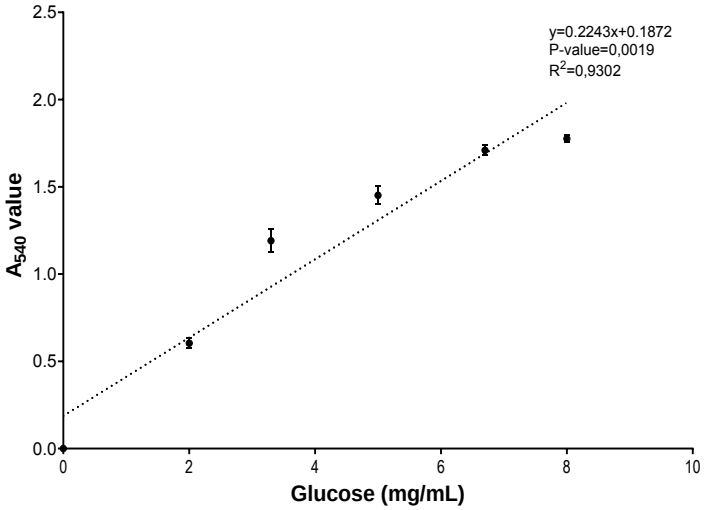

Figure S1. A standard curve that refers to A540 results according to different glucose concentrations.

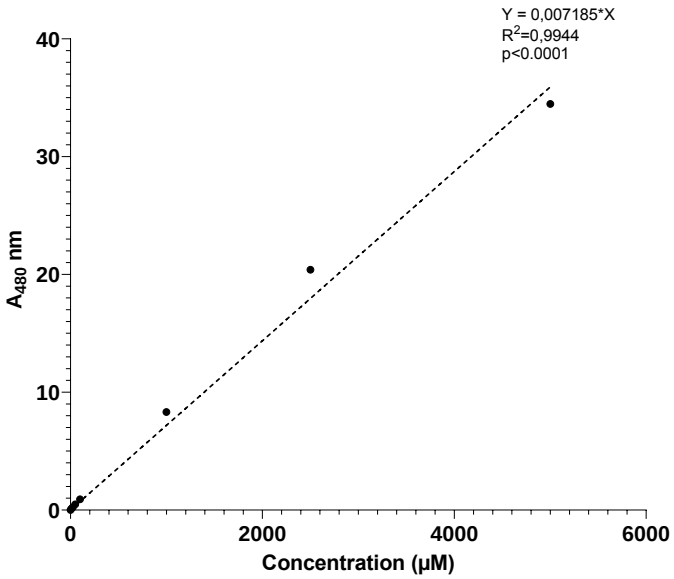

Figure S2. Doxorubicin standard curve

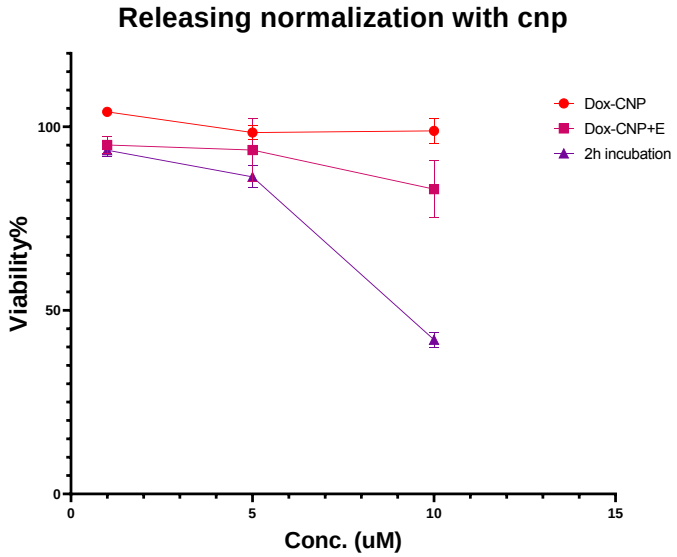

Figure S3. *In vitro* analysis of the targeted drug release method that includes Dox-CNP, Dox-CNP+Enzyme, and 2 hours incubated Dox-CNP+ combination before treatment, and results are normalized with CNP+Enzyme combination.

PUBLICATIONS DERIVED FROM THESIS

CONFERENCE/SEMINAR

- **2024 NANOTR-18 Conference**
  Sarıboğa R., Sarıoğlu Ö.F., Comparative Analysis of Cellulose Nanoparticle Production Methods for Chemotherapy Drug Integration

  Koç University/ Poster Presentation **İstanbul, Türkiye**

- **2024 NANOTR-18 Conference**
  Sarıboğa R., Sarıoğlu Ö.F., A Controlled-Release Drug Delivery Strategy Based on Doxorubicin-Loaded Cellulose Nanoparticles and a Cellulolytic Bacterial Strain

  Koç University/ Oral Presentation **İstanbul, Türkiye**

- **2024 ACTS'24 Seminar**
  Sarıboğa R., Sarıoğlu Ö.F., A Targeted Drug Release Therapy with Cellulolytic Bacteria &Cellulose Nanoparticles

  Bilkent University/ Poster Presentation **Ankara, Türkiye**

ARTICLES

- **Review Article**

Sariboga, R., & Sarioglu, O. F. (2024). Applications of Cellulose- Based Nanomaterials for Sustainability and Therapeutics: A Review. *ChemBioEng Reviews*, *11*(4), e202300069.

- **Research Article**

Sariboga, R., & Sarioglu, O. F. (2024). Cellulolytic characterization of the rumen-isolated Acinetobacter pittii ROBY and design of a potential controlled-release drug delivery system. *Engineering Microbiology*, *4*(3), 100164.